TU Delft

Introduction to Reflection Seismology
AESB2140 (B.Sc.)

G.G. Drijkoningen

August 2017

(Version 3.1 - with exercises)

Contents

1 Fourier analysis **5**

1.1 Continuous Fourier Transform. 5

1.2 Discrete Fourier Transform and Sampling Theorem. 7

1.3 LTI Systems and Convolution 10

1.4 Convolution Theorem 11

1.5 Filters 12

1.6 Correlation 12

1.7 Deconvolution 14

1.8 Time- and frequency characteristics 18

2 Basics of the seismic method: kinematics **21**

2.1 Introduction 21

2.2 Basic physical notions of waves 22

2.3 The interface : Snell's law, refraction and reflection 24

2.4 Application of basic concepts: Interpretation of some raw field seismic records. 29

2.5 Application of Fourier analysis: Spectral analysis and filtering of field seismic records 35

2.6 *EXERCISES* 39

3 Seismic instrumentation **43**

3.1 Seismic data acquisition 43

3.2 Seismic sources 46

3.2.1 Airguns 46

3.2.2 Vibroseis 50

3.2.3 Dynamite . . . 56
3.3 Seismic detectors . . . 60
3.3.1 Geophones . . . 61
3.3.2 Hydrophones . . . 64
3.4 Seismic recording systems . . . 68
3.4.1 (Analog) filters . . . 68
3.4.2 The Analog-to-Digital (A/D) converter . . . 71
3.5 Total responses of instrumentation . . . 72
3.6 *EXERCISES* . . . 74

4 Fundamentals of the seismic method: wave theory 75
4.1 Introduction . . . 75
4.2 Wave motion in fluids: acoustic waves . . . 76
4.3 Reflection and transmission at boundaries . . . 77
4.4 Wave motion in an elastic solid . . . 80
4.5 *EXERCISES* . . . 83

5 Processing of Seismic Reflection Data 85
5.1 Seismic processing and imaging . . . 85
5.2 Sorting of seismic data . . . 87
5.3 Normal move-out and velocity analysis . . . 92
5.4 Stacking . . . 99
5.5 Zero-offset migration . . . 101
5.6 Conversion from time to depth . . . 113
5.7 *EXERCISES* . . . 116

A Discrete Fourier Transform and Sampling Theorem 119

B Correlation 123

C Advantages and disadvantages of Vibroseis and dynamite 125

D Network outline 127

E Derivation of basic equations for 1-D acoustic wave motion 129

F Strain, P- and S-waves 133

Chapter 1

Fourier analysis

In this chapter we review some basic results from signal analysis and processing. We shall not go into detail and assume the reader has some basic background in signal analysis and processing. As basis for signal analysis, we use the Fourier transform. We start with the continuous Fourier transformation. But in applications on the computer we deal with a discrete Fourier transformation, which introduces the special effect known as aliasing. We use the Fourier transformation for processes such as convolution, correlation and filtering. Some special attention is given to deconvolution, the inverse process of convolution, since it is needed in later chapters of these lecture notes.

1.1 Continuous Fourier Transform.

The Fourier transformation is a special case of an integral transformation: the transformation decomposes the signal in weigthed basis functions. In our case these basis functions are the cosine and sine (remember $\exp(i\phi) = \cos(\phi) + i\sin(\phi)$). The result will be the weight functions of each basis function.

When we have a function which is a function of the independent variable t, then we can transform this independent variable to the independent variable frequency f via:

$$A(f) = \int_{-\infty}^{+\infty} a(t) \exp(-2\pi i f t) dt \tag{1.1}$$

In order to go back to the independent variable t, we define the inverse transform as:

$$a(t) = \int_{-\infty}^{+\infty} A(f) \exp(2\pi i f t) df \tag{1.2}$$

Notice that for the function in the time domain, we use lower-case letters, while for the frequency-domain expression the corresponding uppercase letters are used. $A(f)$ is called the *spectrum* of $a(t)$.

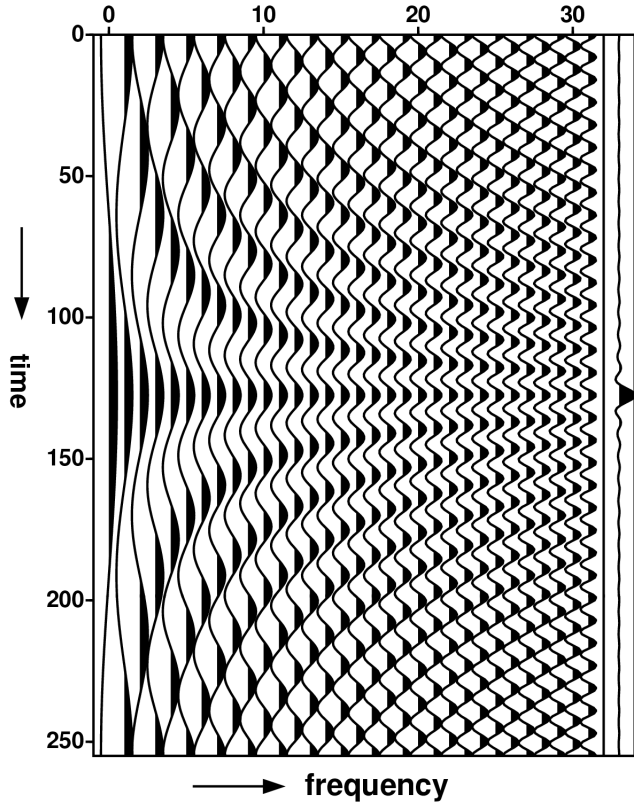

Figure 1.1: 32 cosine's with increasing frequencies; when added together, the rightmost trace is obtained.

A total signal can be built up via using cosines of different frequencies. If we would add many cosines together, we can make some specific signals. Let us consider Figure (1.1). We see 32 cosines with increasing frequencies. When we add the first 32 traces together, we obtain the trace as plotted on the right of the Figure: it has only one peak.

In this figure we used cosines with constant amplitudes, so the cosines were not shifted and the weights were just 1. We can shift the cosines, and we can vary the weights of the different frequency components, to obtain a certain signal. Actually, one can synthesize any signal by using shifted and weighted cosines. This is the Fourier Transform. As an example of this, consider Figure (1.2). On the leftmost trace, we see a time signal. When we look at the different components of this signal, we obtain the other traces. On the horizontal axis the frequency is given. First, it can be seen the weights of the frequency components is different, with the largest amplitudes around 24 Hz. Next, it can be seen that the different cosines are slightly time–shifted compared to its neighbour.

The amplitude of the components are obtained as the *amplitude* spectrum of the Fourier transformation of the signal. The shift of each cosine, is obtained via the *phase* spectrum

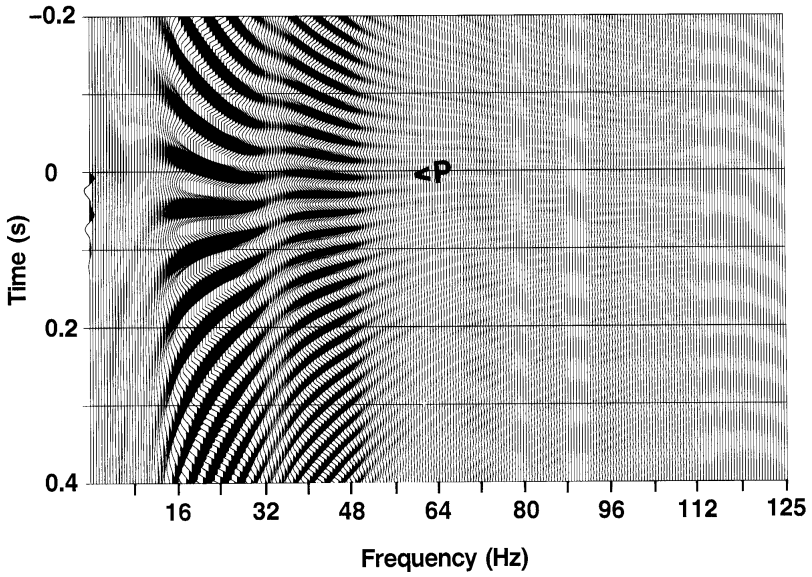

Figure 1.2: A time signal (leftmost trace) decomposed into shifted, weighted cosines (From: Yilmaz, 1987).

of the Fourier transformation of the signal. The Fourier transform of a signal gives, in general, complex values for the frequency components. The amplitude gives the amplitude spectrum, and the phase of the complex value gives the phase spectrum.

1.2 Discrete Fourier Transform and Sampling Theorem.

The above continuous integrals are nearly always used in deriving any mathematical results, but, in performing transforms on data, the integrals are always replaced by summations. The continuous signal becomes a discrete signal. As is shown in appendix A, discretisation of the continuous Fourier integral *makes the spectrum periodic:*

$$A_{\text{Discrete}}(f) = \sum_{m=-\infty}^{\infty} A_{\text{Continuous}}(f + \frac{m}{\Delta t}) \tag{1.3}$$

So this is an infinite series of shifted spectra as shown in Figure (1.3)(b). The discretisation of the time signal forces the Fourier transform to become periodic. In the discrete case we get the same spectrum as the continuous case if we only take the interval from $-1/(2\Delta t)$ to $+1/(2\Delta t)$, and else be zero; the signal must be *band-limited*. So this means means that the discrete signal must be zero for frequencies $|f| \geq f_N = 1/(2\Delta t)$. The frequency f_N is known as the Nyquist frequency. Equivalently, we can say that if there is no information in the continuous time signal $a(t)$ at frequencies above f_N, the maximum sampling interval

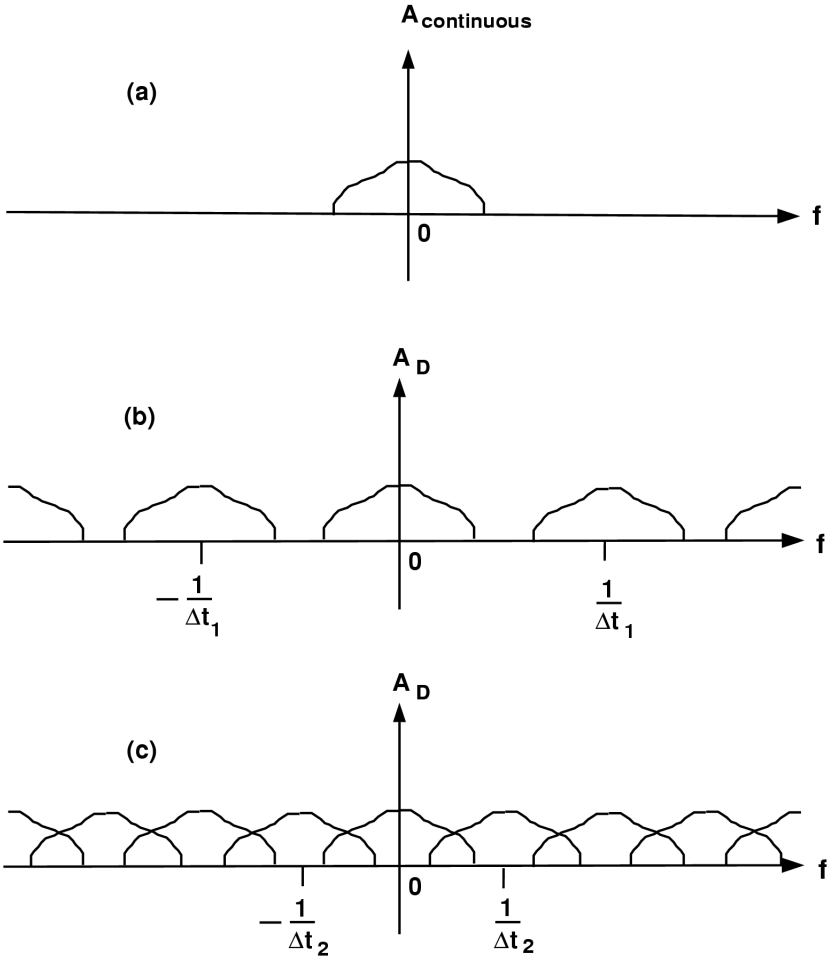

Figure 1.3: Effect of time-discretisation in frequency domain: (a) continuous spectrum; (b) properly time-sampled spectra giving rise to periodicity (period $1/\Delta t_1$); (c) too coarse time sampling Δt_2 such that spectra overlap (= aliasing in time domain).

Δt is

$$\Delta t_{\max} = \frac{1}{2f_N} \tag{1.4}$$

This is the sampling theorem. If we choose Δt too large, we undersample the signal and we get aliasing as shown in Figure 1.4. The original signal appears to have a lower frequency.

Another basic relation originates from the discretisation of the inverse Fourier transformation. The frequencies become discrete and therefore the *time* signal becomes periodic. The interval $1/\Delta t$ is divided up into N samples at Δf sampling so that we obtain the relation:

$$N\Delta t\Delta f = 1 \tag{1.5}$$

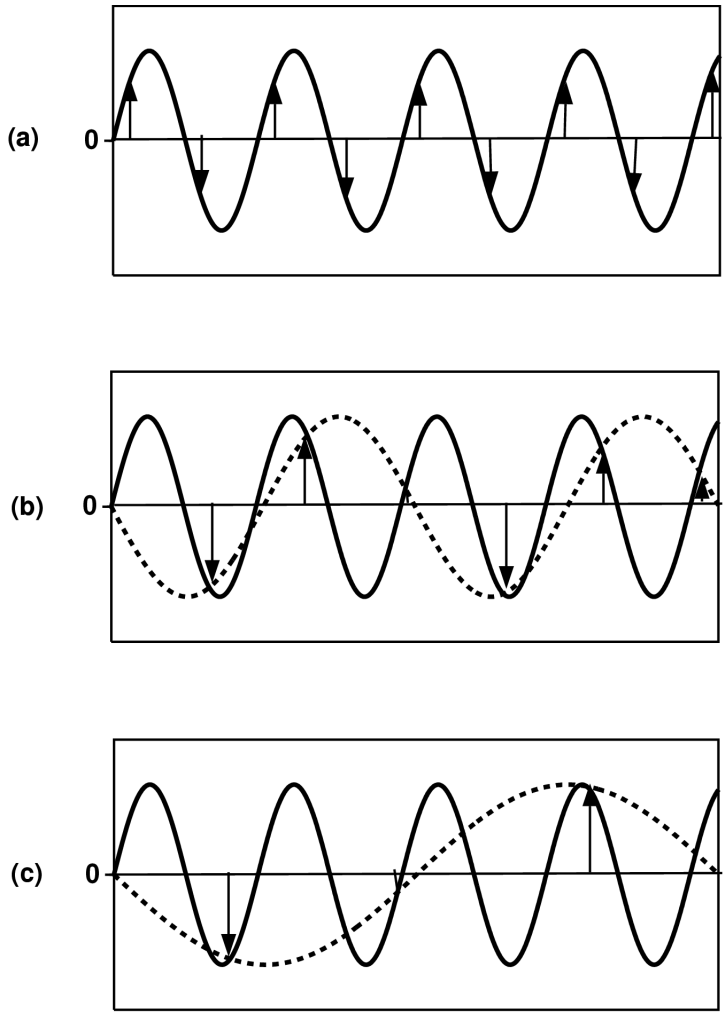

Figure 1.4: Effect of discretisation in time: (a) properly sampled signal; (b) just undersampled signal; (c) fully undersampled signal.

This relation can be used when we want increase the number of samples, for instance. In that case, if the time sampling remains the same, the frequency sampling decreases! This can be useful for interpolating data.

Finally, we obtain the pair:

$$A_n = \Delta t \sum_{k=0}^{N-1} a_k \exp(-2\pi i n k/N) \qquad n = 0, 1, 2, ..., N-1 \tag{1.6}$$

$$a_k = \Delta f \sum_{n=0}^{N-1} A_n \exp(2\pi i n k/N) \qquad k = 0, 1, 2, ..., N-1 \tag{1.7}$$

in which a_k and A_n are now the discrete-time and discrete-frequency values of the continuous signals $a(t)$ and $A_{\text{Continuous}}(f)$. These two equations are the final discrete-time and discrete-frequency Fourier transform pair.

1.3 LTI Systems and Convolution

In this section a signal is fed into a linear time-invariant system. To that purpose a signal $s(t)$ can be written as:

$$s(t) = \int_{-\infty}^{+\infty} s(\tau)\delta(t-\tau)d\tau \tag{1.8}$$

Let us feed the integral to the system by building up the signal from the δ-pulse responses, as shown in Figure 1.5.

- On top, $\delta(t)$ is fed into the system giving $h(t)$ as output.
- Next, a time-shifted pulse $\delta(t-\tau)$ is fed into the system: because the system is time-invariant, the response will be $h(t-\tau)$.
- Next, a scaled pulse $s(\tau)\delta(t-\tau)$ is fed into the system: because the system is linear, the response is $s(\tau)h(t-\tau)$. This is valid for each τ, so for all values of the integrand.
- Then, finally, scaling the input each by $d\tau$, we can feed the whole integral into the system: because the system is linear, the total response $x(t)$ to this signal will be:

$$x(t) = \int_{\infty}^{+\infty} s(\tau)h(t-\tau)d\tau \tag{1.9}$$

The integral on the right-hand side is a *convolution*: the output $x(t)$ is the convolution of the input $s(t)$ with the impulse response $h(t)$. A physical system is causal and assuming the input signal starts at $t = 0$, the responses $s(t)$ and $h(t)$ are zero for times smaller than zero. Substituting this in the above, the equation becomes:

$$x(t) = \int_{0}^{t} s(\tau)h(t-\tau)d\tau \tag{1.10}$$

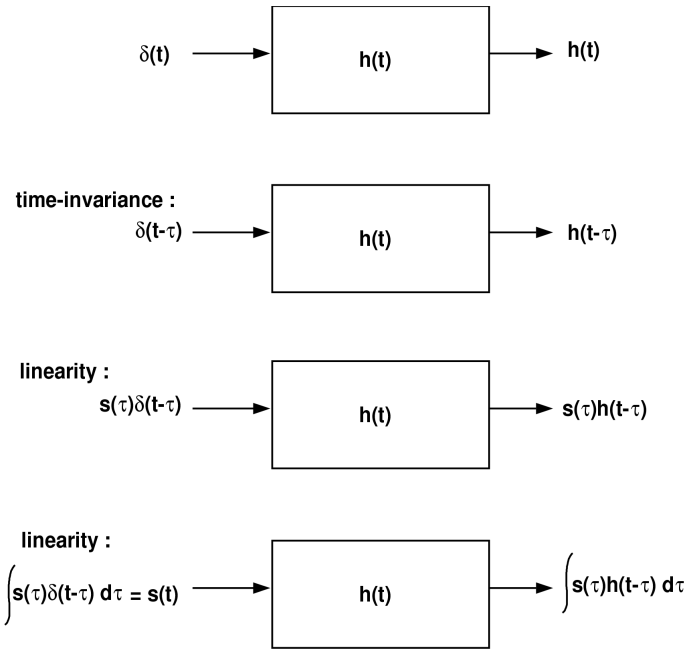

Figure 1.5: Convolution built up from scaled, time-shifted δ-pulses.

The convenient shorthand notation for the convolution integral is

$$x(t) = s(t) * h(t) \tag{1.11}$$

1.4 Convolution Theorem

The convolution theorem states that convolution in one Fourier domain is equivalent to multiplication in the other Fourier domain. Thus, the result of convolving of two time signals is equivalent, in the frequency domain, to multiplying their Fourier transforms. Equally, convolution of two (complex) signals in the frequency domain is equivalent to multiplication of their inverse Fourier transforms in the time domain. Of course, this result applies to all Fourier-transformable functions, including functions of space.

The theorem may be stated mathematically as follows

$$\mathcal{F}_t\left(\int_{-\infty}^{+\infty} h(t')g(t-t')dt'\right) = \mathcal{F}_t[h(t) * g(t)] = H(f)G(f) \tag{1.12}$$

in which $\mathcal{F}_t$ means "Fourier transform of".

1.5 Filters

A filter is a system that has an input and an output. The linear time-invariant systems considered previously can also be treated as filters. Filters usually have a purpose to do something to a signal: the input signal needs to be shaped or formed, depending on the application.

Fourier analysis can give very much insight in how a signal is built up : one cannot only recognize certain features arriving at certain times, such as a reflection in reflection seismics, but one can also recognize certain resonances in systems: many electronic circuits have their own resonances, and they can be analyzed by Fourier analysis. One can do more than just analyze signals: one can also *remove* features from a signal. Thus, removal cannot only be done in the time domain, but also in the frequency domain. This is called *filtering*.

An example of filtering is given in the next figure (Fig. 1.6). Let us now consider a signal as given in Figure (1.6). The signal is built up of a part which is slowly varying (low-frequent), and a part which is rapidly varying (high-frequent). Say, we are interested in the slowly varying part, so the rapidly varying (high-frequent) part needs to be removed. This removal cannot be done in the time domain since the two parts are not separated. From the previous sections it may be obvious that we can establish a separation via the frequency domain. For that reason, we transform the signal to the frequency domain. This is shown on the upper right figure. Two peaks can be seen, each associated with the parts which were described above. Now the signal is fed into a filter, which is a window function. This means simply that the spectrum of the input signal is multiplied with the transfer function of the system, which is a window function. When the multiplication is performed, the figure as given in the right-bottom figure is obtained: only the low-frequency part is retained. When the signal is transformed back to the time domain, the left-bottom figure is obtained : we have got rid of the high-frequency part using the window-function in the frequency domain as filter.

The procedure as given in the above is called *filtering*. Filtering in this case is nothing else than windowing in the frequency domain.

1.6 Correlation

In the same way as convolution, we can easily derive that a correlation in the time domain is equivalent to a multiplication *with the complex conjugate* in the frequency domain. The derivation of this, is given in appendix B. We can recognize two types of correlations, namely an autocorrelation and a cross-correlation. For the autocorrelation, the Fourier

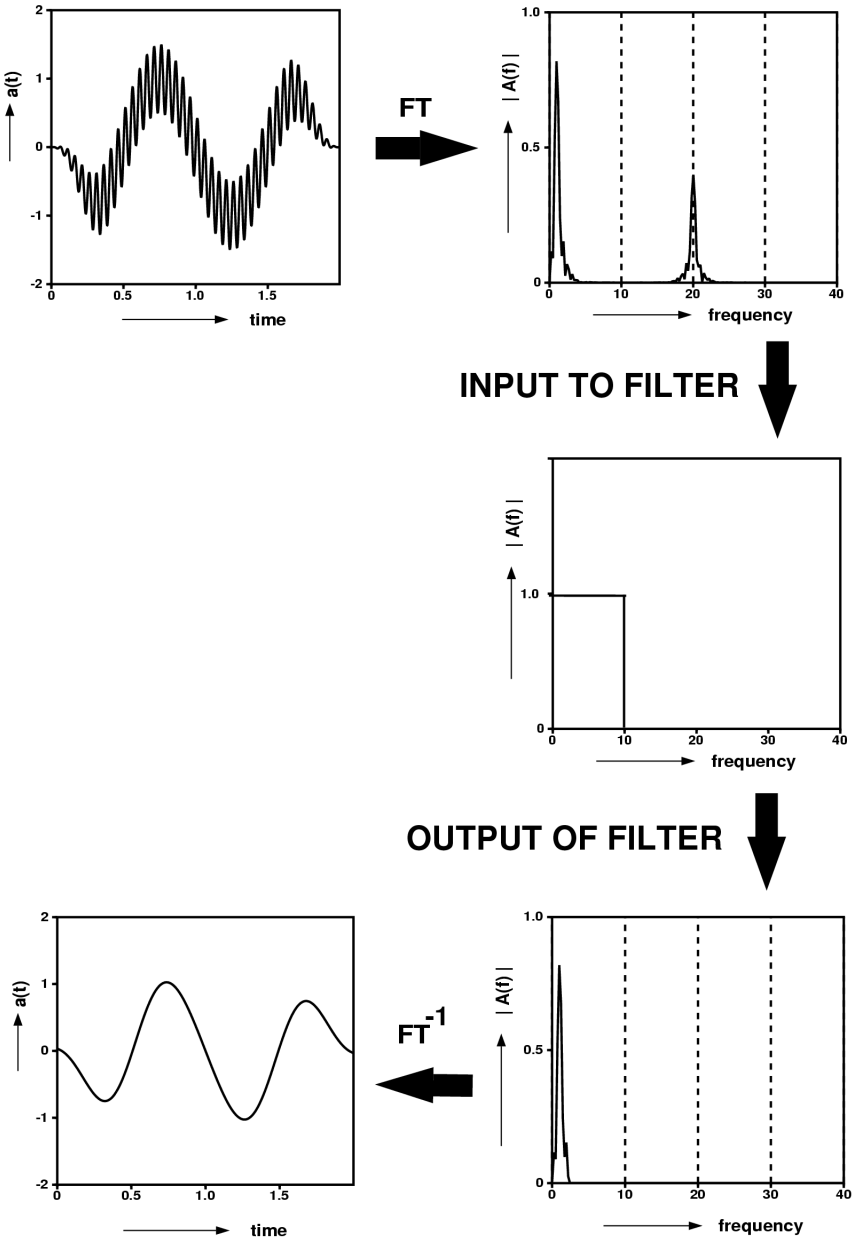

Figure 1.6: Filtering of two-sine signal using window in frequency domain. Upper left: two superposed sine waves. Upper right: amplitude spectrum. Lower right: amplitude spectrum of filtered signal. Lower left: filtered signal in time-domain.

transform is given by:

$$\begin{aligned}\mathcal{F}_t\left(\int_{-\infty}^{+\infty} a(\tau)a^*(\tau-t)d\tau\right) &= A(f)A^*(f)\\ &= [|A(f)|\exp\{i\phi_A(f)\}]\ [|A(f)|\exp\{i\phi_A(f)\}]^*\\ &= |A(f)|\exp\{i\phi_A(f)\}\ |A(f)|\exp\{-i\phi_A(f)\}\\ &= |A(f)|^2 \qquad (1.13)\end{aligned}$$

where $|A(f)|$ denotes the amplitude and ϕ_A the phase of the signal A. Note here that the *phase* of the spectrum is absent in the result, and therefore the signal is called zero phase. In the time domain, it can be shown mathematically that this autocorrelation-signal is symmetric around $t = 0$.

In the same way, it is shown in appendix B that the Fourier transform of a cross-correlation is given by:

$$\mathcal{F}_t\left(\int_{-\infty}^{+\infty} a(\tau)b^*(\tau-t)d\tau\right) = A(f)B^*(f) \qquad (1.14)$$

1.7 Deconvolution

Deconvolution concerns itself with neutralizing a part of a signal which is convolutional. We consider that the output signal $x(t)$ consists of the convolution of an input signal $s(t)$ and the impulse response $g(t)$ of an LTI system, i.e.,

$$x(t) = s(t) * g(t). \qquad (1.15)$$

Often, we are interested in the impulse response response of the system. Ideally, we would like the input signal to have a flat amplitude spectrum of 1, with no phase, which corresponds to a delta-function in time. In practice, this will never be the case. Generally, the input signal $s(t)$ has a certain shape and amplitude. So therefore we want to find a filter $f(t)$ that converts the signal $s(t)$ into a δ-function:

$$f(t) * s(t) = \delta(t). \qquad (1.16)$$

By applying the filter $f(t)$ to the output signal $x(t)$, we neutralize the effect of the input signal since

$$\begin{aligned}f(t) * x(t) &= f(t) * s(t) * g(t)\\ &= \delta(t) * g(t) \qquad (1.17)\\ &= g(t).\end{aligned}$$

Neutralizing the effect of the input signal from a output signal is called a *deconvolution* process.

Let us assume we have a signal $s(t)$ with a known spectrum, $S(f)$. Then the convolution (1.15) becomes a multiplication in the frequency domain:

$$X(f) = S(f)G(f), \tag{1.18}$$

in which $X(f)$ is the spectrum of the output signal, and $G(f)$ is the spectrum of the system response. Now if we want to neutralize the input signal, then we have to divide each side by $S(f)$, or equivalently apply the inverse operator $F(f) = 1/S(f)$ to each side, obtaining:

$$\frac{X(f)}{S(f)} = G(f). \tag{1.19}$$

Of course, this states the problem too simple: the signal $x(t)$ always contains some noise. When the signal $x(t)$ is taken as the convolution above together with some noise term, i.e., $X(f) = S(f)G(f) + N(f)$ in which $N(f)$ denotes the noise term, then the deconvolution in the frequency domain becomes:

$$\frac{X(f)}{S(f)} = G(f) + \frac{N(f)}{S(f)}. \tag{1.20}$$

The next problem is that due to this division, the noise is blown up outside the bandwidth of signal $S(f)$, i.e., there where the amplitude of $S(f)$ is (very) small. This effect is shown in Figure (1.7).

There are two ways to tackle this problem. The first one is that we stabilize the division. This is done by not applying a filter $F(f) = 1/S(f)$ but first multiplying both the numerator and the denominator by the complex conjugate of the input-signal spectrum, $S^*(f)$, and since the denominator is now real we can add a small (real) constant ϵ to it. Thus instead of $1/S(f)$, we apply the filter:

$$F(f) = \frac{S^*(f)}{S(f)S^*(f) + \epsilon^2}. \tag{1.21}$$

Often we take ϵ as a fraction of the maximum value in $|S(f)|$, e.g. $\epsilon = \alpha MAX(|S(f)|)$ with α in the order of 0.01 - 0.1. In this way we have controlled the noise, but it can still be large outside the bandwidth of $S(f)$ (see Figure (1.7)). As an example, Figure (1.8) shows the result for deconvolution.

The other way of dealing with the blowing up of the noise is only doing the division in a certain bandwidth which is equivalent to shaping the input signal $s(t)$ into a shorter one, which we call $d(t)$. In this case we do not apply the filter $1/S(f)$ but instead we use $D(f)/S(f)$. Then the deconvolution amounts to:

$$\frac{X(f)D(f)}{S(f)} = G(f)D(f) + \frac{N(f)D(f)}{S(f)}, \tag{1.22}$$

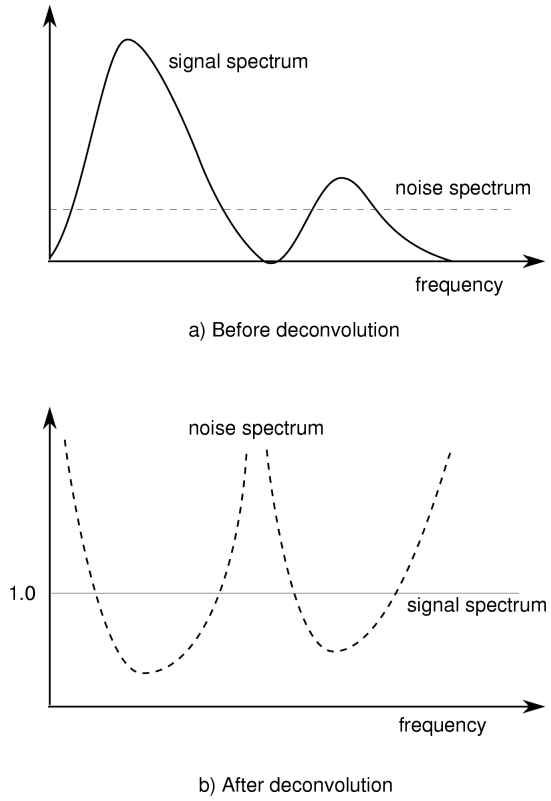

Figure 1.7: The effect of deconvolution in the frequency domain in the presence of noise.

where $|D(f)|$ is approximately equal to $|S(f)|$, i.e.:

$$a < \frac{|D(f)|}{|S(f)|} < b, \tag{1.23}$$

in which b/a is less than 10, say. Often in seismics, we would like to end up with a signal that is short in the time domain. This means that the spectrum of $D(f)$ must be smooth compared to the true input-signal spectrum $S(f)$. Note that a short signal in time corresponds with a smooth (i.e. oversampled) signal in frequency, as the major part of the time signal will be zero. Practically this means when we know the spectrum we can design some smooth envelope around the spectrum $S(f)$, or we can just pick a few significant points in the spectrum and let a smooth interpolator go through these picked points. An example of designing such a window is given in Figure (1.9).

As a last remark of deconvolution in the frequency domain it can be said that in practice both ways of control over the division by $S(f)$ are used. We then apply a filter :

$$F(f) = \frac{D(f)S^*(f)}{S(f)S^*(f) + \epsilon^2} \tag{1.24}$$

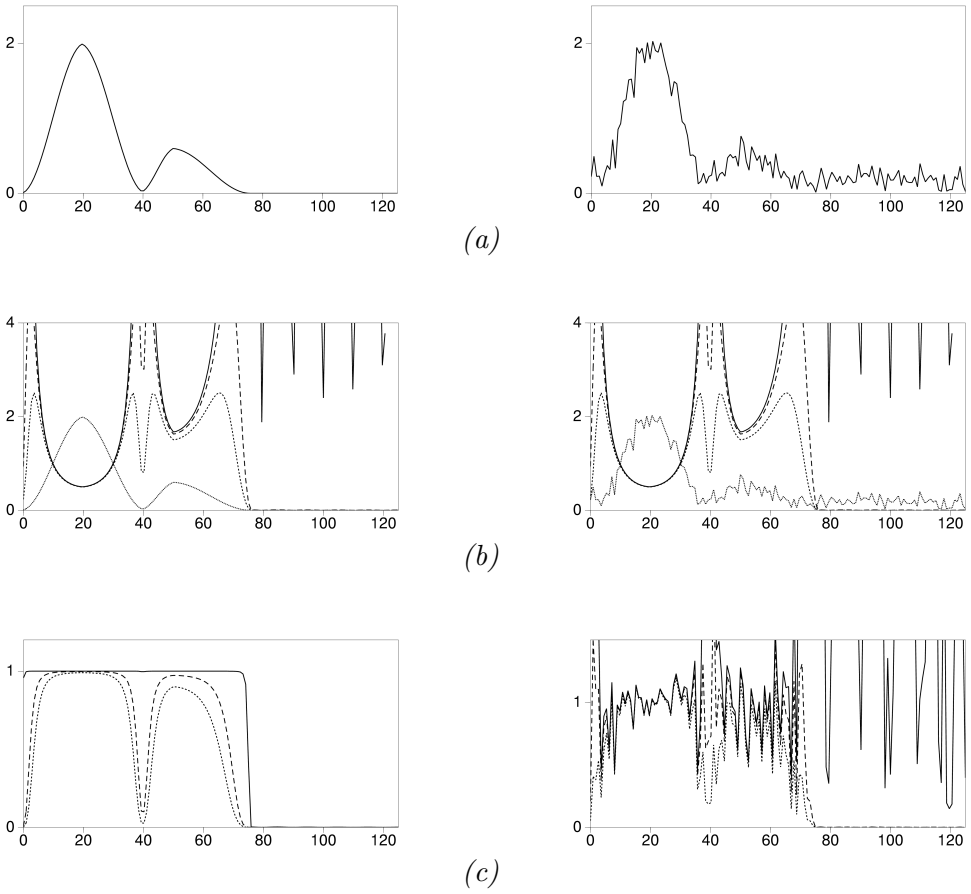

Figure 1.8: Applying stabilized inversion in the frequency domain, left for a noise free input signal, right for a noisy input signal. (a) Spectrum of signal to be inverted. (b) Spectra of inverse operators with 3 stabilization constants ($\epsilon = 0,\ 0.05,\ 0.1$). (c) Multiplication of inverse filters with original spectrum of (a), i.e. the deconvolution results.

to the output signal $x(t)$, resulting in:

$$\frac{X(f)D(f)S^*(f)}{S(f)S^*(f)+\epsilon^2} = \frac{G(f)D(f)S(f)S^*(f)}{S(f)S^*(f)+\epsilon^2} + \frac{N(f)D(f)S^*(f)}{S(f)S^*(f)+\epsilon^2}. \tag{1.25}$$

This is about the best we can do given the constraints of bandwidth and signal-to-noise ratio.

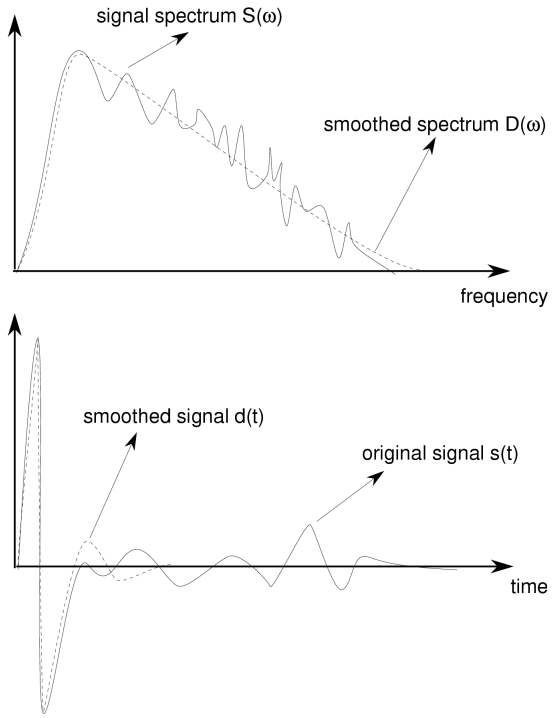

Figure 1.9: Designing a desired input signal via smoothing in the frequency domain.

1.8 Time- and frequency characteristics

In the table we below, we list the characteristics that we will use throughout these lecture notes. Some of them have been discussed in this chapter, others will be discussed in the coming chapters.

time domain	**frequency domain**
discretisation with Δt $a(t = k\Delta t)$	making periodic with $\frac{1}{\Delta t}$ $\sum_{m=-\infty}^{\infty} A_{\text{Continuous}}(f + \frac{m}{\Delta t})$
convolution of signals $\int_{\infty}^{+\infty} s(\tau)h(t-\tau)d\tau$	multiplication of spectra $S(f)H(f)$
correlation with $\int_{\infty}^{+\infty} a(\tau)b^*(\tau - t)d\tau$	multiplication by complex conjugate $A(f)B^*(f)$
purely symmetric $a(t) = a(-t)$	zero phase (imaginary part zero) $\lvert A(f)\rvert$
time shift $\delta(t - T)$	linear phase $\exp(-2\pi i f T)$
signal and inverse both causal	minimum phase
deconvolution $f(t) * s(t) = \delta(t)$	division $F(f) = \frac{1}{S(f)}$
differentiation in time d/dt or $\partial/\partial t$	multiplication with term: $2\pi i f$

Table 1.1: Some characteristics in time- and frequency domain.

Chapter 2

Basics of the seismic method: kinematics

In this chapter we introduce the basic notion of seismic waves from a kinematic point of view, which means that we do not concern ourselves with the causes of the motion. (These causes, the physics behind them, are treated in a later chapter (Chapter 4.) In the earth, seismic waves can propagate as longitudinal (P) or as shear (S) waves. The wave phenomena occurring at a boundary between two layers are discussed, such as Snell's Law, reflection and transmission. For seismic-exploration purposes, where measurements are taking place at the surface, the different arrivals of direct waves, reflected waves and refracted/head waves are discussed. Then, some typical records as obtained on land and at sea are interpreted, in terms of these arrivals. From these events velocities and estimates of depths can be obtained. And from those, a first model for the subsurface is estimated (where the model is here seen as the first interpretation of the data). Using the Fourier transformation, a filtering example is shown with the aim to separate different events in these raw records.

2.1 Introduction

The seismic method makes use of the properties of the velocity of sound. This velocity is different for different rocks and it is this difference which is exploited in the seismic method. When we create sound at or near the surface of the earth, some energy will be reflected back (bounced back). They can be characterized as echoes. From these echoes we can determine the velocities of the rocks, as well as the depths where the echoes came from. In this chapter we will discuss the basic principles behind the behaviour of sound in solid materials. When we use the seismic method, we usually discuss two types of seismic methods, depending on whether the distance from the sound source to the detector (the "ear") is large or small with respect to the depth of interest: the first is known as refraction seismics, the other as reflection seismics. Of course, there is some overlap between those

two types and that will be discussed in this chapter. When features really differ, then that will be discussed in next chapter for refraction and the chapters on reflection seismics. The overlap lies in the physics behind it, so we will deal with these in this chapter. In the following chapters will deal with instrumentation, field techniques, corrections (which are not necessary for refraction data) and interpretation.

2.2 Basic physical notions of waves

Everybody knows what waves are when we are talking about waves at sea. Sound in materials has the same kind of behaviour as these waves, only they travel much faster than the waves we see at sea. Waves can occur in several ways. We will discuss two of them, namely the longitudinal and the shear waves. Longitudinal waves behave like waves in a large spring. When we push from one side of a spring, we will observe a wave going through the spring which characterizes itself by a thickening of the wires running through the spring in time (see also figure (2.1)). A property of this type of wave is that the motion of a piece of the wire is in the same direction as the wave moves. These waves are also called Push-waves, abbreviated to P-waves, or compressional waves. Another type of wave is the shear wave. A shear wave can be compared with a chord. When we push a chord upward from one side, a wave will run along the chord to the other side. The movement of the chord itself is only up- and downward: characteristic of this wave is that a piece of the chord is moving perpendicular to the direction of that of the wave (see also figure (2.1)). These types of waves are referred to as S-waves, also called shear waves. Characteristic of this wave is that a piece of the chord is pulling its "neighbour" upward, and this can only occur when the material can support shear strain. In fluids, one can imagine that a "neighbour" cannot be pulled upward simply because it is a fluid. Therefore, in fluids only P-waves exist, while in a solid both P- and S-waves exist.

In the real world, we deal with three dimensions, so a wave will spread in three directions. In a homogeneous medium (so the properties of the material are everywhere constant and the same) the wave will spread out like a sphere. The outer shell of this sphere is called the wave front. Another way of describing this wave front is in terms of the normal to the wavefront: the ray. We are used to rays in optics and we can use the same notion in the seismic method. When we were explaining the behaviour of P- and S-waves, we are already using the term "neighbour". This was an important feature otherwise the wave would not move forward. A fundamental notion included in this, is Huygens' principle. When a wave front arrives at a certain point, that point will behave also as a source for the wave, and so will all its neighbours. The new wavefront is then the envelope of all the waves which were generated by these points. This is illustrated in figure (2.2). Again, the ray can then be defined as the normal to that envelope which is also given in the figure.

So far, we only discussed the way in which the wave moves forward, but there is also another property of the wave we haven't discussed yet, namely the amplitude : how does the amplitude behave as the wave moves forward? We have already mentioned spherical

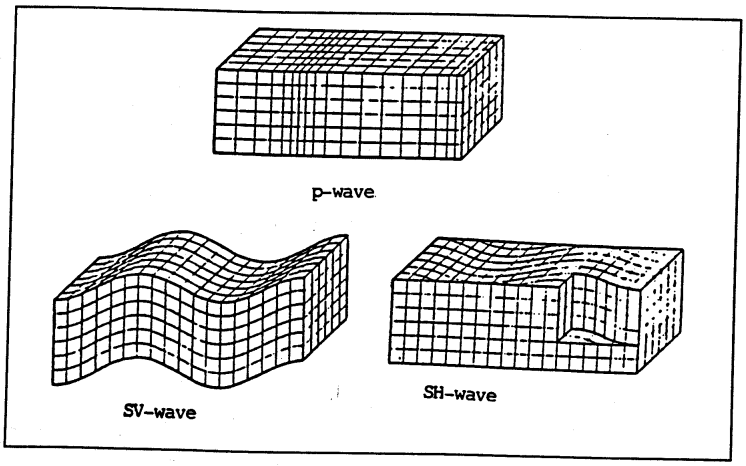

Figure 2.1: Particle motion of P and S waves

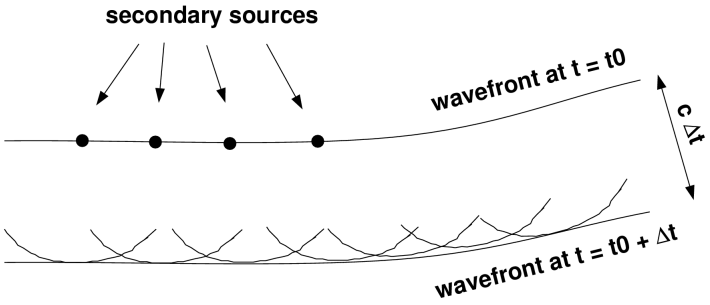

Figure 2.2: Using Huygens' principle to locate new wavefronts.

spreading when the material is everywhere the same. The total energy will be spreaded out over the area over the sphere. This type of energy loss is called spherical divergence. It simply means that if we put our "ear" at a larger distance, the sound will be less loud. There is also another type of energy loss, and that is due to losses within the material, which mainly consists of internal friction losses. This means that the amplitude of a wave will be extra damped because of this property. S-waves usually show higher friction losses than P-waves. Finally, we give a table of common rocks and their seismic wave velocities in table (2.1).

Material	velocity (m/s)	Material	velocity (m/s)
Air	330	Sandstone	2000-4500
Water	1500	Shales	3900-5500
Soil	20-300	Limestone	3400-7000
Sands	600-1850	Granite	4800-6000
Clays	1100-2500	Ultra-mafic rocks	7500-8500

Table 2.1: Seismic wave velocities for common materials and rocks.

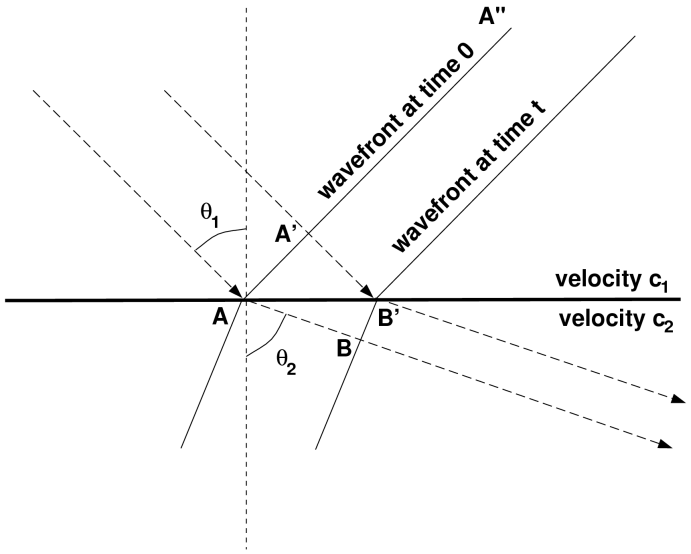

Figure 2.3: Snell's law

2.3 The interface : Snell's law, refraction and reflection

So far, we discussed waves in a material which had everywhere the same constant wave velocity. When we include a boundary between two different materials, some energy is bounced back, or reflected, and some energy is going through to the other medium. It is nice to perform Huygens' principle graphically on such a configuration to see how the wavefront moves forward (propagates), especially into the second medium. From this picture, we could also derive the ray concept. In this discussion, we will only consider the notion of rays. A basic notion in the ray concept, is Snell's law. Snell's law is a fundamental relation in the seismic method. It tells us the relation between angle of incidence of a wave and velocity in two adjacent layers (see Figure (2.3)).

$AA'A''$ is part of a plane wave incident at angle θ_1 to a plane interface between medium 1 of velocity c_1, and medium 2 of velocity c_2. The velocities c_1 and c_2 are constant. In a

time t the wave front moves to the position AB and are normals to the wave front. So the time t is given by

$$t = \frac{A'B'}{c_1} = \frac{AB}{c_2} \tag{2.1}$$

Considering the two triangles and this may be written as:

$$t = \frac{AB' \sin\theta_1}{c_1} = \frac{AB' \sin\theta_2}{c_2} \tag{2.2}$$

Hence,

$$\frac{\sin\theta_1}{c_1} = \frac{\sin\theta_2}{c_2} \tag{2.3}$$

which is Snell's law for transmission. So far, we have taken general velocities c_1 and c_2. However, in a solid, two velocities exist, namely P- and S-wave velocities. Generally, when a P-wave is incident on a boundary, it can transmit as a P-wave into the second medium, but also as a S-wave. So in the case of the latter, Snell's law reads:

$$\frac{\sin\theta_P}{c_P} = \frac{\sin\theta_S}{c_S} \tag{2.4}$$

where c_P is the P-wave velocity, and c_S the S-wave velocity. The same holds for reflection: a P-wave incident on the boundary generates a reflected P-wave and a reflected S-wave. Finally, the same holds for an incident S-wave: it generates a reflected P-wave, a reflected S-wave, a transmitted P-wave and a transmitted S-wave.

A special case of Snell's law is of interest in refraction prospecting. If the ray is refracted along the interface (that is, if $\theta_2 = 90\,\mathrm{deg}$), we have

$$\frac{\sin\theta_c}{c_1} = \frac{1}{c_2} \tag{2.5}$$

where θ_c is known as the critical angle.

So far, we have looked at basic notions of refraction and reflection at an interface. When we measure in the field, and there would be one boundary below it, we could observe several arrivals: a direct ray, a reflected ray and a refracted ray. We will derive the arrival time of each ray as depicted in figure 2.4.

The direct ray is very simple: it is the horizontal distance divided by the velocity of the wave, i.e.,:

$$t = \frac{x}{c_1}, \tag{2.6}$$

so in a time-distance graph this is a linear event.

When we look at the reflected ray, we have that the angle of incidence is the same as the angle of reflection. This also follows from Snell's law: when the velocities are the same, the angles must also be the same. When we use Pythagoras' theorem, we obtain for the traveltime:

$$t = \frac{\left(4z^2 + x^2\right)^{1/2}}{c_1} \tag{2.7}$$

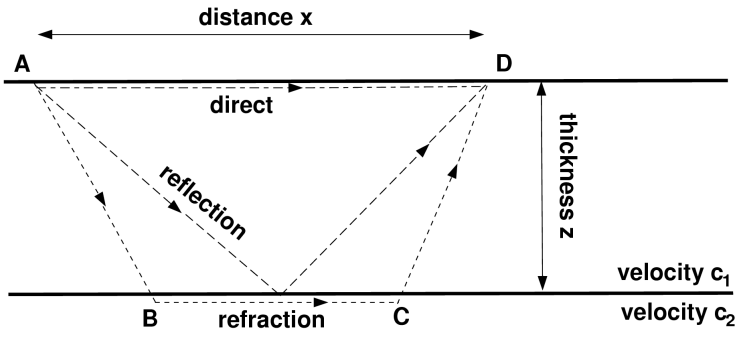

Figure 2.4: The direct, reflected and refracted ray.

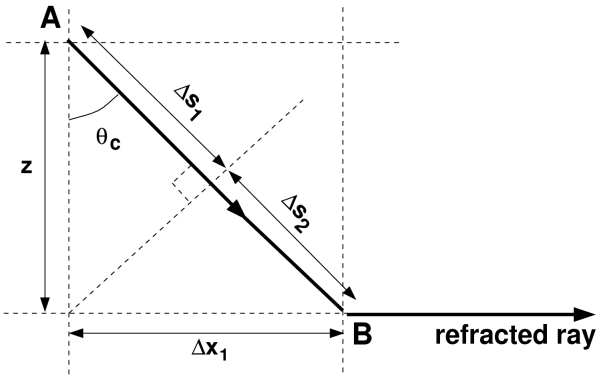

Figure 2.5: An element of the ray with critical incidence

Squaring this equation:

$$t^2 = \left(\frac{2z}{c_1}\right)^2 + \left(\frac{x}{c_1}\right)^2, \tag{2.8}$$

we see that for a time-distance graph this is the equation of a hyperbola (; notice that in a $(x, 2z)$ graph it would be a circle).

When we look at the refracted ray, the derivation is a bit more complicated. Take each ray element, so take the paths AB, BC and CD separately. Then, for the first element, as shown in figure (2.5), we obtain the traveltime:

$$\Delta t_1 = \frac{\Delta s_1 + \Delta s_2}{c_1} = \frac{\Delta x_1 \sin\theta_c}{c_1} + \frac{z\cos\theta_c}{c_1} \tag{2.9}$$

where θ_c is the critical angle.

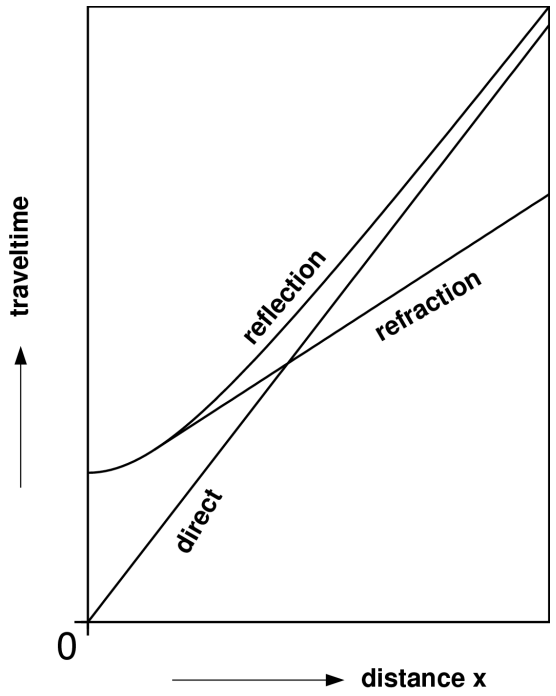

Figure 2.6: Time-distance (t, x) curve for direct, reflected and refracted ray.

We can do this also for the paths BC and CD, and we obtain the total time as:

$$t = \Delta t_1 + \Delta t_2 + \Delta t_3 \tag{2.10}$$

$$= \frac{\Delta x_1 \sin\theta_c}{c_1} + \frac{z\cos\theta_c}{c_1} + \frac{\Delta x_2}{c_2} + \frac{\Delta x_3 \sin\theta_c}{c_1} + \frac{z\cos\theta_c}{c_1} \tag{2.11}$$

where $\Delta x_2 = BC$ and Δx_3 is the horizontal distance between C and D. When we use now Snell's law, i.e., $\sin\theta_c/c_1 = 1/c_2$, in the terms with Δx_1 and Δx_3, then we can add all the terms with $1/c_2$, using $x = \Delta x_1 + \Delta x_2 + \Delta x_3$ to obtain:

$$t = \frac{x}{c_2} + \frac{2z\cos\theta_c}{c_1} \tag{2.12}$$

We recognize this equation as the equation of a straight line when t is considered as a function of distance x, the line along which we do our measurements. We will use this equation later in the next chapter. We have now derived the equations for the three rays, and we can plot the times as a function of distance x. This is done in figure (2.6).

This picture is an important one. When we measure data in the field the characteristics in this plot can most of the time be observed.

Now we have generated this figure, we can specify better when we are performing a reflection survey, or a refraction survey. In refraction seismics we are interested in

the refractions and only in the travel times. This means that we can only observe the traveltimes well if it is not masked by the reflections or the direct ray, which means that we must measure at a relatively large distance with respect to the depth of interest. This is different with reflection seismics. There, the reflections will always be masked by refractions or the direct ray, but there are ways to enhance the reflections. What we are interested in, is the arrival at relatively small offsets, thus distances of the sound source to the detector which are small with respect to the depth we are interested in.

Before discussing any more differences between the refraction method and the reflection method, we would like to discuss amplitude effects at the boundary. Let us first introduce the acoustic impedance, which is the product of the density ρ with the wave velocity c, i.e., ρc. When a ray encounters a boundary, some energy will be reflected back, and some will be transmitted to the next layer. The amount of energy reflected back is characterized by the reflection coefficient R:

$$R = \frac{\rho_2 c_2 - \rho_1 c_1}{\rho_2 c_2 + \rho_1 c_1} \tag{2.13}$$

That this is the case, will be derived from basic physical principles in a later chapter on wave theory (Chapter 4). Obviously, the larger the impedance contrast between two layers, the higher the amplitude of the reflected wave will be. Notice that it is the impedance contrast which determines whether energy is reflected back or not; it may happen that the velocities and densities are different between two layers, but that the impedance is (nearly) the same. In that case we will see no reflection. We can now state another difference between refraction and reflection seismics. With refraction seismics we are only interested in traveltimes of the waves, so this means that we are interested in contrasts in velocities. This is different in reflection seismics. Then we are interested in the amplitude of the waves, and we will only measure an amplitude if there is a contrast in acoustic impedance in the subsurface.

Generally speaking the field equipment for refraction and reflection surveys have the same functionality: we need a source, detectors and recording equipment. Since reflection seismics gives us a picture of the subsurface, it is much used by the oil industry and therefore, they put high demands on the quality of the equipment. As said before, a difference between the two methods is that in reflection seismics we are interested in amplitudes as well, so this means that high-precision instruments are necessary to pick those up accurately. Source, detectors and recording equipment will be discussed in the chapter on seismic instrumentation (chapter 3).

Finally, we tabulate the most important differences between reflection and refraction seismic in table 2.2.

REFRACTION SEISMICS	REFLECTION SEISMICS
Based on contrasts in : seismic wave speed (c)	Based on contrasts in : seismic wave impedances (ρc)
Material property determined : wave speed only	Material properties determined: wave speed and wave impedance
Only traveltimes used	Traveltimes and amplitudes used
Source-receiver distances large compared to investigation depth	Source-receiver distances small compared to investigation depth

Table 2.2: Important differences between refraction and reflection seismics.

2.4 Application of basic concepts: Interpretation of some raw field seismic records.

In this section, we will look at the interpretation of raw seismic data as recorded in the field.

Land record

Let us consider first a record that has been recorded on land. In Figure 2.7 such a field record is shown. The first event we are considering, is the "first arrival". It shows itself by giving a pulse after a quiet period. This arrival can be a *direct* arrival or a *refraction*, both of which we discussed earlier. When looking closely at the record, it can be seen that there a slight change of dip, occurring at around an offset of 800 m. Therefore, the arrival until this distance is a direct arrival, while beyond that distance, it is the refraction. By drawing a straight line through the direct arrival, the velocity with which it propagates along the surface is: 2400 meters in 670 ms is approximately 3600 m/s. This is a relatively high velocity so there is probably some very hard rock at the surface. The velocity of the refracted arrival can also be determined by a straight line through that arrival; it amounts to 2400 meters in around 500 ms (note that the arrival does not go through the origin so it is the difference between the time at x=0 m and at x=2400 m), so a velocity of 4800 m/s. Below the record in figure 2.7, a simple model is shown that explains this first arrival; the synthetic record belonging to this model, is given on the top right of the figure.

The next events we consider are the strong events which crosses 2400 meter at some 1.3 seconds. This event is interpreted as ground-roll or surface waves (they propagate along the surface). Calculating the velocity, we come to 1850 m/s. Again, the simple model below the record explains this ground roll; the synthetic record on the top right of the figure also shows this arrival.

Also in this field record, a "high-frequency" event can be observed which goes through the 4-seconds mark at about 1300 meters distance. Calculating the velocity from this, we come to some 325 m/s. It may be clear that this is a wave that goes through the air. This event is also synthesized in the top right figure, using the model as given below it.

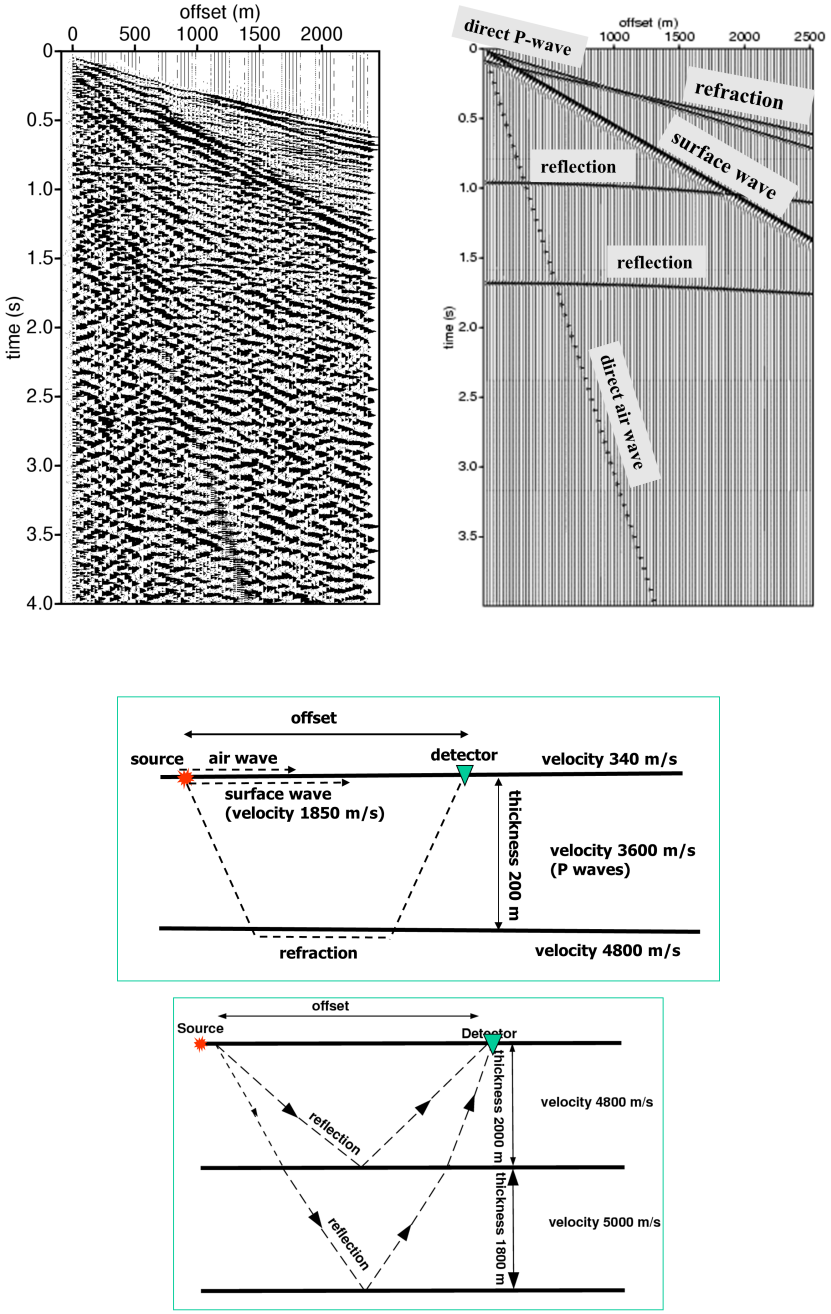

Figure 2.7: Field seismic shot record from land survey (top left), its synthetic seismogram (top right) using model of near surface (middle) and model at larger depths (bottom).

Last, but not least, are "high-frequency" events which are slightly curved, e.g. the ones at 0.9 and 1.6 seconds. These events are interpreted as reflections from layer boundaries in the deep subsurface. Those are usually the events we are interested in, when we want to obtain an image of the subsurface. Using a simple model as given at the bottom of the figure (which explains the deeper part of the earth), the synthetic record for these events is also shown in the top right of the figure.

In the above, we have interpreted five types of events, which can be captured in one combined model and are shown in one combined synthetic seismogram. These synthetics explain the most important events in the raw seismic record. Still, when looking at the resulting synthetic seismogram, we see that we are very over-simplifying the situation since the synthetic and field record are only resembling in the arrival times of the most important events. When looking at the general characteristics, they are very different indeed.

The field record we discussed so far, was recorded on some hard rocks where the velocities are relatively high. However, when shooting data on land with some loose top soil, the characteristics are much different. In Figure 2.8, a field record of such a situation is given. Again, we can determine the main events in this record. Let us first consider the "first arrival", i.e. the arrival that is coming in first after a quiet period. As usual, this is interpreted as a refraction as shown in the figure below the record. The velocity can be determined: we come to some 1600 m/s. This velocity is very near the velocity of water, so this refraction may be due to the water table. In the right figure, the synthetic shows this arrival.

The next event is the most prominent one, namely the event which goes through the 1-second mark at some 180m, so its velocity is around 180 m/s. This arrival is interpreted as "ground-roll"/surface waves, which travel along the surface. The model which explains this arrival, is given again below the record, and its synthetic shown on the top right.

The most important events for this record, are the "high-frequency" events which are the sightly curved arrivals, which can all be interpreted as reflections from deep layers. The number of reflections are too many; only a few are synthesized in the record on the top right, using the model as given at the bottom of the figure.

Again, when comparing the synthetic to the field seismogram, it is obvious that we have very over-simplified the earth; the positive side is that we have probably been able to understand most of the events in the field record.

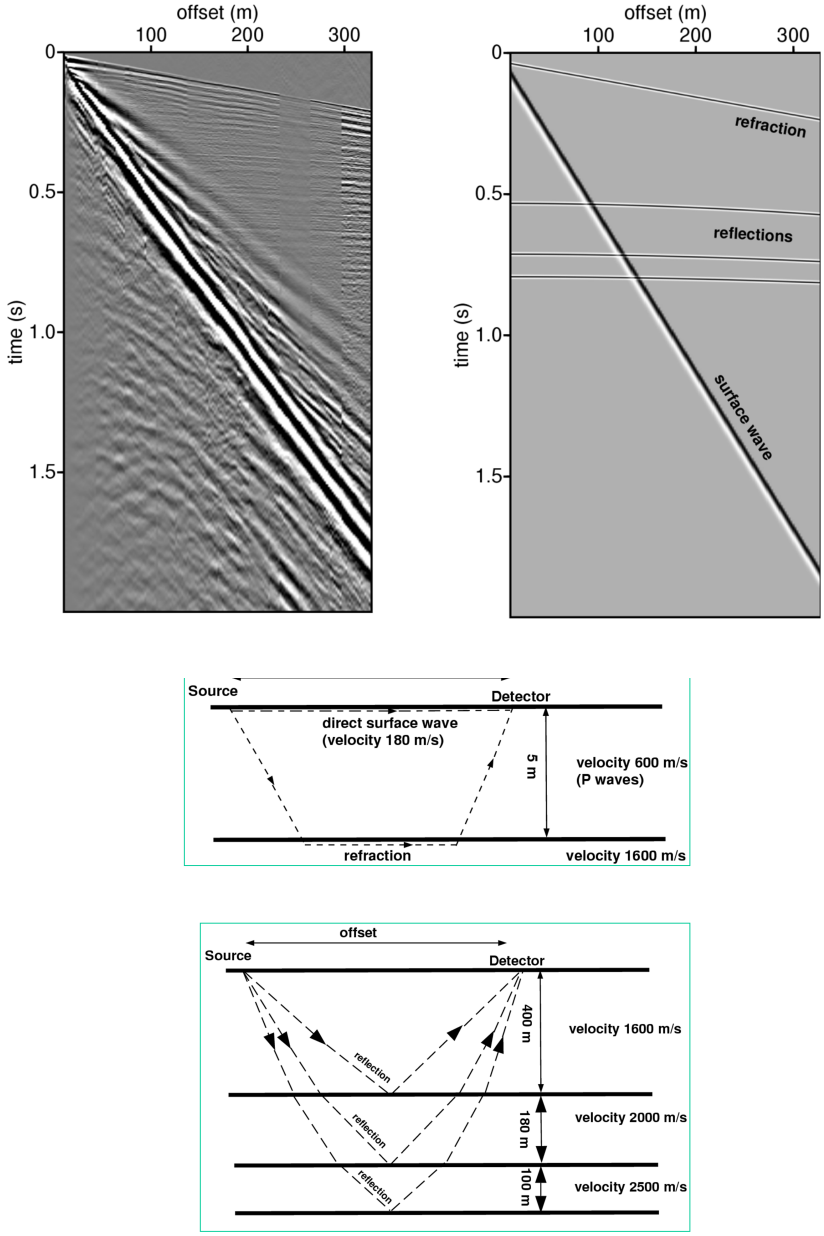

Figure 2.8: Field seismic shot record from land survey with loose top soil (top left), its synthetic seismogram (top right) using model of near surface (middle) and model at larger depths (bottom).

Marine record

Figure 2.9 shows a raw seismic recordings, made at sea. This record is much "cleaner" than the land record, as we measure in a water layer, which is a very homogeneous layer.

Let us analyze some separate events again. The first event in the marine record is the faint one, going nearly through the origin. It crosses the 500 meter at some 340 ms; this means a velocity of some 1470 m/s. It may be clear that this is the direct arrival from the source to the receivers through the water, as explained in the model below the record. This direct arrival is thus a body wave, since it travels with the velocity of water.

The next event is the first arrival at farther offsets; this arrival is interpreted as a refractive event. When analyzing the distance travelled over time, i.e. the apparent velocity, a velocity of roughly 2000 m/s is obtained. Using the results for a refraction in the first chapter, a depth of 300 meter is obtained. This is quantified in the model below the figure, and its associated synthetic seismogram in the figure on the top right.

The third event we analyze is the first strong event that looks hyperbolic: starting at some 0.4 seconds and bending down to some 2.2 seconds at 3200 m offset. Clearly, because of its hyperbolic behaviour, it is interpreted as a reflection. When looking at later times, we some more strong hyperbolic events, such as at 0.8 seconds (bending downward toward some 2.3 seconds), and at 1.2 seconds (bending downwards toward 2.4 seconds), and even more. These events are interpreted as so-called multiply reflected waves, i.e., waves that bounce up and down in the water layer. In fact almost all events we see below 0.8 seconds are due to multiply reflected waves, or short-hand: multiples. The times at which the multiply reflected waves arrive, seem to be periodic; this is indeed the case.

Combining the interpretation of the refraction and the reflaction, it must be noted that the refracted arrival does not converge to the first reflection but to a later reflection. This means that the refraction occurs at a deeper layer; the shallower layers are probably loosely consolidated so that the velocity of sound has not changed much compared to the one from water.

A simple model explaining all these events, is shown in the figure below the record, with a water layer of 300 meter. The refracted layer is estimated at a depth of 550 meter, where we assumed that the velocity was a constant of 1500 m/s above. The resulting synthetic seismogram is shown on the top right of the figure. It may be clear that the multiply reflected waves come from the same reflective boundary in the subsurface, namely the sea bottom (and the sea surface, of course), and are therefore superfluous. They are considered as noise, the only one being "signal" is the one at around 0.4 seconds.

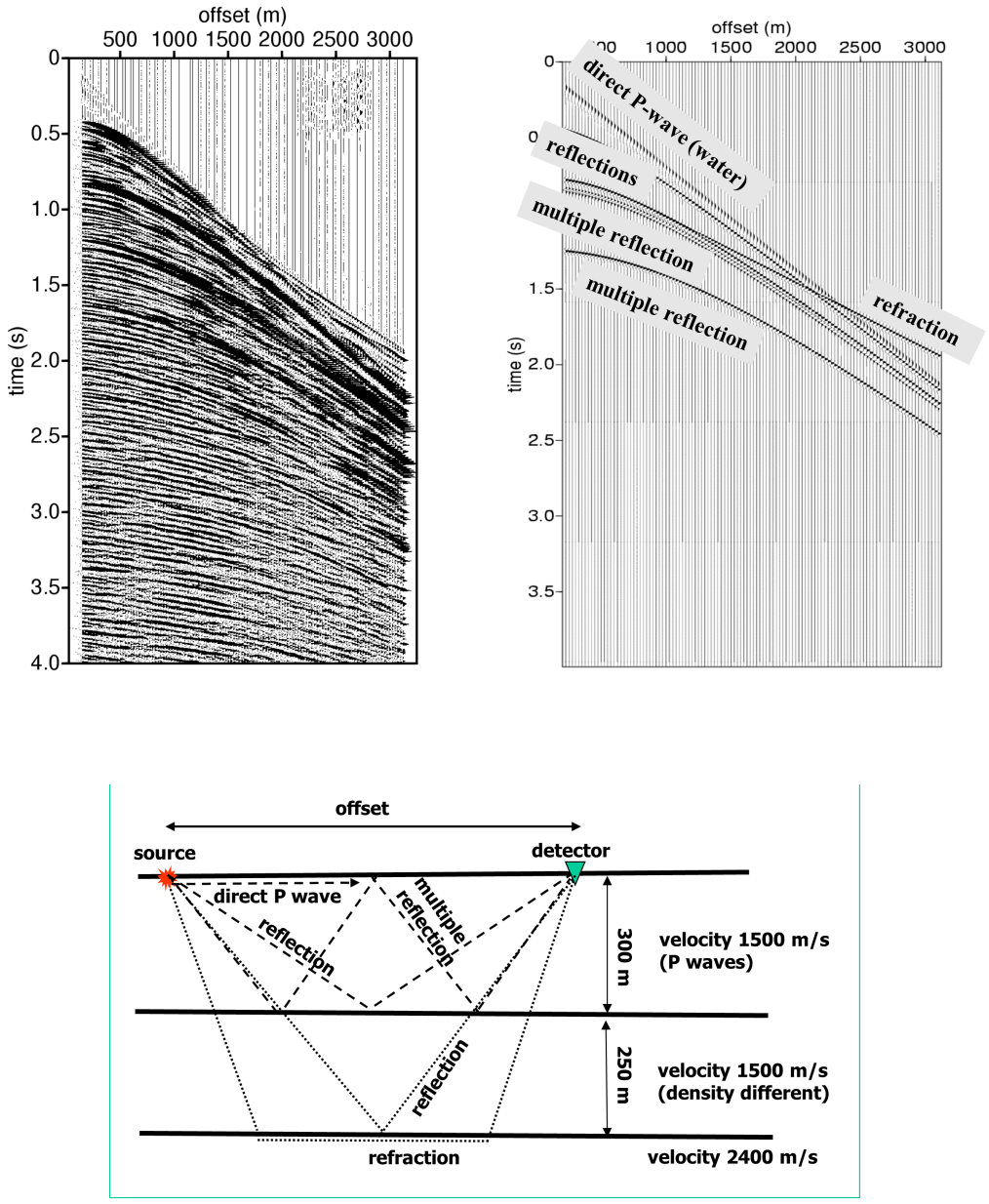

Figure 2.9: Seismic shot record from marine survey (top left), its synthetic seismogram (top right) using model of water layer and sea-water bottom, where only the path of one multiple reflection is drawn (bottom).

2.5 Application of Fourier analysis: Spectral analysis and filtering of field seismic records

In the previous section, we analyzed the data as they are recorded in the field. However, we only looked at the data as a function of *time*, not of frequency. When we look at the data of the previous section in more detail, we see that the events have a wavelength which differs for the type of event. In particular, let us consider the data from figure 2.8. The surface wave has a longer waveshape (lower-frequency) than the reflections and refractions; in the modelling we already took account of this, as can be seen in the synthetic seismogram on the top right of the figure. Also in the other land record, figure 2.7, a difference in length of waveshape can be observed. The surface wave has also here a longer waveshape than the reflections. The event with even another length of waveshape is the air wave. It has a very "high-frequency" shape.

It may now be clear that when we make *spectra* of these data, i.e., transform the time-axis to a frequency axis using the Fourier transformation, that different arrivals will give different peaks in the Fourier spectra. What we achieve is that we can analyze and interpret different frequencies in terms of different events. Moreover, we can start thinking about using the Fourier-transformed data for filtering purposes, i.e., removing certain frequency bands with the aim to remove undesired signal, like, e.g. the surface wave. Let us look at some spectra.

In figure 2.10, we have selected only 3 traces to illustrate our points. On the left of the figure, we plotted the 3 traces as a function of time; we can still observe the first arrival and the surface wave, which is characterized by its long waveshape. In the plot next to it, we have plotted the amplitude spectra of these 3 traces. First of all, notice that we obtain frequencies up to 500 Hz, which is the Nyquist frequency $f_N = 1/(2\Delta t)$, associated with the sampling interval: $\Delta t = 1$ ms. Next, it is evident that the largest amplitudes occur at the low frequencies, i.e., around 10 to 15 Hz. It may be clear that these frequencies are associated with the surface wave. Finally, it is not clear from the amplitude spectra where the reflection information is; when we look at the whole record we would expect it to be at higher frequencies.

Let us now *filter* the data, i.e., make the amplitudes zero at certain frequencies. Since we are *not* interested in the surface waves, we can make the amplitudes zero at the low frequencies. This is done in the next plot; notice that the plot is scaled to the maximum of the spectrum, so now other amplitudes become visible. When we transform this data back to the time domain, we obtain the rightmost plot. We see that we have effectively removed the surface wave.

From this plot, we cannot see whether we have changed the character of the whole record. To that end, all the traces of the original field record have been filtered with the same filter as we did for the 3 traces, and the result before and after filtering is shown in figure 2.11. What we can now see is that the surface wave is indeed pretty well removed, although not completely, and that the reflection are hardly affected. We can now even see

the reflections that were masked by the surface wave before we did any filtering.

It may now be clear that we have removed the most important "noise" in the field record. Before we did the filtering, we had a signal-to-noise ratio which was well below 1; after filtering the signal-to-noise ratio is larger than 1 since the highest amplitudes now seem to be the reflections themselves. What is important to realize is that, using the Fourier transformation, we have obtained a method to *separate* the surface waves from the reflections. In the time-domain, the surface waves crossed the reflections and therefore we could not make the "time"-amplitudes of the surface wave zero: we would then also have removed part of the reflections.

In this example, we have shown the power of filtering via analysis of Fourier-transformed data. This has solved one problem, namely the one of surface waves. However, many cases exist where such a filtering is partly successfull, and other types of filters are necessary. In the case of multiple reflections, as seen in the marine record (figure 2.9), transforming the time axis to a frequency axis does not solve anything since the multiple reflections have the same frequency contents as the primary reflections: we cannot achieve a separation between "signal" (primaries) and "noise" (multiples), so filtering as discussed above cannot help us here.

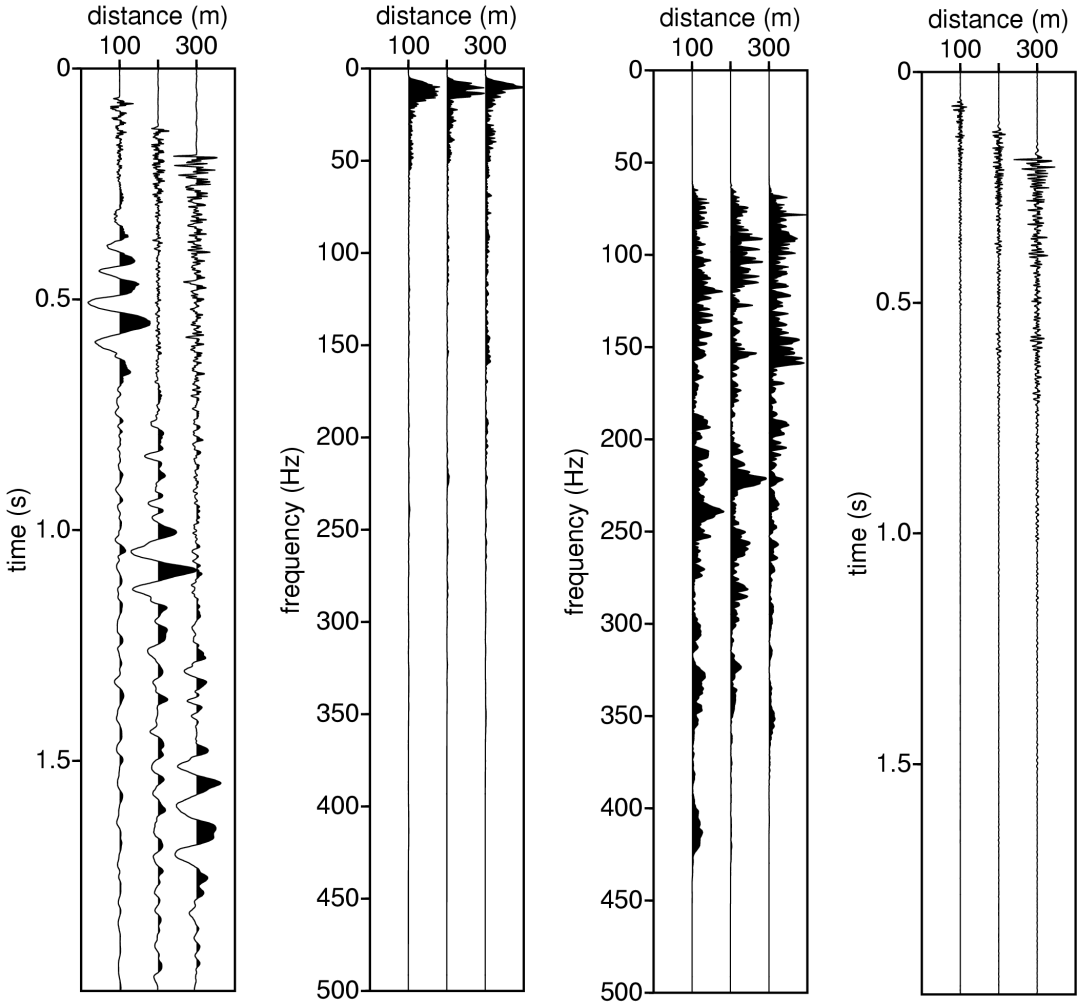

Figure 2.10: 3 seismic traces from raw seismic field record for analysis. From left to right: 3 original traces; amplitude spectra from Fourier-transformed traces; amplitude spectra from Fourier-transformed filtered traces; filtered traces.

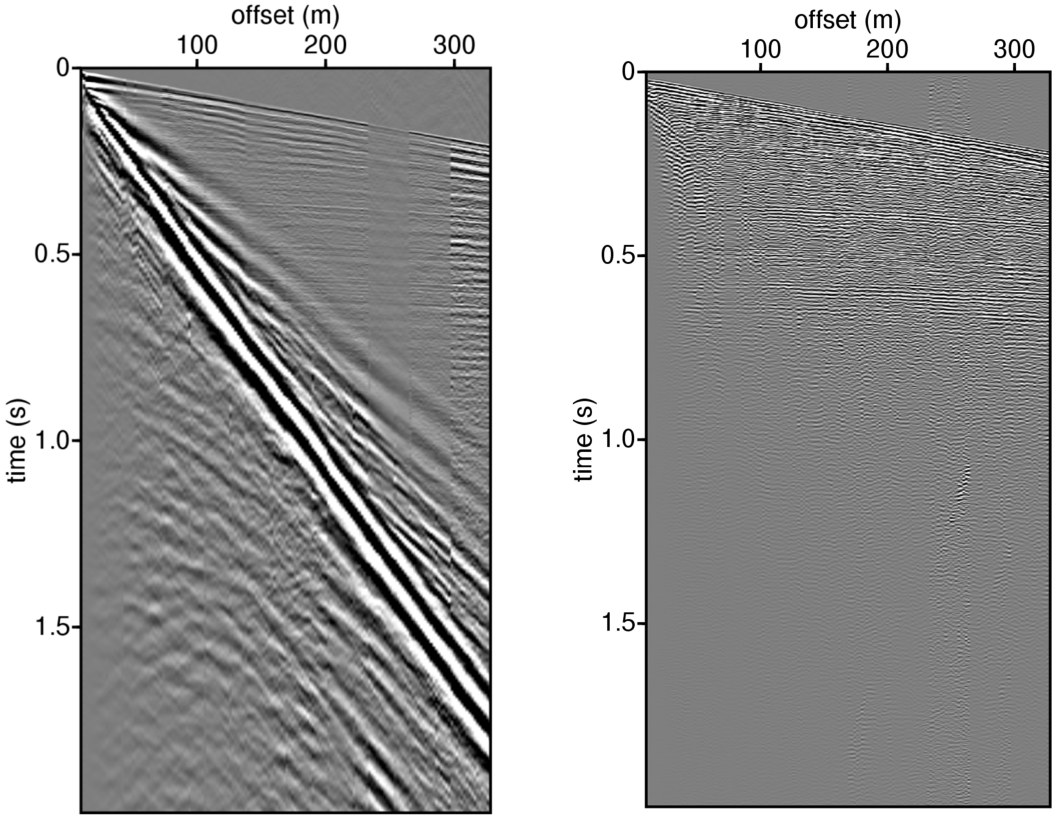

Figure 2.11: Seismic shot record from land survey with loose top soil. Original record (left) and record after removing low frequencies (right).

2.6 *EXERCISES*

1. In the figure (2.12) below, a ray is reflected multiple times (twice) between the top and bottom boundary. A source is located at the origin $(0, 0)$ and a receiver at position $(x, 0)$. For this ray, derive the traveltime as a function of horizontal distance.

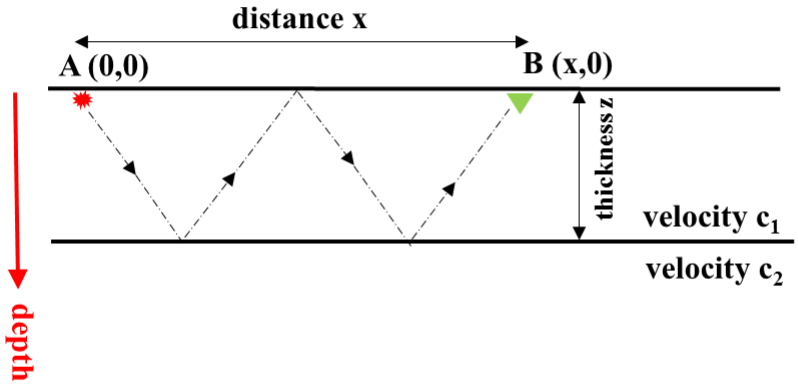

Figure 2.12: Ray path for a multiply reflected wave.

2. The earth is 3-D and common recordings are done over an area, retrieving 3-D information from the subsurface, the recording time being the third dimension. A typical situation is sketched in the figure (2.13) below where a source is away from a receiver line. For a direct wave from the source to receiver: derive the travel time as a function of the horizontal distances x and y.

3. In the figure (2.14) below, a ray is reflected against a diffractor, located at position (x_D, z_D). A source is located at the origin $(0, 0)$ and a receiver at position $(x, 0)$. For this ray, derive the traveltime as a function of horizontal distance.

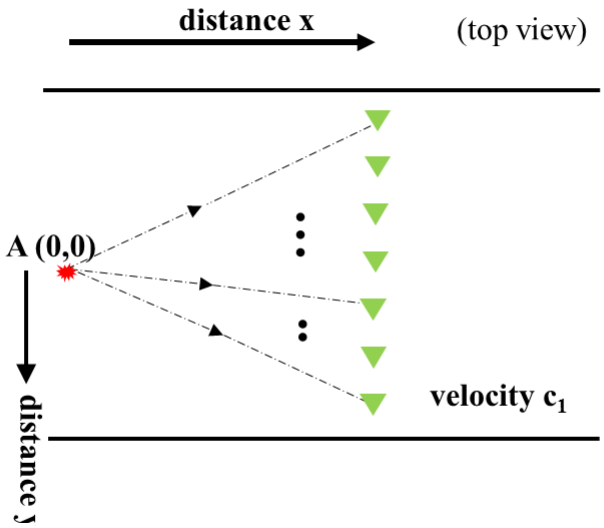

Figure 2.13: Ray paths of direct waves for 3D recordings; top view.

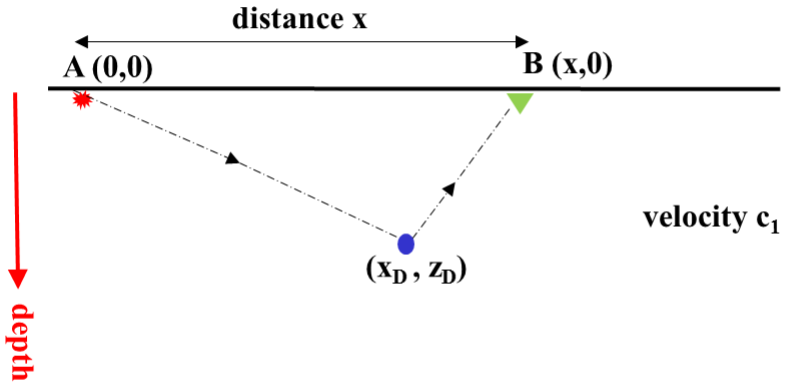

Figure 2.14: Ray path for a wave bouncing back from a diffractor.

4. In figure (2.15) a seismic land record from a 3D survey is given. These data have been sensed with receivers with a distance of 2 meter from each other.

   - On this record, indicate which event(s) can be interpreted as:
     - Direct/refracted P-wave
     - (Direct) surface waves
     - P-wave reflections
   - Determine the velocity of:
     - Direct/refracted P-wave
     - (Direct) surface waves

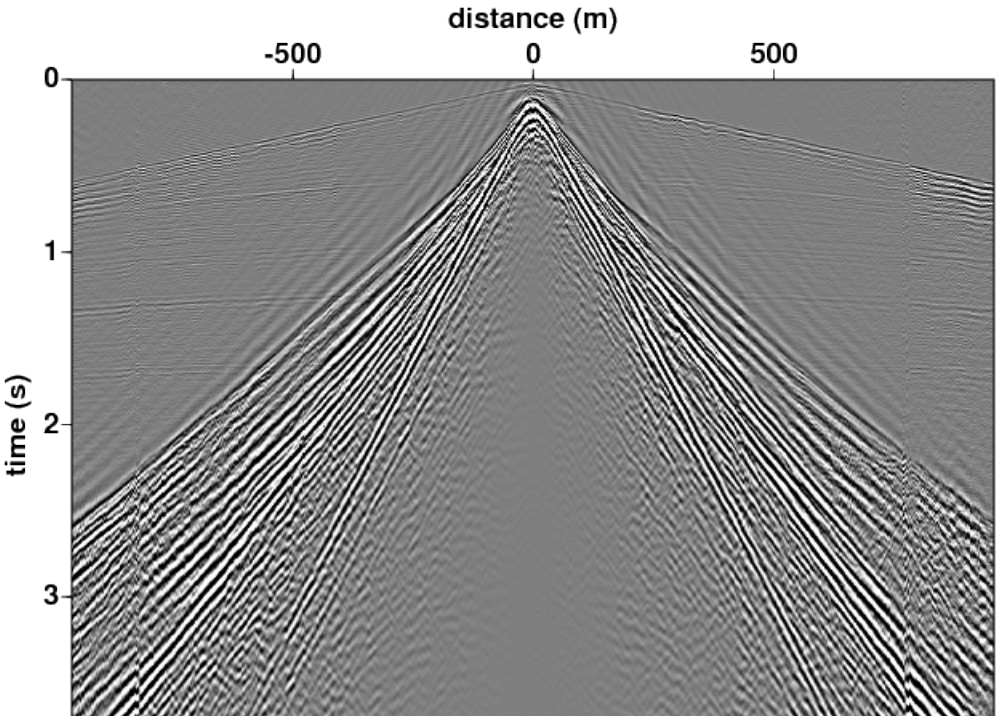

Figure 2.15: Shot record obtained from the North-East polder in the Netherlands. Spacing between receivers is 2 m.

5. In figure (2.16) a seismic marine record is given. These data have been sensed with receivers where the first one was 114 meters away from the source (= offset).
   - On this record, indicate which event(s) can be interpreted as:
     - Refracted P-wave
     - P-wave reflection from the sea bottom
     - Deeper P-wave reflections than the one from the sea bottom
   - Determine the velocity of:
     - Sea water from the reflection of the sea bottom
     - Refracted P-wave

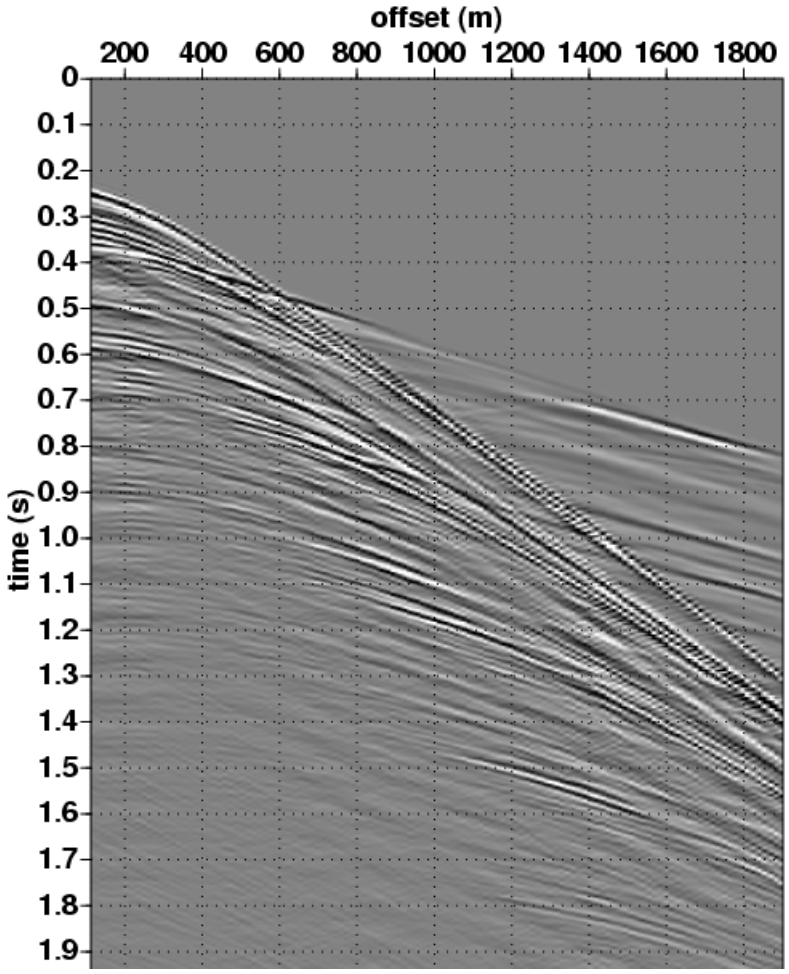

Figure 2.16: Shot record obtained at sea where the first receiver was 114 m away from the source. Offset is distance between the source and receiver.

Chapter 3

Seismic instrumentation

In this chapter we discuss the different instrumentation components as used for gathering seismic data. It discusses briefly these components as typically used in seismic exploration: the seismic sources (airgun at sea and dynamite and the so-called vibroseis source on land), the seismic sensors (hydrophones at sea and geophones on land) and the seismic acquisition system. The effects of these components can usually be directly observed in the seismic records, and the aim of this chapter is that the reader should become aware of the contribution of these components. (For the readers with a background in signal analysis, the effects are quantified in terms of signals and Fourier spectra.)

3.1 Seismic data acquisition

The object of exploration seismics is obtaining structural subsurface information from seismic data, i.e., data obtained by recording elastic wave motion of the ground. The main reason for doing this is the exploration for oil or gas fields (hydro-carbonates). In exploration seismics this wave motion is excitated by an active source, the seismic source, e.g. for land seismics (onshore) dynamite. From the source elastic energy is radiated into the earth, and the earth reacts to this signal. The energy that is returned to the earth's surface, is then studied in order to infer the structure of the subsurface. Conventionally, three stages are discerned in obtaining the information of the subsurface, namely data *acquisition*, *processing* and *interpretation*.

In *seismic data acquisition*, we concern ourselves only with the data gathering in the field, and making sure the data is of sufficient quality. In seismic acquisition, an elastic wavefield is emitted by a seismic source at a certain location at the surface. The reflected wavefield is measured by receivers that are located along lines (2D seismics) or on a grid (3D seismics). After each such a *shot record* experiment, the source is moved to another location and the measurement is repeated. Figure 3.1 gives an illustration of seismic acquisition in a land (onshore) survey. At sea (in a marine or offshore survey) the source and receivers are towed behind a vessel. In order to gather the data, many choices have

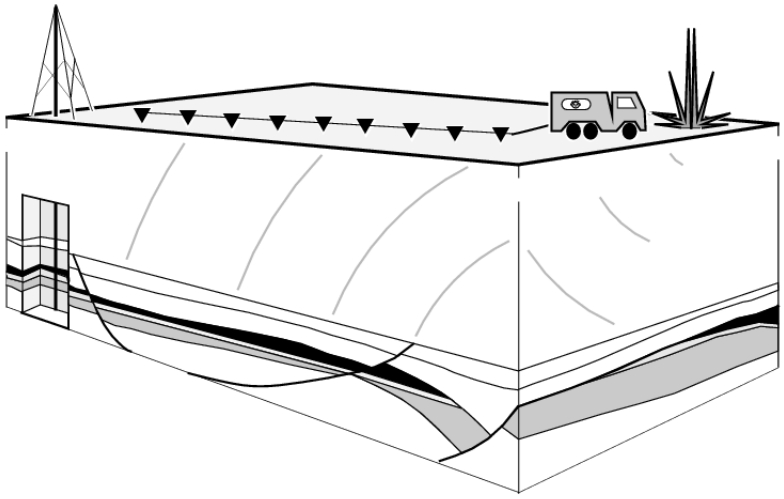

Figure 3.1: Seismic acquisition on land using a dynamite source and a cable of geophones.

to be made which are related to the physics of the problem, the local situation and, of course, to economical considerations. For instance, a choice must made about the seismic source being used: on land, one usually has the choice between dynamite and vibroseis; at sea, air guns are deployed. Also on the sensor side, choices have to be made, mainly with respect to their frequency characteristics. With respect to the recording equipment, one usually does not have a choice for each survey but one must be able to exploit its capabilities as much as possible.

Various supporting field activities are required for good seismic data acquisition. For example, seismic exploration for oil and gas is a complex interaction of activities requiring good management. Important aspects are:

- General administration/exploration concession and permit work ("land and legal"); topographic surveying and mapping, which is quite different for land- or marine work.
- More specific seismic aspects: placing and checking the seismic source, which on land is either an explosive (for example dynamite) or Vibroseis and at sea mostly an array of airguns; positioning and checking the detectors, geophones on land, hydrophones at sea; operating the seismic recording system.

The organisation of a seismic land crew, often faced with difficult logistics, terrain- and access road conditions is quite different from that of marine seismic crew on board of an exploration vessel, where a compact streamlined combination of seismic and topo operations is concentrated on the decks of one boat; different circumstances require different strategies and different technological solutions.

This chapter deals with seismic instrumentation, i.e., all the necessary hardware to make seismic measurements in the field.

First of all, we have to generate sound waves, with sufficient power and adequate frequency content in order to cause detectable reflections. This will be discussed in the section on sources. Then, when the waves have travelled through the subsurface, we want to detect the sound, and convert the motion to an electrical signal. This will be discussed in section on geophones and hydrophones. Then, the electrical signal is transported via cables to the recording instrument where it will be converted such that it can be stored, usually on tape, and can be read again at a later time. This is necessary when we want to process the data to obtain a seismic image of the subsurface. Recording systems are discussed in the section of recording systems.

The general model which is assumed behind the whole seismic system, is that all the components are linear time-invariant (LTI) systems. This means that the digital output we obtain after a seismic experiment in the field is a convolution of the different components, i.e.,:

$$x(t) = s(t) * g(t) * r(t) * a(t) \tag{3.1}$$

in which

$x(t)$ = the seismogram (digitally) on tape or disk

$s(t)$ = the source pulse or signature

$g(t)$ = the impulse response (or Green's function) of the earth

$r(t)$ = the receiver impulse response

$a(t)$ = the seismograph impulse response (mostly A/D conversion)

As may be obvious, in each of the following sections, we will discuss each of these impulse responses, apart that from the earth, since that is the function we would like to know at the end. That will be part of the chapter on processing.

3.2 Seismic sources

This section deals with the seismic source. The source generates the (dynamical) mechanical disturbance that cause a seismic wave motion with a characteristic signal shape ("signature") to travel through the subsurface from source to receivers. The seismic source has a dominant influence on the signal response resulting from the total acquisition system, i.e. the response due to source, receiver(s) and seismic recording system. In this chapter the seismic sources as routinely used by the oil industry in the exploration for oil and gas will be treated: airguns as used in marine operations, Vibroseis and dynamite as used for seismic operations on land. For each type of source the most important aspects of the mechanical principles of operation will be treated and then the characteristic seismic signal produced by the source (the source's "signature").

3.2.1 Airguns

Many oil and gasfields are found in water-covered areas, such as the Gulf of Mexico and the North Sea. Ever since the 1960's companies were not allowed to use dynamite any more as seismic source because of fish dying massively due to the sharp and destructive strong shockwave from the dynamite. Exploration companies had to look for alternatives. Many sources were developed since then, such as airguns, waterguns and even a marine equivalent of the Vibroseis. Airguns became the most popular marine source in the oil industry because of their renowned reliability and signature repeatability. The signature of one airgun has an inconveniently long and oscillatory character, the reason why airguns are used in specifically designed arrays, consisting of airguns with different volumes.

The mechanics of the airgun

As is obvious from the name, the driving mechanism of the airgun is supplied by (compressed) air. In Figure (3.2) we have given a schematic view of an airgun. Air under pressure is pumped into a chamber. Using the piston, the air is suddenly released and the air leaves the chamber and starts to create a bubble in the surrounding water. Inside the bubble we have the air but there is a turbulent region which consists of many little bubbles, the non-linear zone. This is schematically given in figure (3.3) (a). The mechanism behind the behaviour of the airgun is depicted in figure (3.3) (b) and (c). The bubble increases in the beginning but after a while the pressure from outside, the hydrostatic pressure, is larger than the pressure from inside of the bubble and the expansion slows down. The expansion comes to an end and the bubble reaches its maximum radius when the kinetic energy of the outward moving water is fully converted into potential energy related to bubble radius, hydrostatic pressure and some heat losses. From there on, the bubble starts to collapse since the hydrostatic pressure from outside is larger than the pressure inside. The collapse slows down when we have again passed the equilibrium position (where the pressure inside the bubble is equal to the hydrostatic pressure) until we have reached a minimum radius where it will start to expand again, and so on.

The collapses and expansions will not go on forever because of the heat dissipation

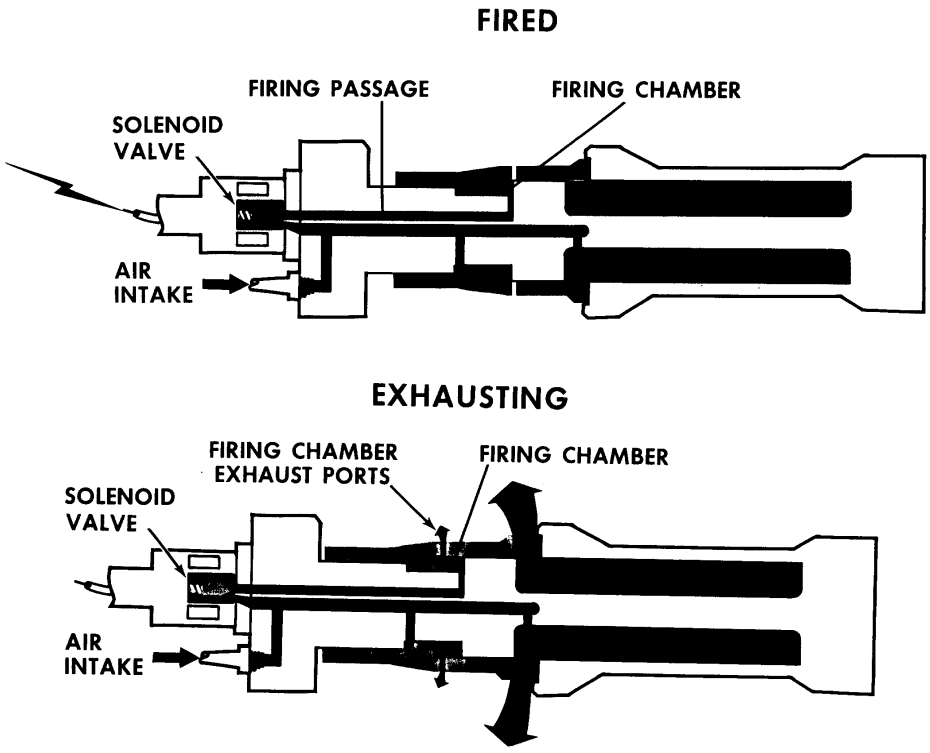

Figure 3.2: Cross-section of an airgun just when it is fired, and when the air is released.

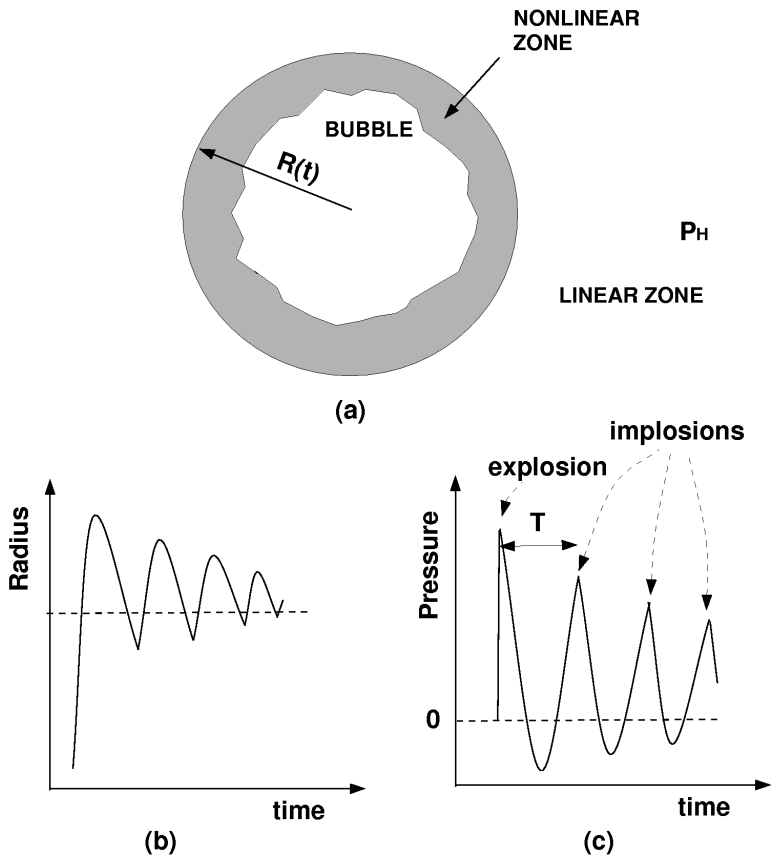

Figure 3.3: (a) Schematic section of the released air bubble; the radius (b) and the pressure (c) as a function of time for the air bubble of an airgun.

into the water. The result from this behaviour is a damped oscillatory pressure signal, somewhat similar to a damped sine curve. The behaviour is depicted in the figure (3.3) (b) and (c), where both bubble radius and the pressure have been plotted as a function of time.

The signal from an airgun

The signal from a single airgun has a length of some 200 ms. Of course, this depends on the type of airgun and the pressure of the air supplied to the airgun. The larger the size, i.e. airgun airchamber volume, or the higher the pressure the longer the period in the oscillations (or, the lower the frequency content). Common pressures are 2000 and 3000 psi. The gun sizes are specified airchamber volume. Common values are 10, 20, 30 up to 100 cubic inches. Much used by many contractors these are the so-called sleeve guns. With the sleeve gun, as the name suggests, the air escapes via a complete ringed opening.

The signature resulting from one airgun is an oscillatory signal which does not resemble the ultimate goal: creating a short seismic signature, preferably a delta pulse. This is the main reason why arrays are used. Airguns of different sizes and at different distances from each other are used such that the first pressure peaks coincide but the other peaks cancel, i.e., destructive interference for the other peaks. Usually with the design of airgun arrays, the largest gun is chosen to give the desired frequency content needed for a survey. Then smaller guns are used to cancel out the second, third, etc. peaks from this large gun. This is done in the frequency domain rather than in the time domain: a delta pulse in time corresponds to a flat amplitude spectrum in frequency. This has resulted in a few configurations of airgun arrays of which the so-called Shell array is the mostly used one. This array has seven guns in one array. The quality of an array is measured via the so-called primary-to-bubble ratio, that means the ratio between the first peak and the second-largest peak. An example of such a signature is given in Figure (3.4). These days P/B ratios of 16 can be achieved.

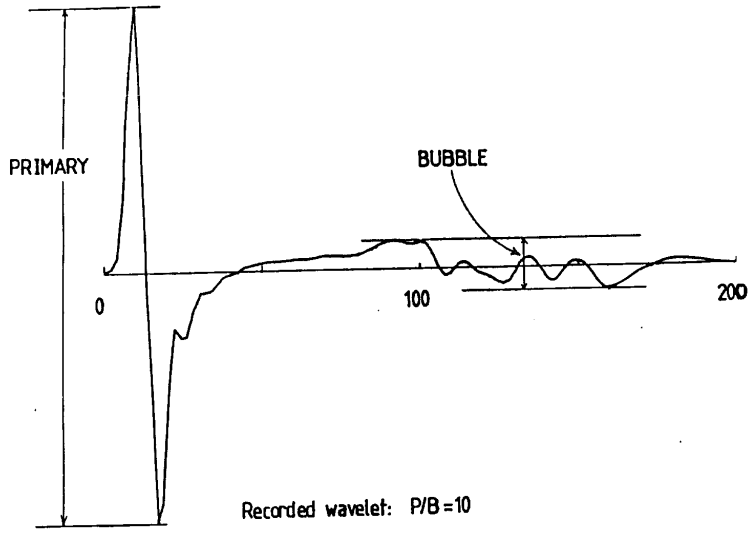

Figure 3.4: Far-field wavelet of tuned air-gun array.

3.2.2 Vibroseis

In seismic exploration, the use of a vibrator as a seismic source has become widespread ever since its introduction as a commercial technique in 1961. In the following the principles of the Vibroseis[1] method are treated and the mechanism which allows the seismic vibrator to exert a pressure on the earth is explained. The basic features of the force generated by the seismic vibrator is discussed: the non-impulsive signal generated by a seismic vibrator having a duration of several seconds.

The vibrator is a surface source, and emits seismic waves by forcing vibrations of the vibrator baseplate which is kept in tight contact with the earth through a pulldown weight. The driving force applied to the plate is supplied either by a hydraulic system, which is the most common system in use, or an electrodynamic system, or by magnetic levitation. The direction in which the plate vibrates can also vary: P wave vibrators (where the motion of the plate is in the vertical direction) as well as S wave vibrators (vibrating in the horizontal direction) are used. Finally, a marine version of the seismic vibrator has been developed, however not in frequent use. For all these vibrator types, the general principle which governs the generation of the driving force applied to the plate (usually referred to as the baseplate) can be described by the configuration shown in Figure (3.5). A force F is generated by a hydraulic, electrodynamic or magnetic-levitation system. A reaction mass supplies the system with the reaction force necessary to apply a force on the ground. The means by which this force is actually generated is illustrated in Figure (3.6), in which the principle of the hydraulic drive method is shown. By pumping oil alternately into the lower and upper chamber of the piston, the baseplate is moved up and down.

[1]Registered trademark of Conoco Inc.

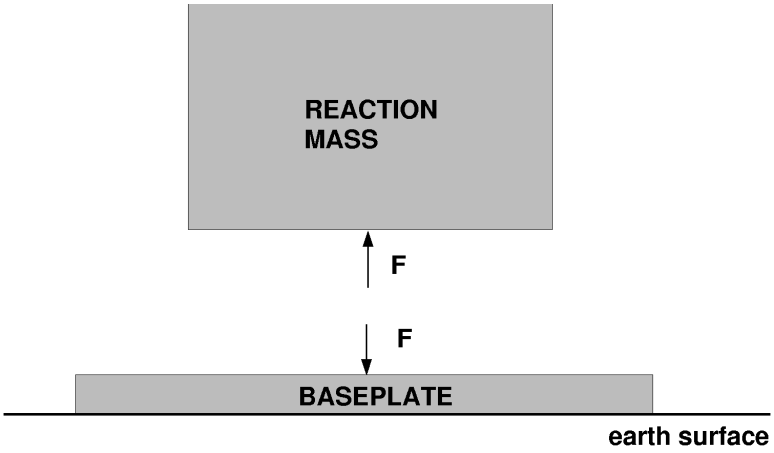

Figure 3.5: The force-generating mechanism of the seismic vibrator source.

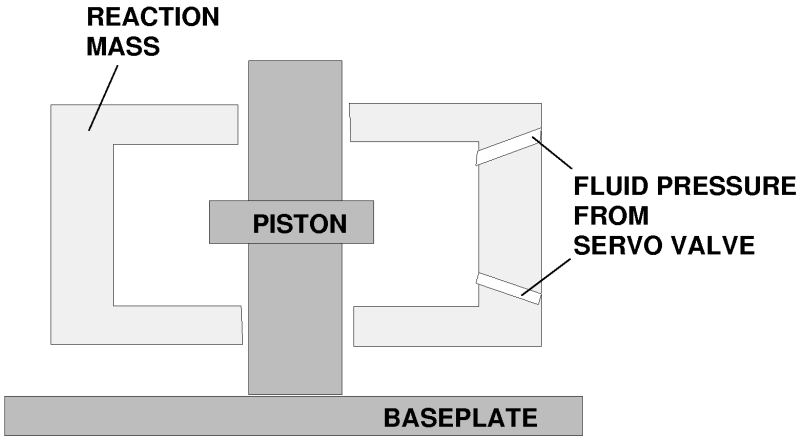

Figure 3.6: Schematic view of the generation of the driving force for a hydraulic vibrator.

The fluid flow is controlled by a servo valve. The driving force acting on the baseplate is equal and opposite to the force acting on the reaction mass, as can easily be inferred from Figure (3.6). In general, the peak force is such that the accelerations are in the order of several g's, so that an additional weight has to be applied to keep the baseplate in contact with the ground. For the hydraulic and electrodynamic vibrators, the weight of the truck is used for this purpose. This weight, commonly referred to as the holddown mass, is vibrationally isolated from the system shown in Figure (3.6) by an air spring system with a low spring stiffness (shown in figure (3.7)), and its influence on the actual output of the system is usually neglected. The resonance frequency of the holddown mass is in the order of 2 Hz, the lowest frequency of operation in Vibroseis seismic surveys for exploration purposes being usually not less than 5 Hz.

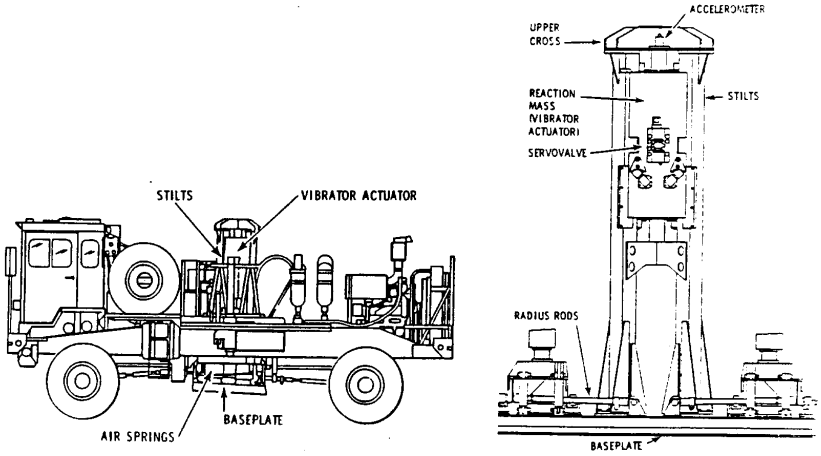

Figure 3.7: (a) schematic view of the Vibroseis truck with the air springs, the baseplate and the vibrator actuator (reaction mass), and (b) detailed view of the middle part of the truck.

The force exerted on the baseplate

The mechanism by which the seismic vibrator applies a force to the baseplate is very complicated, and differs for different vibrators. In this section, the applied force is described using a simplified mechanical model for a hydraulic P wave vibrator.

A model of a compressional wave vibrator is introduced here which describes the different components of the vibrator in terms of masses, springs and dashpots (i.e. shock absorbers). The model, shown in Figure (3.8), contains three masses. These are the holddown mass, which represents the weight of the truck and is used to keep the baseplate in contact with the ground; the reaction mass, which allows the vibrator to exert a force on the baseplate; and the baseplate, which is in contact with the earth's surface. The input force i, which is supplied by the vibrator's hydraulic system, is not the same as the force f exerted on baseplate and reaction mass due to the compressibility of the oil pumped in the cylinder. The suspension s_1 represents the means to support the reaction mass in its neutral position. The connection between truck and the baseplate by means of isolated air bags is represented by the dashpot K and suspension s_2. Gravity forces are not included in the analysis because they represent a static load, and do not affect the dynamic behaviour of the seismic vibrator.

The signal emitted by a seismic vibrator

The signal emitted by the seismic vibrator is not impulsive, but typically has a duration of some 10-15 sec. The use of such a relatively long signal seems to be in contradiction with the fact that seismic exploration methods aim at detecting the impulse response of the earth. This apparent contradiction can be clarified by taking a closer look at the

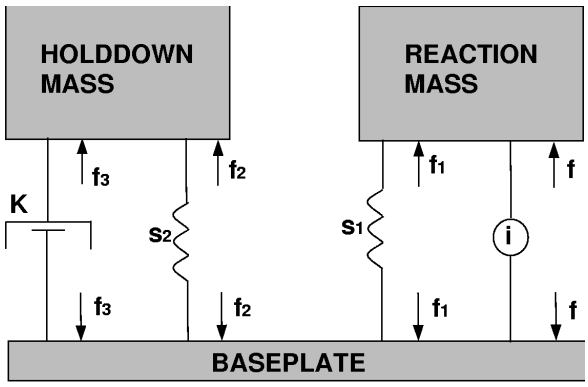

Figure 3.8: The mechanical model of the Vibroseis truck.

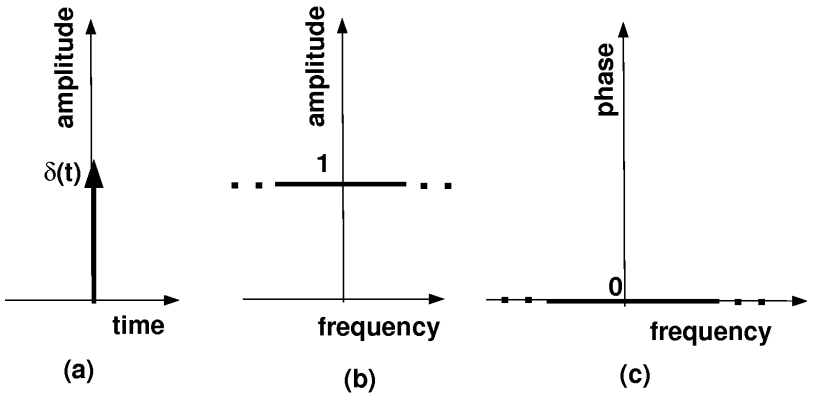

Figure 3.9: The notion of a perfect impulse, (a) in the time domain, and (b),(c) its corresponding frequency domain version.

properties of an impulse and the earth response to such an impulse.

A perfect impulse at time $t = 0$ contains all frequency components with equal amplitude and zero phase. This is illustrated in Figure (3.9). In practice, one cannot generate a perfect impulse because this would require an infinite amount of energy; the best one can achieve is to emit a bandlimited impulse, resulting in a finite-amplitude wavelet whose time duration is small compared with any dominant signal periods present in the earth's response.

The Vibroseis source emits a bandlimited, expanded impulse. The band limitation has two aspects: at the low frequency end, it is dictated by the mechanical limitations of the system and the size of the baseplate. The high frequency limit is determined by the mass and stiffness of the baseplate, the compliance of the trapped oil volume in the driving system for a hydraulic vibrator and mechanical limitations of the drive system.

The notion of an "expanded " impulse can be explained in terms of the amount of energy per unit time, known as energy density. In an impulsive signal, all energy is concentrated in a very short time period, leading to a very high energy density. In the Vibroseis method, a comparable amount of energy is transmitted over a longer time (i.e., smeared out over a longer time), so that the energy density of the signal is reduced considerably. This reduction in energy density is achieved by delaying each frequency component with a different time delay, while keeping the total energy contained in the signal constant. Thus, instead of emitting a signal with a flat amplitude spectrum and a zero phase spectrum, a signal is created which has the same flat amplitude spectrum in the frequency band of interest, however having a non-zero phase spectrum. The frequency-dependent phase shifts cause time delays which enlarge the duration of the signal. However, the total energy of the signal is determined only by its amplitude spectrum (Parseval's theorem!). The effect of the increased time duration of the emission on the recorded seismogram has to be eliminated. This is achieved by having full control of the phase function of the emitted signal. Then, the signal received at the geophone can be corrected for the non-zero phase spectrum of the source wavelet by performing a cross-correlation process of the received seismogram and the outgoing signal (source signal). To clarify this point, let the source wavelet be denoted by $s(t)$. If the convolutional model is adopted to describe the response at the geophone, $x(t)$, the following expression is obtained in the absence of noise:

$$x(t) = s(t) * g(t) \tag{3.2}$$

where $g(t)$ denotes the impulse response of the earth, i.e., the layered geology, and $*$ denotes a convolution. Transforming equation (3.2) to the frequency domain yields

$$X(\omega) = S(\omega)G(\omega) \tag{3.3}$$

If the received signal $x(t)$ is cross-correlated with the source signal $s(t)$, the signal $c(t)$ is obtained which, in the frequency domain, is given by

$$C(\omega) = X(\omega)S^*(\omega) = |S(\omega)|^2 G(\omega) \tag{3.4}$$

since cross-correlation of $x(t)$ with $s(t)$ in the time domain corresponds to a multiplication in the frequency domain of $X(\omega)$ with the complex conjugate of $S(\omega)$. In this equation, the complex conjugate is denoted by the superscript $*$. This cross-correlation is merely a special deconvolution process, in which we exploit the feature that we send out a signal whose amplitude spectrum is constant. This can be seen by looking at the deconvolution as discussed in the chapter on Fourier theory. Applying the deconvolution filter with stabilisation constant amounts to:

$$F(\omega)X(\omega) = \frac{X(\omega)S^*(\omega)}{S(\omega)S^*(\omega) + \epsilon^2}. \tag{3.5}$$

It can be seen here that the numerator is equal to equation (3.4), so the cross-correlation is a partial deconvolution. The main achievement of the cross-correlation is that it *undoes* the phase of the signal. The denominator has the term $S(\omega)S^*(\omega)$. This is a purely

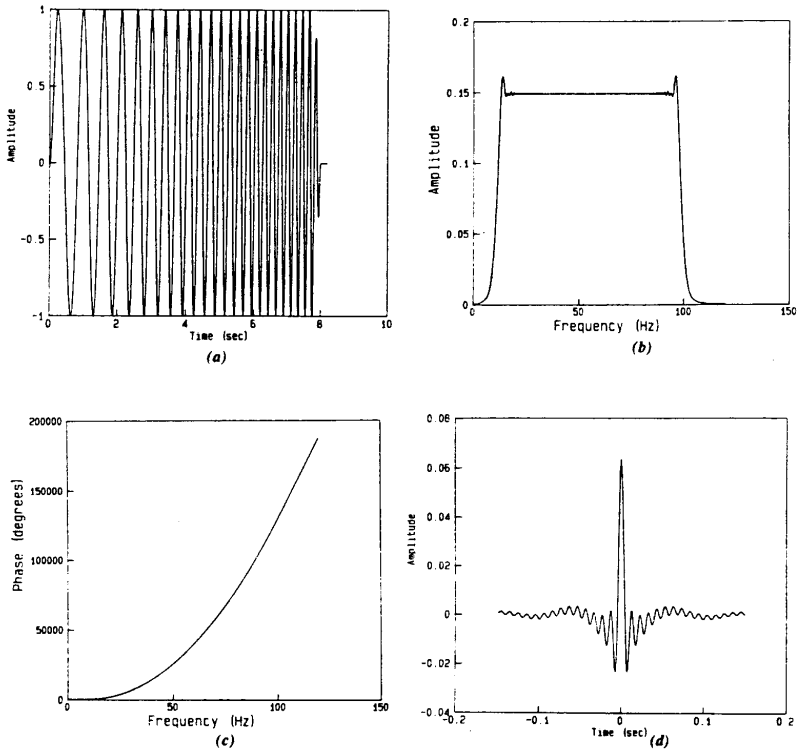

Figure 3.10: An 8 sec, 10-100 Hz upsweep with a taper length of 250 msec. (a) the sweep in the time domain; the frequency range for this Figure is 1-5 Hz for display purposes, (b) the amplitude spectrum of the sweep, (c) the phase spectrum of the sweep, in degrees, and (d) the autocorrelation of the sweep.

real number and therefore only affects the amplitude. In the case that the amplitude is flat, the amplitude does not depend on frequency any more and becomes a simple scaling factor in the deconvolution process. So when the amplitude spectrum of $S(\omega)$ is flat over the frequency band of interest , and zero outside this frequency band, it follows that by cross-correlating the measured seismogram $x(t)$ with the source function $s(t)$, the (scaled) bandlimited impulse response $g(t)$ of the earth is obtained.

In Figure (3.10) the concepts are illustrated for the example of an upsweep, a signal which ends with a larger frequency than it started off with. An 8 sec, 10-100 Hz linear upsweep is used with a taper length of 250 msec. Figure (3.10) (a) shows the sweep. Because the oscillations in the sweep are too rapid to yield a clear picture, the frequency limits for this figure are 1-5 Hz. Figures (3.10) (b) and (3.10) (c) show the amplitude and phase, respectively. It can be observed from these figures that the phase indeed is a quadratic function of frequency, and that the amplitude spectrum of the sweep is constant over the bandwidth. Finally, Figure (3.10) (d) shows the autocorrelation of the sweep.

3.2.3 Dynamite

Until the arrival of the Vibroseis technique, dynamite was the mostly used seismic source on land. Dynamite itself is very cheap, the costs involved are mainly the costs of drilling the shotholes to place the dynamite. These costs may run up so high as to make the Vibroseis a good competitor of the dynamite source. Dynamite is usually used in non-urban areas for obvious reasons. A nice characteristic of dynamite is that it is resembling a (bandlimited) form of the delta pulse, something we would ideally like to have, since we are interested in the impulse response of the earth. In this section some features of the dynamite source and the signature resulting from it will be discussed.

The chemical working of dynamite and its mechanical impact

Dynamite is a chemical composition which burns extremely fast when detonating. Typically, 1 kilogram of dynamite burns in about 20 microseconds. In this very short time it vaporizes and generates very high pressures and temperatures. The dynamite is usually ignited with a detonator which is a small-size charge of dynamite as well, but enough to ignite the larger charge. The detonator must get a large current through it in order to be set off. For safety reasons, the detonator is designed such that a large current has to be applied. A typical current strength is some 5 Amp.

Explosives can be classified by their chemical composition. Dynamite itself consists of a combination of the explosives glyceroltrinitrate and glycoldinitrate. Since the combination of these two give a fluid, they are mixed with celluloid-nitrate and then give a gelatinous material. Additives of certain (secret) components result in different types of dynamite. Because all of these dynamites contain glyceroltrinitrate, contact with the skin or inhalation, causing head aches, must be avoided.

Since the burning of the dynamite takes place in a very short time generating sudden high pressures and temperatures, it is obvious that in the ground, immediately around the explosive a non-linear zone is created, that means the rock or soil will have undergone some permanent change by the explosion. Three processes are at work there: deformation of the material, conversion of work into heat and geometrical spreading. There will be a distance from the source where there will be no deformation any more; this is given in figure (3.11). The behaviour of the dynamite as a function of time is given in the lower of figure (3.11). In time, we first have an intense shock wave with a complete shattering of the rock or soil. Then, at a certain time, we get two effects, namely a cavity expansion and anelastic rock deformation, until we reach finally a time where we left a cavity which stays there, and an elastic wave originating from this area. So there will always be a cavity left when using dynamite. This cavity is not the same as the radius where the anelastic wave becomes an elastic wave. There has actually been some people who have dug out these cavities in order to see how the cavity changed with a different charge of dynamite. It turned out that the cavity radius was proportional to the cube root of the charge mass.

The dynamite signature

Let us now look at the pressure resulting from a dynamite explosion. It will not be

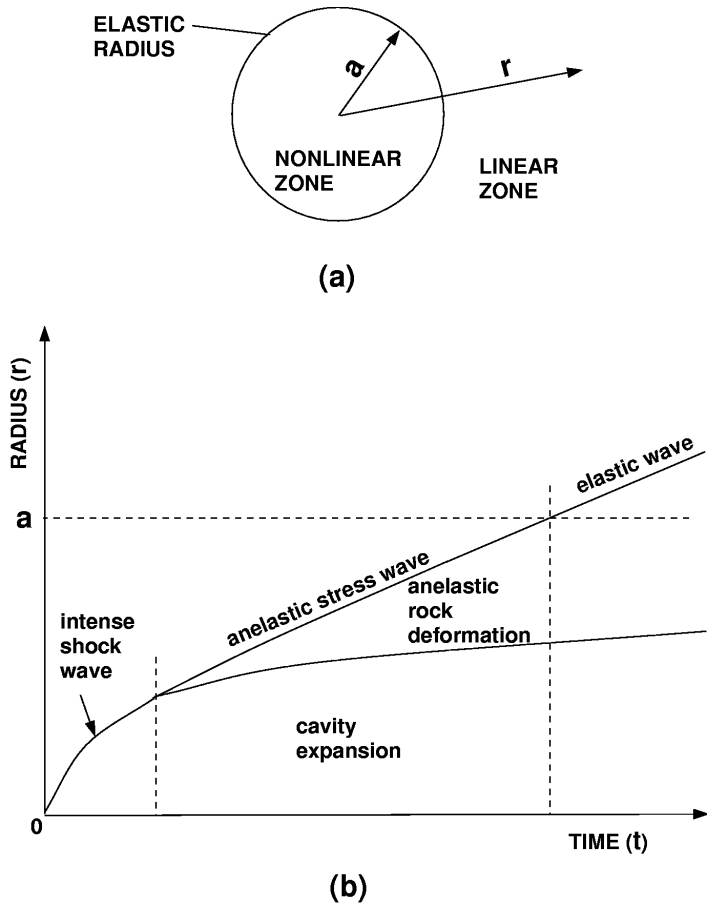

Figure 3.11: The behaviour of dynamite: (a) the characteristic zones in space, and (b) the radius as a function of time with its characteristic zones.

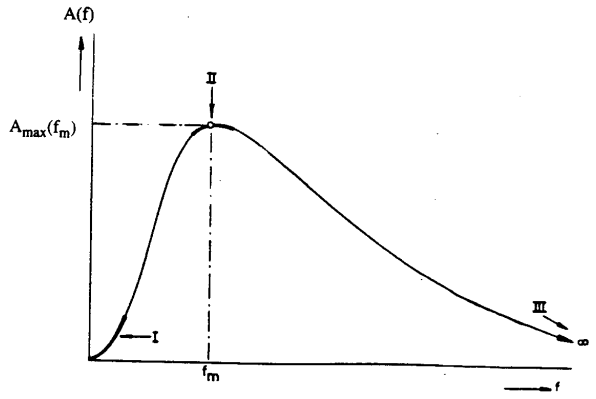

Figure 3.12: Amplitude as function of frequency of dynamite signature (from: Peet, 1964)

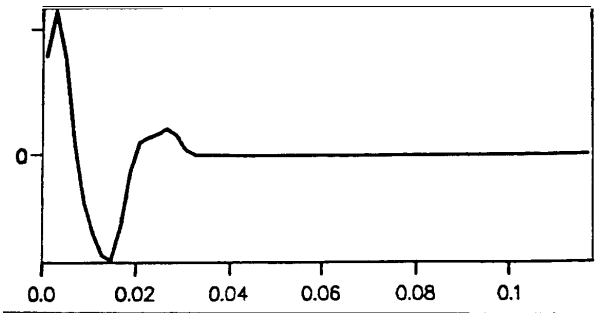

Figure 3.13: Time-domain signal of dynamite, obtained from measurements in the field.

shown how the following results are obtained; that is beyond the scope of these course notes. These results were derived theoretically from shock-wave theory, and are shown in Figure 3.12. In this figure we see that the spectrum has a maximum and that is also what is observed in field experiments.

Also, from experiments in the field, the dynamite signature has been determined, although the experiments are not always reliable. The results are shown in Figure (3.13), showing a pulse with a sharp peak at the beginning. Actually, most of the energy of the signal is in the beginning. In signal-theoretical terms, this is called minimum-delay. This is a very nice property: For instance, with refraction seismic, we are interested in the first arrival. So a wavelet with the fastest energy build-up is the best we can have. It is the best part to pick the arrival times. Therefore with refraction seismic, nearly always dynamite is used, if allowed.

The amplitude and phase spectrum are given in Figure (3.14) and Figure (3.15).

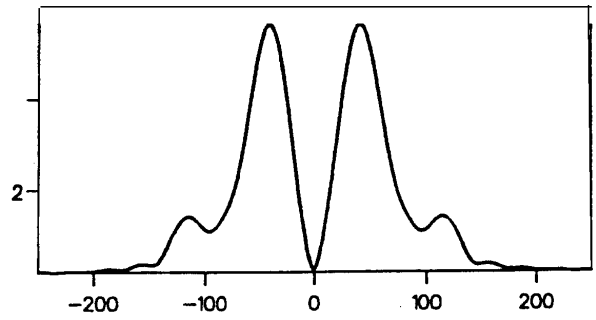

Figure 3.14: Amplitude spectrum of dynamite signature.

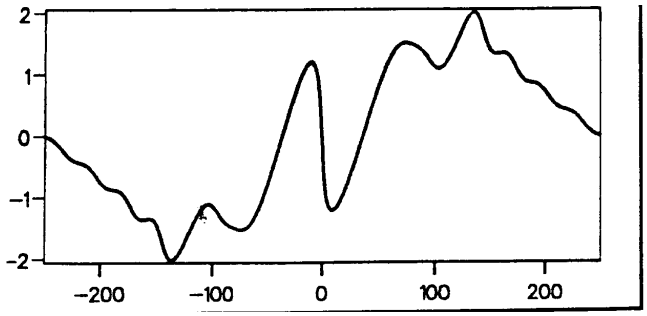

Figure 3.15: Phase spectrum of dynamite signature.

The advantages and disadvantages of dynamite compared to Vibroseis

Some final words on why to use which method: dynamite or vibroseis. Nowadays, Vibroseis is the most used seismic source on land: Technically, one has more control over the signal sent out; Environmentally, it can be used in populated areas; Financially, the cost per km is less than for dynamite. Still, dynamite has advantages too, such as the minimum-delay property. A detailed discussion on the pros and cons of each of these sources can be found in Appendix C.

3.3 Seismic detectors

The source generates a mechanical disturbance which propagates in the ground, is reflected, refracted or diffracted, and returns to the surface. When the disturbance propagates in a fluid such as water a temporary variation of pressure is created. Elastic deformation results in movements of the surface and at some point of the surface the acceleration, the velocity or the displacement of a point can be measured. In any case, whether a movement or a variation of pressure is observed, we have to represent it by some other physical quantity which can be easily stored and manipulated. Considering the development of electronic technology, a representation by an electrical voltage is evidently a good solution. The first field component of a seismic data acquisition system is the detector group. The detectors convert the seismic disturbance into a voltage of which the variations represent faithfully the variations of the mechanical disturbance detected, a voltage which is the analog of the seismic disturbance.

The detectors used for seismic exploration work are called geophones since they are used to "hear" echoes from the earth underneath. Sometimes, they are called seismometers but this term is more often applied to long period seismographs used for recording natural earthquakes. The term "detector" applies to all types of seismic-to-electrical transducers. From what has been said before, it will be clear that they can be classified into two main groups: motion-sensitive, mainly for land operations, and pressure-sensitive for operations in water (or fluids), be it for marine seismic work or in the mud column of a borehole, for well-shooting or a VSP. Pressure-sensitive geophones are also called hydrophones.

The types of detectors commonly used in practice, are electromagnetic and piezoelectric transducers and we shall omit all others. Piezoelectric transducers which are pressure-sensitive are used as hydrophones and electromagnetic transducers are used on land. In the moving coil geophone of the electromagnetic type, a voltage is generated by the movement of a conductor in a strong permanent magnetic field. These types are used nowadays.

Geophones are the parts of the system which undergo the roughest treatment. They are planted and picked up many times, they are flung down, run over by the trucks, stamped into the ground by the line men. And yet, they are expected to generate an accurate, noise-free reproduction of the earth movements. They are built to withstand rough handling but a minimum of care on the part of the line men can help in obtaining good quality data.

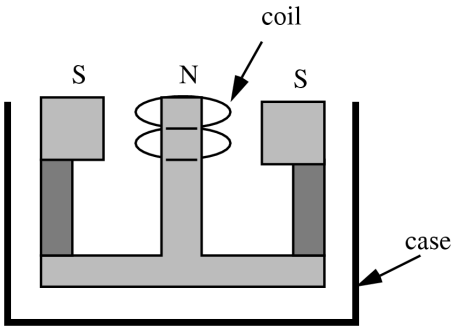

Figure 3.16: Schematic cross-section of a moving-coil geophone.

3.3.1 Geophones

A moving coil geophone (Figure 3.16) operates according to the principle of a microphone or a loudspeaker: the coil consisting of copper wire wound on a thin non-conducting cylinder ("former") moves in the ring-shaped gap of a magnet. Figure 3.16 is the cross section of a cylindrical structure. The annular magnet and polar pieces N and S in soft iron create a radial field in the gap. The only movement allowed for the coil, suspended from springs not shown in the picture, is a translation along the direction of the axis and in the gap. As the coil moves, its windings cut magnetic lines of force and an electromotive force is generated. The output voltage is proportional to the rate at which the coil cuts the lines of magnetic force, that is to say, proportional to the velocity at which it moves. Therefore this type of detector is known as "velocity geophone".

The main parts of the geophone are:

- the moving mass, made up by the coil and the "former" on which it is wound;
- the coil suspension, usually two flat springs, one at the top and one at the bottom, to avoid lateral displacement of the coil;
- the case, with the magnet and polar pieces inside a cylindrical container which protects the other elements against dust and humidity.

The case is placed on the ground and is supposed to follow the ground movement exactly (Figure 3.17). The output voltage is proportional to the velocity of the mass relative to the case and what we are interested in is this relative movement as a function of the movement of the case.

A complete description of geophones must take into account many phenomena beyond the scope of these lecture notes. The final design of a geophone is usually a compromise between conflicting requirements. For a geophysicist it is often sufficient to know the basic operating principle of the geophone in order to understand the behaviour of this component

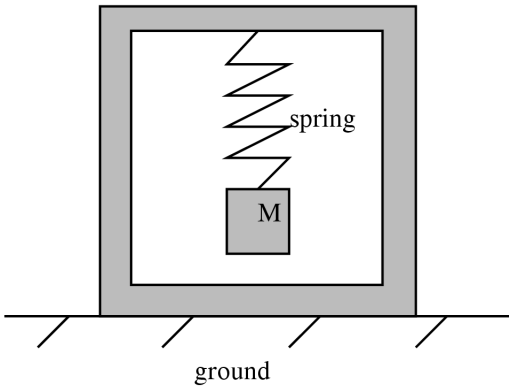

Figure 3.17: The geophone on the ground.

as part of the whole data acquisition network. Consequently, the considerations which follow are restricted to the response of an ideal geophone.

Assuming the vertical component of the velocity is:

$$v_z = \frac{dz}{dt}, \tag{3.6}$$

and the output voltage is given by V, the conversion of the motion to the electric signal takes place via the transfer function:

$$R(\omega) = \frac{\text{Voltage}}{\text{Particle Velocity}} = \frac{V(\omega)}{v_z(\omega)} = \frac{\omega^2 K}{\omega^2 - 2ih\omega\omega_0 - \omega_0^2} \tag{3.7}$$

where ω_0 is the resonance frequency of the spring, and K and h are some constants depending on mechanical and electrical components; K represents a sensitivity (proportionality constant) and h a damping factor. Consider now three situations:

$$\begin{aligned} \omega \to 0: &\qquad R(\omega) \to -\frac{\omega^2}{\omega_0^2} K = \frac{\omega^2}{\omega_0^2} K \exp(\pi i) \\ \omega = \omega_0: &\qquad R(\omega) \to \frac{K}{-2ih} = \frac{K}{2h} \exp(\pi i/2) \\ \omega \to \infty: &\qquad R(\omega) \to K \end{aligned} \tag{3.8}$$

These are depicted in Figure 3.18 and Figure 3.19. The received voltage is proportional to the velocity of the ground only at frequencies well above the resonance frequency of the geophone. At these frequencies the constant K is the sensitivity of the geophone, with units of, for example, volts/mm/s.

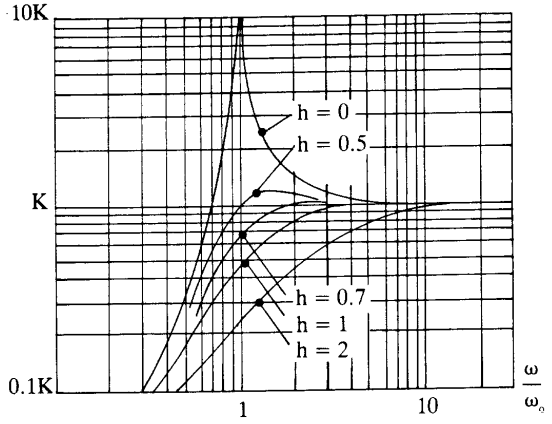

Figure 3.18: Amplitude response of geophone at constant velocity drive (From: Pieuchot, 1984)

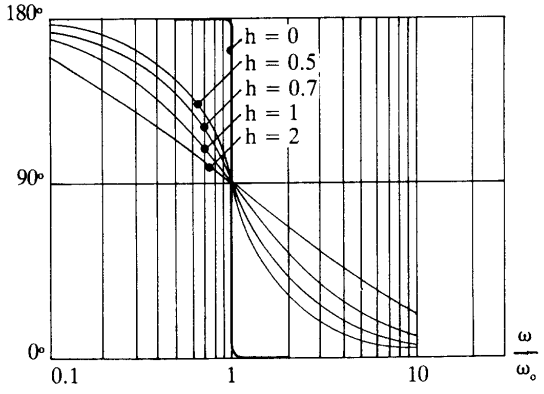

Figure 3.19: Phase response of geophone at constant velocity drive (From: Pieuchot, 1984)

3.3.2 Hydrophones

As has been shown in the foregoing section, the geophone exhibits a flat pass-band characteristic from a few Hertz above the resonance frequency to the spurious frequency. In that pass-band the output voltage V_{Geop} is proportional to the particle velocity v:

$$V_{\text{Geop}} = constant \cdot v_z \tag{3.9}$$

We will show in the next paragraph that in the pass band of the hydrophone, the output voltage V_{Hydr} is proportional to the acoustic pressure p, i.e.,:

$$V_{\text{Hydr}} = constant \cdot p \tag{3.10}$$

Hydrophones are thus pressure-sensitive detectors and they are used for operations in water-covered areas.

At present often hydrophones with ceramic pressure sensitive elements are used. They operate on the principle of piezoelectricity. A piezoelectric material is one which produces an electrical potential when it is submitted to a physical deformation. The phenomenon is observable in some crystalline structures such as quartz and tourmaline and is used in record player pick-ups. It can also be produced by in artificially-made poly-crystalline ceramics after they have been submitted to a high-intensity electric field (several tens of thousands volts per centimeter). The most commonly used material in seismic applications, is lead zirconate titanate (PZT).

In order to show the principle of piezo-electricity, we consider an hexagonal quartz crystal as shown in Figure 3.20. In such a crystal, the charges can be represented by positive or negative charges at the corners, inherently because of its crystallic structure. When the crystal is at rest, i.e., no force is applied as shown on the left in Figure 3.20, the resultant total charge, expressed by the positive (+) and negative (-) in the middle of the crystal, is zero. However, when a force is applied, as shown on the right of Figure 3.20, the positive and negative charges do not cancel each other any more, represented by the plus and minus-sign in the middle. Because of the force, there will be a resultant voltage difference observed. The magnitude of piezoelectric forces, actions, and voltage is relatively small. For example, the maximum relative dimensional change of a single element is in the order of 10^{-8}. Amplification is often required and accomplished by other components in the system, such as electronic circuits. In some cases, the design of a ceramic element itself provides the required mechanical amplification. The use of ceramic elements as seismic (pressure) detectors / hydrophones is based on these principles.

As with the geophones in land operations, the hydrophones are always assembled in multiple arrays at each trace. They are often assembled so as to increase the capacitance (more hydrophones in parallel than in series) and decrease the low-frequency cut-off. The network model for the hydrophone is given in Figure 3.21.

V/E is the transfer function since E represents the variations of pressure in the water.

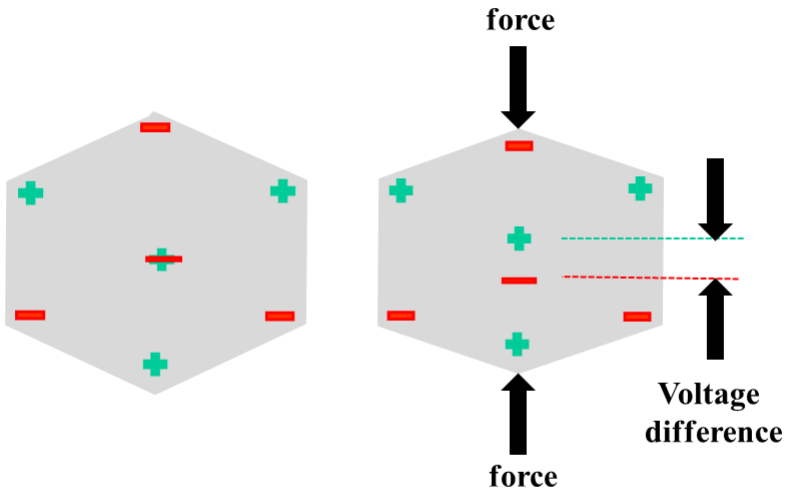

Figure 3.20: Piezoelectric voltages from applied force on hexagonal quartz crystal. Left: positive (+) and negative charges (-) cancel each other (at rest). Right: Applying force make that positive (+) and negative charges (-) do not cancel each other, resulting in a voltage difference.

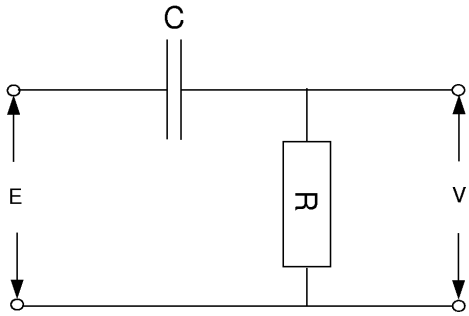

Figure 3.21: Simplified circuit for deriving the hydrophone response.

From the circuit given in Figure 3.21, the transfer function $R(\omega)$ can be derived:

$$R(\omega) = \frac{\text{Voltage}}{\text{Pressure}} = \frac{V}{E} = \frac{R}{R + \frac{1}{i\omega C}} = \frac{i\omega CR}{1 + i\omega CR} = \frac{\omega}{\omega - i\omega_0}. \tag{3.11}$$

(For an overview or recap of impedances in networks, for a resistor, inductor or capacitor, see appendix D.)

Consider now three situations:

$$\begin{aligned} \omega \to 0 : \qquad & \frac{V(\omega)}{E} \to i\omega CR = \omega CR \exp(\pi i/2) \\ \omega = \omega_0 = 1/CR : \qquad & \frac{V(\omega)}{E} \to \frac{i}{1+i} = \frac{1}{2}\sqrt{2}\exp(\pi i/4) \\ \omega \to \infty : \qquad & \frac{V(\omega)}{E} \to 1 \end{aligned} \tag{3.12}$$

The amplitude and phase response are given in Figure 3.22.

It is now interesting to compare this response to the one from the geophone. At low frequencies the responses are out of phase by $\pi/2$, decreasing to $\pi/4$ at higher frequencies and in phase at high frequencies. This can be important when comparing two seismic sections, one shot on land and the other one shot at sea.

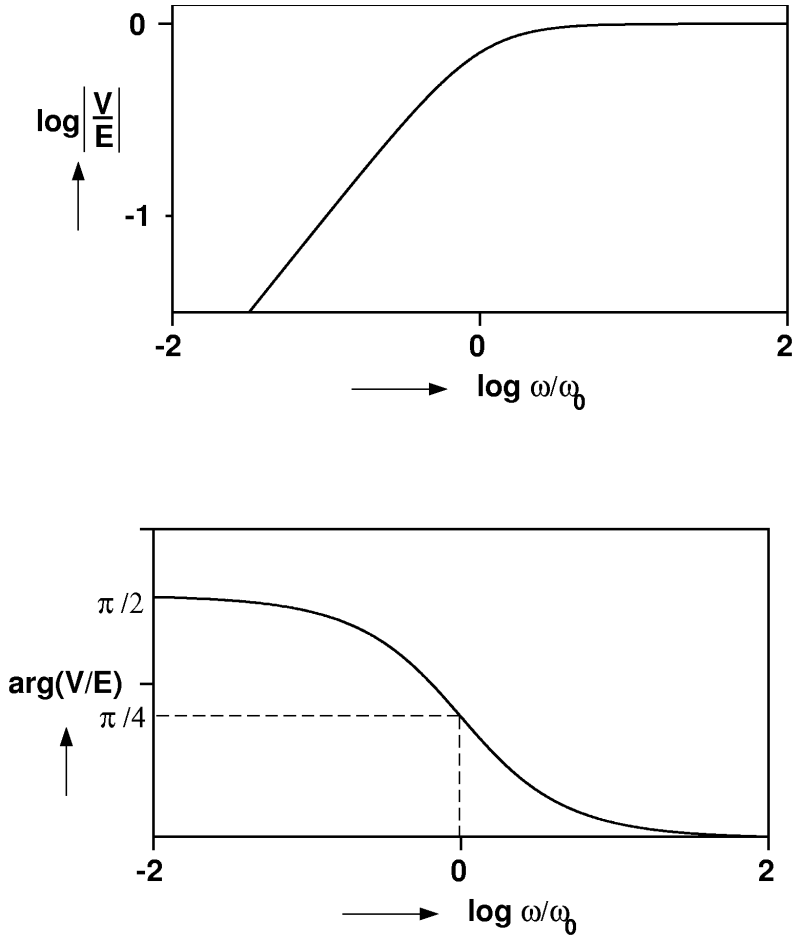

Figure 3.22: Amplitude and phase response of a hydrophone.

3.4 Seismic recording systems

The modern seismic data recording system is a compound of electric subsystems (amplifiers, filters, etc.). The (glasfibre) cable system may often be considered integral part of it. It has as input analog electrical signals from the seismic detectors (see section on geophones and hydrophones) and puts digital data out on magnetic tape. Nearly all systems offer the facility of instant data verification through the creation of output on paper record, the so-called "monitor recording".

In a very general sense, a recorder consists of several parts, namely amplifiers, filters and an A/D converter, before it is stored on (magnetic) tape. The analog signal comes from the geophones into the system, where it is first amplified. The data can be filtered, the most important one being the anti-alias (high-cut) filter. Then the data is converted to a digital signal using the A/D converter, giving digital data which can be stored on disc or computer tape.

3.4.1 (Analog) filters

An important setting of a data recording system is that of different filters. The filters are analog filters. Some of these filters may be predetermined but others must be left at the discretion of the user and must be adjustable in the field. These filters can be categorised into two groups, namely passive and active filters. Passive filters are built from passive electrical elements: resistors, capacitors and coils. Active filters have an amplifier as an integral part of the filter. Usually there are three types of filters available to the user in the field: low-pass (high-cut), notch and high-pass (low-cut) filters.

In the following the principles of passive filters will be dealt with. Let us look at a general scheme of a filter by considering figure (3.23). When a potential difference E is put over a series connection of two passive elements with impedances Y and Z, and when we measure the potential difference V over the Y component, the ratio of the two potentials is given by:

$$\frac{V}{E} = \frac{Y}{Z+Y} \tag{3.13}$$

The components Y and Z can be any components as tabulated in appendix C.

For a resistance, the impedance is R, for an inductance $i\omega L$, and for a capacitance $1/i\omega C$. So, when the component Y is an capacitance and Z a resistance, the measured potential difference is a "high-cut" (or "low-pass") version of the input voltage E. This can be seen by substituting the values in the above equation:

$$\frac{V}{E} = \frac{\frac{1}{i\omega C}}{\frac{1}{i\omega C} + R} = \frac{1}{1 + i\omega CR} \tag{3.14}$$

which is a ratio, dependent on the frequency ω. When we write this in polar coordinates,

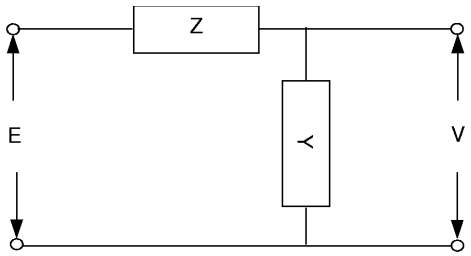

Figure 3.23: A passive filter.

we get:

$$\frac{V}{E} = \frac{1}{1+i\omega CR}\frac{1-i\omega CR}{1-i\omega CR} = \frac{1}{1+\omega^2C^2R^2} + i\frac{-\omega CR}{1+\omega^2C^2R^2} = \frac{1}{(1+\omega^2C^2R^2)^{1/2}}\exp(i\phi) \tag{3.15}$$

where ϕ is the phase angle. When ω is small, then ωCR can be neglected compared to 1 in the amplitude factor and thus, V/E behaves like 1 (amplitudewise). When ω is large then 1 can be neglected compared to ωCR, and the numerator approaches ωCR so V/E will behave like $1/\omega$. This is thus a high-cut filter.

In the same way we can derive that when Y is a resistor, the filter acts as a low-cut or high-pass filter. It is customary to specify a filter by its so-called corner frequency, i.e., the frequency where $\omega LCR = 1$. With a high-cut filter as above, the signal will be significantly damped above this frequency, with a low-cut filter the signal will be significantly damped below this frequency. The foregoing filter was an example of a passive filter, i.e., a filter built-up of passive elements (R, L, C).

Why do we need these filters in our geophysical measurements? Let us discuss them separately, first the low-cut filter. As the name says, low-frequency waves can be suppressed with these filters. On land, filtering is sometimes applied to suppress the surface waves or ground roll, although there is a preference for keeping surface waves in the seismogram and remove them later during processing. At sea, a low-cut filter is needed to suppress the waves at the surface of the sea itself.

A most important filter is the anti-alias filter, needed for proper sampling in time of the seismic signal. Aliasing of the seismic signal should be avoided when we sample it in time. This means that the highest frequency in the signal should at least be sampled with 2 samples per full period. But we do not know the frequency content of our signal beforehand and therefore we make sure, using a high-cut filter, that above a certain frequency, the signal is suppressed below a certain level. The high-cut filter must reduce the signal above the Nyquist frequency below the noise level. The Nyquist frequency is given by: $f_N = 1/2\Delta t$. The effect of aliasing in the time domain is illustrated in figure (3.24). Once the frequency content of the signal is suppressed sufficiently above the Nyquist frequency, digitizing the data makes real sense. Because of this application, this filter is also called an anti-alias filter or just alias filter. This filter must always be set according to the sampling

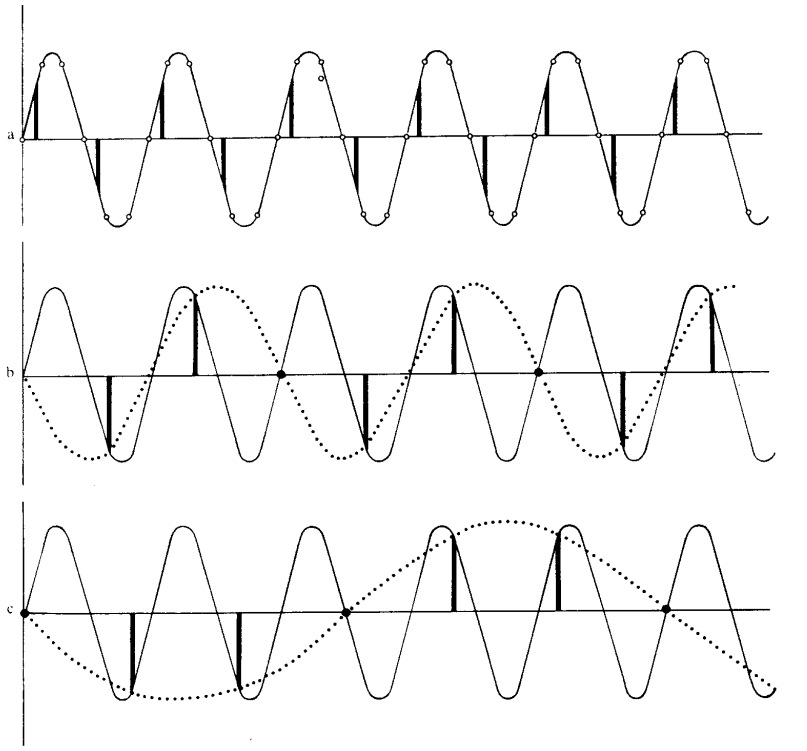

Figure 3.24: The time-domain aspect of aliasing.

rate.

Another type of filter which is usually present in a seismic recording system, is the notch filter. Once in a while, it can happen that 50 or 60 Hz interference from power cables is disturbing the seismic measurement (Europe 50 Hz, America 60 Hz). When input balancing circuits, cable screening fails to cure this problem, it is possible to use an active steep-flank so-called "notch filter" to cut the signal at these frequencies. It should be noted however that by cutting the signal before recording, we may also cut valuable information from our data and we may never be able to retrieve it later on.

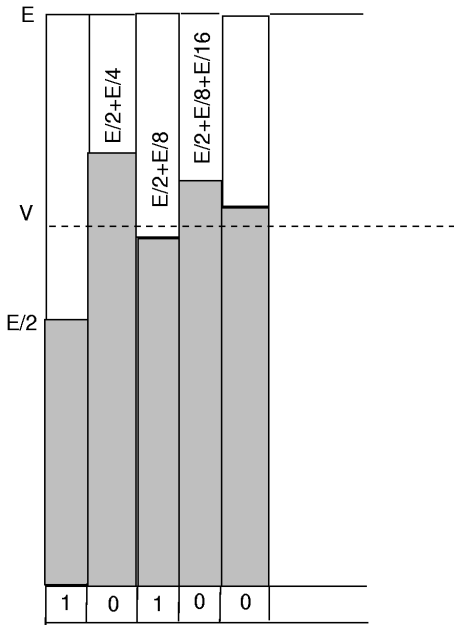

Figure 3.25: Conversion by successive approximations.

3.4.2 The Analog-to-Digital (A/D) converter

In this part the analog-to-digital conversion is discussed. The input is a continuous signal voltage, while the output is a sequence of bits. There are several ways of converting an analog signal to a digital one; we shall only discuss the one called the converter by successive approximations. This type of converter starts to compare the voltage from the side where the signal is largest so which will result in the first bit being the "most-significant" bit. Let us consider figure (3.25). First the voltage is compared to a reference voltage E, divided by 2. If the voltage is larger, then the first bit will be set to 1, otherwise to zero. In the second stage, an amount of $E/4$ is added to or subtracted from the earlier amount of $E/2$, and again the comparison is made with the signal. If the signal is again larger, a bit value of one will added to the earlier one, otherwise a zero. And so we go on with adding or subtracting $E/2^n$, until we have reached the maximum amount of bits. An A/D converter is usually given by the amount of bits, e.g., a 24-bits converter. We can see that we make an error when we digitise the data; the error will be half the so-called least-significant bit (LSB).

The amount of bits resulting from a seismic survey is usually quite large, especially in 3-D seismics. A simple example: assume we have 4000 channels, and we record data for 6 seconds with a sampling rate of 2 ms; the value of the sample is given by 3 bytes (1 byte=8 bits). Then the total number of bytes per shot is: 4000 x 6 x 500 x 3 = $36 \cdot 10^6$ bytes = 36 Megabytes. This is only one shot and for a normal 3D survey thousands of shots are fired, amounting to a dataset that is usually above 1 Terabyte.

3.5 Total responses of instrumentation

In the beginning of this chapter, we defined a general model that was assumed behind the whole seismic system, namely a convolution of the different responses, i.e.,

$$X(t) = S(t) * G(t) * R(t) * A(t)$$

where the responses were defined in the introduction (eq. (3.1)). A convolution in time is equivalent to a multiplication in the Fourier domain, see the chapter on Fourier analysis. Therefore the seismogram can be written in terms of frequencies as:

$$X(\omega) = S(\omega)G(\omega)R(\omega)A(\omega) \tag{3.16}$$

We see that the seismogram consists of (complex) multiplications of the individual transfer functions. Since the multiplications are complex, it can be written as a multiplication of amplitudes and adding of phases, i.e,:

$$\begin{aligned} X(\omega) &= |S(\omega)||G(\omega)||R(\omega)||A(\omega)| \exp(i\phi_S) \exp(i\phi_G) \exp(i\phi_R) \exp(i\phi_A) \\ &= |S(\omega)||G(\omega)||R(\omega)||A(\omega)| \exp\{i(\phi_S + \phi_G + \phi_R + \phi_A)\} \end{aligned} \tag{3.17}$$

where the symbols ϕ_i denote the phase of the component i. In figure 3.26, we have given an example of such a system. In the figure we have taken the example of a recording that is made with dynamite, detected with a geophone and recorded with a certain sampling interval (with then the Nyquist frequency following as $1/2\Delta t$). From this example, we can see that the source is mostly determining the total response. The geophone mostly affects the low frequencies.

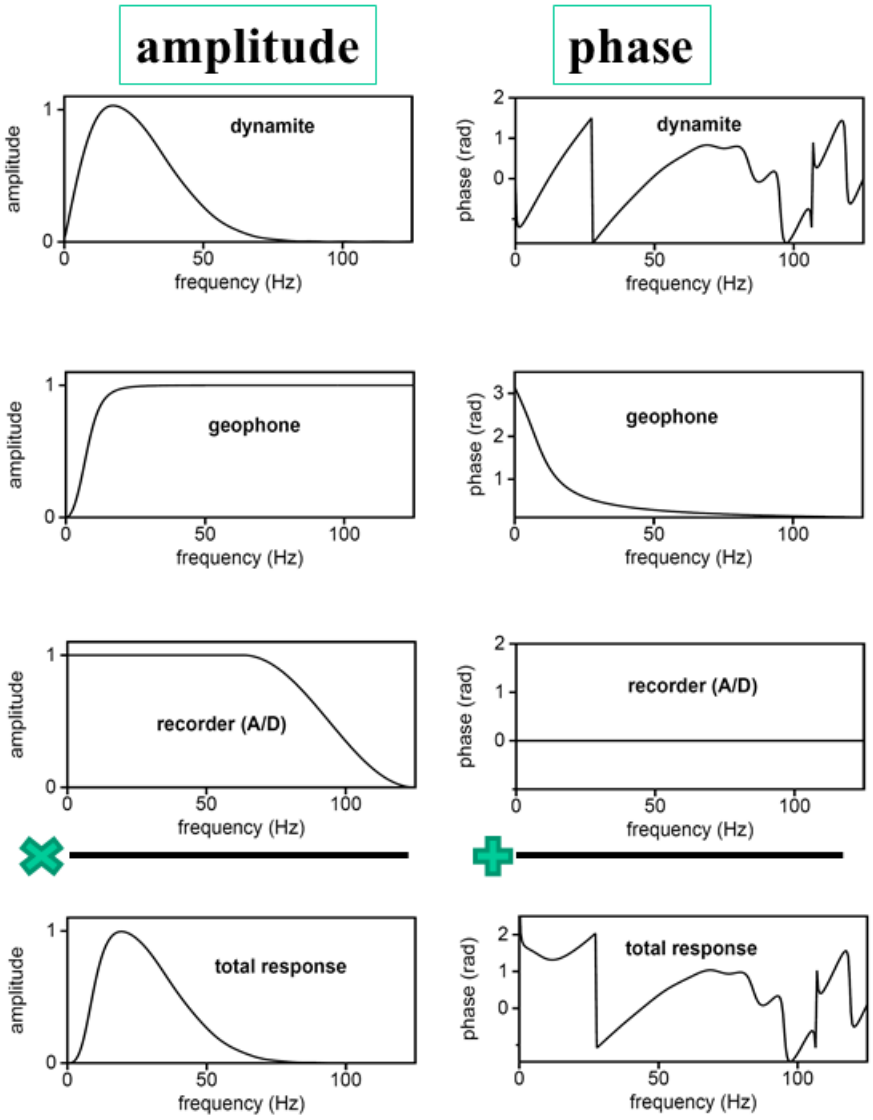

Figure 3.26: The responses due to dynamite source (upper figure), received by geophone of 10 Hz (next two figures), recorded with sampling interval Δt=4 ms (next two figures), resulting in total response (bottom). Note that amplitudes multiply and phases add.

3.6 *EXERCISES*

1. Draw the amplitude and phase spectrum of a seismic record that has been shot with a vibratory source (sweep 20-200 Hz) and correlated afterwards, with a 40-Hz geophone and a time-sampling interval of 1 ms. Put numbers to the axes, if possible.

2. Draw the amplitude and phase spectrum of a seismic record that has been shot with a vibratory source (sweep 5-80 Hz) and correlated afterwards, with a 10-Hz hydrophone and a time-sampling interval of 2 ms. Put numbers to the axes, if possible.

Chapter 4

Fundamentals of the seismic method: wave theory

In this chapter we introduce wave theory, starting from basic laws of physics. For free space, the one-dimensional wave equation is derived for acoustic waves in a fluid, and give the simplest solution to that equation: the direct wave. It is shown how the pressure and the particle velocity are related. Then, in the case of a boundary between two layers with different properties, it is derived which property gives a reflection back from a boundary: the impedance contrast, also called the reflectivity. Finally the one-dimensional wave equations for P- and S-waves in a solid are derived, to which the simplest solutions as given for acoustic waves also apply.

4.1 Introduction

In chapter 2, we discussed the kinematic properties of wave motion, using rays and traveltimes, without worrying ourselves which more fundamental laws were behind it. Here we start from physical fundamentals of mechanics, i.e., Newton's law and deformation laws. Using these laws, we can derive the basic equations for wave motion, which then results in the so-called wave equation. The solution of the wave equation shows the features as discussed in that previous chapter 2: it turns out that rays are obtained from the high-frequency approximation to that wave equation. The attenuation of the wave due to spreading is captured by the wave equation. And reflection and transmission amplitudes are also captured by applying the resulting equations describing the wave motion. So in this chapter we will go into this, giving the fundamental backbone to the seismic method.

4.2 Wave motion in fluids: acoustic waves

With acoustic waves, we assume a fluid in which no shear forces exist, and therefore only P-waves exist. Since waves are physical phenomena, they should have a relation to basic physical laws. The two laws applicable are the Hooke's law and Newton's second law. These two have been used in appendix A to derive the two equations governing the wave motion due to a P-wave. There are some simplifying assumptions in the derivation, one of them being that we consider a 1-dimensional wave. When we denote p as the pressure and v_x as the particle velocity, applying Hooke's law leads to:

$$-\frac{1}{K}\frac{\partial p}{\partial t} = \frac{\partial v_x}{\partial x} \tag{4.1}$$

in which K is called the bulk modulus. This equation is called the deformation equation, in this particular case the equation of elastic deformation. The other relation follows from application of Newton's law:

$$-\frac{\partial p}{\partial x} = \rho\frac{\partial v_x}{\partial t} \tag{4.2}$$

where ρ denotes the mass density. This equation is called the equation of motion.

We are now going to combine these two equations. Therefore we let the operator $\partial/\partial x$ work on the equation of motion:

$$-\frac{\partial}{\partial x}\left(\frac{\partial p}{\partial x}\right) = \frac{\partial}{\partial x}\left(\rho\frac{\partial v_x}{\partial t}\right). \tag{4.3}$$

Now assuming ρ is constant, it can be taken in front of the $\partial/\partial x$ operator. And the differentations with respect to space x and time t are commutative, so:

$$\frac{\partial}{\partial x}\left(\frac{\partial v_x}{\partial t}\right) = \frac{\partial}{\partial t}\left(\frac{\partial v_x}{\partial x}\right). \tag{4.4}$$

Now for $\partial v_x/\partial x$, the deformation equation can be substituted in (4.3) to give:

$$-\frac{\partial^2 p}{\partial x^2} = \rho\frac{\partial}{\partial t}\left(-\frac{1}{K}\frac{\partial p}{\partial t}\right). \tag{4.5}$$

Rewriting gives us the 1-Dimensional wave equation:

$$\frac{\partial^2 p}{\partial x^2} - \frac{1}{c^2}\frac{\partial^2 p}{\partial t^2} = 0 \tag{4.6}$$

in which c can be seen as the velocity of sound, for which we have: $c = \sqrt{K/\rho}$.

This is the basic wave equation for one-dimensional acoustic waves. Equally well, we can derive from the same two equations (4.1) and (4.2) (see also *EXERCISES*) that the particle velocity also satisfies the wave equation:

$$\frac{\partial^2 v_x}{\partial x^2} - \frac{1}{c^2}\frac{\partial^2 v_x}{\partial t^2} = 0 \tag{4.7}$$

where c is the same as in the wave equation of the pressure.

The solution to the wave equation for the pressure is:

$$p(x,t) = s(t \pm x/c) \tag{4.8}$$

where $s(t)$ is some function. Note the dependency on space and time via $(t \pm x/c)$, which denotes that it is a travelling wave, and behaves as a direct wave as discussed in chapter 2. The sign in the argument is depending on which direction the wave travelling in.

In the above, we gave an expression for the pressure, but one can also derive the equivalent expression for the particle velocity v_x. To that purpose, we can use the equation of motion as expressed in equation (4.2):

$$\frac{\partial v_x(x,t)}{\partial t} = -\frac{1}{\rho}\frac{\partial p(x,t)}{\partial x} \tag{4.9}$$

When we subsitute the solution for the pressure from above (equation (4.8)), we get for the negative sign:

$$\begin{aligned} \frac{\partial v_x}{\partial t} &= -\frac{1}{\rho}s'(t - x/c)\frac{-1}{c} \\ &= s'(t - x/c)\frac{1}{\rho c}. \end{aligned} \tag{4.10}$$

We have now an expression for the first derivative of the particle velocity with respect to time; in order to get the particle velocity itself, we have to integrate it with respect to time, taking into account that the particle velocity is a function of space (x) *and* time (t). So formally the particle velocity is:

$$v_x(x,t) = s(t - x/c)\frac{1}{\rho c} + f(x), \tag{4.11}$$

where $f(x)$ is any function that depends solely on x (and not on t). (You can check that this is a solution by substituting this into equation 4.10.) We assume $f(x) = 0$. And we can recognize $s(t - x/c)$ as being the solution for the pressure (see equation (4.8)), so then it can be seen that the particle velocity is a scaled version of the pressure:

$$v_x(x,t) = \frac{p(x,t)}{\rho c}. \tag{4.12}$$

The scaling factor is (ρc), being called the *seismic impedance*.

4.3 Reflection and transmission at boundaries

In this section, we will consider what happens at a boundary between two layers with different mechanical properties. Then we can show which characteristics are responsible

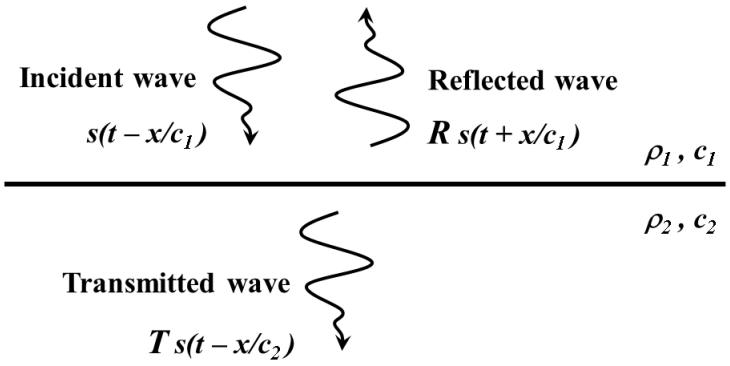

Figure 4.1: Reflection and transmission at boundary between two media with different properties.

for, e.g., a reflection. To that end, we will focus on the basic physical and theoretical principles of reflection and transmission in this section. The basic equations describing wave motion in one direction will be used to derive an expression for the reflection and transmission coefficient at a boundary between two layers with different wave speeds and densities. In the previous section, the solution for the wave equation was given, i.e.:

$$p(x,t) = s(t \pm x/c). \tag{4.13}$$

Let us consider figure (4.1). We defined a plane boundary between two regions with different wave speeds and mass densities. The boundary will reflect some of the energy back, and some will be transmitted. Above the boundary ($x < 0$), we will have a so-called incident wave with some amplitude $s(t)$. In addition, we have a reflected wave above the boundary, which is travelling in the opposite direction of the incident field. This reflected field has a scaled version of the amplitude of the incident field. This scaling factor is called R, which is called the reflection coefficient. Below the boundary ($x > 0$), we have a wave travelling in the same direction as the incident field, but has a scaled amplitude due to the transmission through the boundary. We call this amplitude T, which is the transmission coefficient. So, above the boundary ($x < 0$), we have:

$$p(x,t) = s(t - x/c_1) + Rs(t + x/c_1). \tag{4.14}$$

Notice the sign difference for the incident and the reflected wave, indicating that they travel in opposite directions. Below the boundary ($x > 0$), we have:

$$p(x,t) = Ts(t - x/c_2). \tag{4.15}$$

Notice that the wave speed is now c_2 since the wave is travelling in the medium below the boundary.

We have defined the reflection and transmission coefficient, but we still need to quantify them. This is achieved by posing the boundary conditions, which are that both the pressure and the particle velocity must be continuous across the boundary, i.e.:

$$\lim_{x\uparrow 0} p(x,t) = \lim_{x\downarrow 0} p(x,t) \tag{4.16}$$

$$\lim_{x\uparrow 0} v_x(x,t) = \lim_{x\downarrow 0} v_x(x,t) \tag{4.17}$$

The first boundary condition can be worked out directly from the solutions for the pressure. However, for the second boundary condition, we need to use the equation of motion, which is:

$$\frac{\partial v_x(x,t)}{\partial t} = -\frac{1}{\rho}\frac{\partial p(x,t)}{\partial x} \tag{4.18}$$

Working out the first derivatives of the particle velocity for the the regions above and below the boundary, we obtain respectively:

$$\frac{\partial v_x(x,t)}{\partial t} = \frac{1}{\rho_1 c_1} s'(t - x/c_1) - R\frac{1}{\rho_1 c_1} s'(t + x/c_1) \quad \text{for } x < 0 \tag{4.19}$$

$$\frac{\partial v_x(x,t)}{\partial t} = T\frac{1}{\rho_2 c_2} s'(t - x/c_2) \quad \text{for } x > 0 \tag{4.20}$$

Like in the determination of the impedance in the previous section, we can integrate these two equations with respect to time, assuming that there is no dependence on a function which is solely dependent on x:

$$v_x(x,t) = \frac{1}{\rho_1 c_1} s(t - x/c_1) - R\frac{1}{\rho_1 c_1} s(t + x/c_1) \quad \text{for } x < 0 \tag{4.21}$$

$$v_x(x,t) = T\frac{1}{\rho_2 c_2} s(t - x/c_2) \quad \text{for } x > 0 \tag{4.22}$$

We have obtained the desired expressions needed for the boundary condition on the particle velocity.

Now it is simply substituting the equations in the boundary conditions (4.16) and (4.17), which give:

$$1 + R = T \tag{4.23}$$

$$\frac{1}{\rho_1 c_1} - \frac{1}{\rho_1 c_1} R = \frac{1}{\rho_2 c_2} T. \tag{4.24}$$

Working this out, we obtain for the reflection and transmission coefficients R and T:

$$R = \frac{\rho_2 c_2 - \rho_1 c_1}{\rho_2 c_2 + \rho_1 c_1} \tag{4.25}$$

$$T = \frac{2\rho_2 c_2}{\rho_2 c_2 + \rho_1 c_1} \tag{4.26}$$

These are the desired expressions. First notice that we have expressions in terms of seismic impedances, which are the product of the wave speed with the mass density, i.e., ρc. Secondly, notice that the reflection coefficient is determined by the *contrast in seismic impedances of the different regions.*

4.4 Wave motion in an elastic solid

Stress

Here we will define *stress*. Stress can be defined as the force per unit area exerted on a body across an imaginary surface (see also Fig. 4.2). Since the dimension of stress is of a pressure, i.e., force per unit area, the quantities of stress are also given in the dimension of pressure, i.e., Pa. Therefore the stress can be seen as the equivalent of pressure in an (elastic) solid. One can discern normal stress as the stress perpendicular to a surface, and shear stress as the one parallel to a surface. The normal stress is also called compressional or tensile stress. Since a stress can be in any direction to a surface, the stress can be decomposed into components perpendicular and parallel to the surface. This decomposition matrix is also called the stress tensor. In formula form, this all can be written as:

$$\frac{\underline{F}}{\Delta S} = \underline{\underline{\tau}}\,\underline{n} \tag{4.27}$$

where F is the force, ΔS is the surface, $\underline{\underline{\tau}}$ is the stress tensor and $\underline{n}$ is the vector normal to the surface ΔS. When writing out the matrix of the stress, i.e., the stress tensor, in terms of the coordinates x; y and z, we get:

$$\underline{\underline{\tau}} = \begin{pmatrix} \tau_{xx} & \tau_{xy} & \tau_{xz} \\ \tau_{yx} & \tau_{yy} & \tau_{yz} \\ \tau_{zx} & \tau_{zy} & \tau_{zz} \end{pmatrix} \tag{4.28}$$

Some of these factors are visualized in Figure 4.3.

In order to see the equivalence with the acoustic case, consider the case that no shear stresses exist. Then the diagonal elements of the matrix are the only non-zero ones, and the stress matrix can be written as:

$$\underline{\underline{\tau}}_{\text{noshear}} = \begin{pmatrix} -p & 0 & 0 \\ 0 & -p & 0 \\ 0 & 0 & -p \end{pmatrix} \tag{4.29}$$

where p is the pressure. Notice that there is a minus sign since commonly the positive sign for pressure is for a compressional force, while for stress it is for a tensile force.

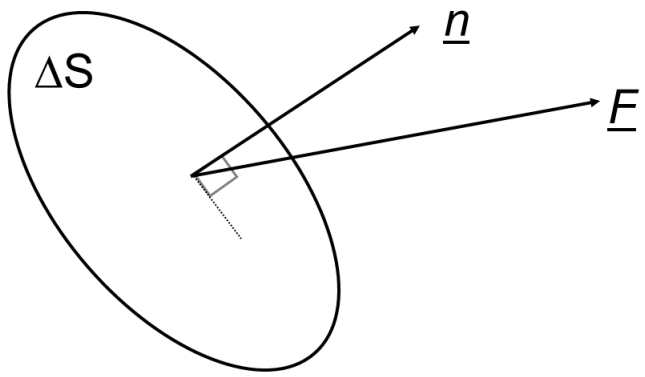

Figure 4.2: Definition of stress for a force working on a surface ΔS.

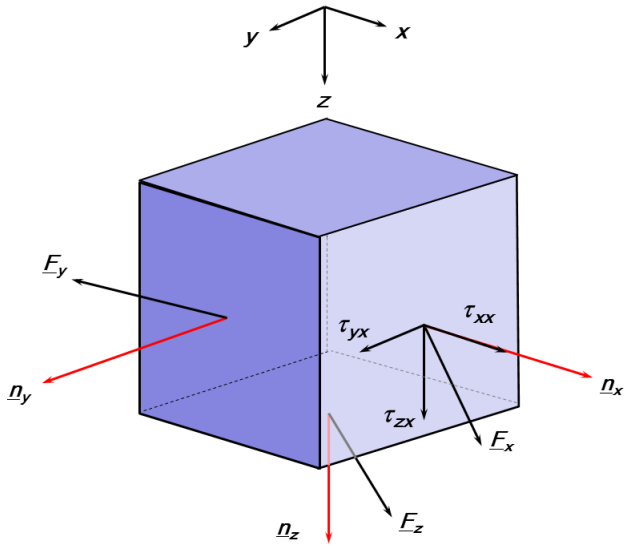

Figure 4.3: Definition of stress components for stresses working on a infinitesimal parallelopiped.

P-waves in an elastic solid

For 1-D wave motion in the x–direction, Hooke's law gives for the plane tensile stress τ_{xx} (see appendix F):

$$\frac{\partial \tau_{xx}}{\partial t} = (\lambda + 2\mu)\frac{\partial v_x}{\partial x} \tag{4.30}$$

where λ and μ are the so-called Lamé parameters. λ is the first Lamé parameter, and μ is the shear modulus; in 3-D, λ is related to the bulk modulus K via $K = \lambda + (2/3)\mu$. This equation is called the deformation equation for a P-wave in an elastic solid. Note that this equation has the same form as the deformation equation for acoustic waves (see eq.(4.1)).

Then applying Newton's law gives an equation nearly equivalent to the one for the acoustic case but now having tensile stress instead of pressure (see also appendix F):

$$\frac{\partial \tau_{xx}}{\partial x} = \rho\frac{\partial v_x}{\partial t} \tag{4.31}$$

This is the equation of motion for a P-wave. Combining the deformation equation and the equation of motion gives, as for the acoustic case, the wave equation for the stress, assuming the density being constant:

$$\frac{\partial^2 \tau_{xx}}{\partial x^2} - \frac{1}{c_P^2}\frac{\partial^2 \tau_{xx}}{\partial t^2} = 0 \tag{4.32}$$

where $c_P^2 = (\lambda + 2\mu)/\rho$ is the squared P-wave velocity. This wave equation describes the wave propagation for P-waves in an elastic solid.

S-waves in an elastic solid

Let us now consider shear stresses which will, as we shall see, result in a wave equation for S-waves. To that end, we consider 1-D displacement in the z-direction for a wave propagating in the x–direction for 1-D shear motion. The equivalent of Hooke's law for shear stress results in (see appendix F):

$$\frac{\partial \tau_{zx}}{\partial t} = \mu\frac{\partial v_z}{\partial x} \tag{4.33}$$

where τ_{zx} is the shear stress. This is the deformation equation for an S-wave.

Then applying Newton's law for a shear stress gives (see also appendix F):

$$\frac{\partial \tau_{zx}}{\partial x} = \rho\frac{\partial v_z}{\partial t} \tag{4.34}$$

which is the equation of motion for S-waves. Combining the deformation equation and the equation of motion gives the wave equation for the shear stress, assuming the density being constant:

$$\frac{\partial^2 \tau_{zx}}{\partial x^2} - \frac{1}{c_S^2}\frac{\partial^2 \tau_{zx}}{\partial t^2} = 0 \tag{4.35}$$

where $c_S^2 = \mu/\rho$ is the squared S-wave velocity. This wave equation describes the wave propagation for S-waves in an elastic solid.

With respect to the (1-D) reflection coefficients for P- and S-waves at the boundary of two elastic solids: the derivations go similar as for the acoustic case, as worked out in the previous section:

- For P-waves, we require the continuity of the tensile stress τ_{xx} and the particle velocity v_x at the interface, and
- For S-waves we require the continuity of the shear stress τ_{zx} and the particle velocity v_z at the interface.

The resulting expressions for the reflection and transmission coefficient are the same as for the acoustic case, only now the velocities are for the elastic solid. (See *EXERCISES*)

4.5 *EXERCISES*

1. From the deformation equation and the equation of motion for acoustic waves (equations 4.1 and 4.2) show that the particle velocity v_x also satisfies the wave equation, i.e., equation 4.7.
2. Here we look at deriving the wave equation in a different way:
   - Show that from substituting the deformation equation (4.1) and the equation of motion (4.2) in the commutative property for the pressure as expressed in equation 4.4, the wave equation for the particle velocity is nicely obtained.
   - In the same way show that from substituting the deformation equation (4.1) and the equation of motion (4.2) in the commutative property for the *particle velocity*, the wave equation for the pressure is nicely obtained.
3. From the deformation equation and the equation of motion for shear waves (equations 4.33 and 4.34) show that the particle velocity v_z also satisfies the wave equation.
4. Here we consider shear waves:
   - How can the solution of the wave equation for the shear stress (equation 4.35) be written?
   - Based on this solution, *derive* the solution for the particle velocity v_z.
   - What is the difference between the two? And how is that called?
5. Here we consider shear waves arriving at an interface:

- When we look at a reflection and transmission across an interface between two materials: we have an incident S-wave coming from above. How would you write the wave field (shear stress and particle velocity) above the interface? And how below?
- At the interface, we require the continuity of the shear stress and particle velocity, as given above: from this, *derive* the reflection and transmission coefficients.

Chapter 5

Processing of Seismic Reflection Data

In this chapter, the steps are discussed of how to obtain a seismic reflectivity image from seismic records. Here, we assume that the records only contain reflections. We will discuss the main basic steps of a processing sequence, commonly used to obtain a seismic image and common to seismic data gathered on land (on-shore) as well as at sea (off-shore): CMP sorting, velocity analysis and NMO correction, stacking, (zero-offset) migration and time-to-depth conversion.

5.1 Seismic processing and imaging

A goal of exploration seismics is obtaining structural subsurface information from seismic data. In the chapter on Instrumentation (Chapter 3) we discussed the elements which do *NOT* say anything about the earth itself. *Seismic processing* concerns itself with removing or compensating for the effects of waves that propagate through the earth such that an *image* is obtained from the subsurface.

Wave propagation versus signal to noise ratio

We can consider two ways of introducing seismic processing to a newcomer. One is in terms of wave theory. We have to understand the physical processes that are involved all the way from the seismic source, through the subsurface, to the seismic recording instrument. We have to try to obtain only those features which are due to the structure of the subsurface and not related to other features. For instance, we want to know the source signal we put into the earth such that we can compensate for it from our data later: the structure of the subsurface does not depend on the source we use. In this way we can remove or suppress certain unwanted features in the image.

Another way of introducing seismic processing to a newcomer is more in terms of the

image we obtain: signal-to-noise ratio and resolution. In order to see the image we need to have at least a moderate signal-to-noise ratio. We would like this ratio to be as large as possible by trying to suppress unwanted features in the final image. The other aspect of the final seismic image is the resolution: we would like the image to be as crisp as possible. As you may know, these two aspects cannot be seen separately. Usually, given a certain data set, an increase in signal-to-noise ratio decreases the resolution (as information is stacked together), and also an increase in resolution (by correctly incorporating wave theory) has normally the consequence that the signal-to-noise ratio gets worse. In seismic processing we would like to obtain the optimum between the two: a good, although not perfect, signal-to-noise ratio with a good resolution.

In these notes we take the view of trying to understand each process in the wave problem, and try to find ways to cope with them. In this way we hope at least to increase the signal-to-noise ratio, perhaps at some costs with respect to resolution. This is a very important characteristic of raw seismic data: it has a very poor signal-to-noise ratio, and it needs a lot of cleaning up before the reflection image of the subsurface can be made visible. It is along this line that we will discuss seismic processing: trying to understand the physical processes. Sometimes, we will refer to the effect it can have on the total signal in terms of signal-to-noise ratio and resolution.

With seismic processing, we have many physical processes we have to take into account. Actually, there are too many and this means that we must make simplifying assumptions. First, we only look at reflected energy, not at critically refracted waves, direct body waves, surface waves, etc. Of course, these types of waves contain much information of the subsurface (e.g. the surface waves contain information of the upper layers) but these waves are treated as noise. Also critically refracted waves contain useful information about the subsurface. That information is indeed used indirectly in reflection seismics via determining static corrections, but in the seismic processing itself, this information is thrown away and thus treated as noise. Another important assumption in processing is that the earth is not elastic, but acoustic. In conventional processing, we mostly look at P-wave arrivals, and neglect any mode-conversion to S-waves, and even if we consider S-waves, we do not include any conversions to P-waves. Some elastic-wave processing is done in research environments, but are still very rarely used in production. Money is better spent on 3-D "P-wave" seismics, rather than on 2-D "elastic" seismics; 3-D seismics with three-component sources and receivers are still prohibitively expensive in seismic data acquisition.

As said previously, the conventional way of processing is to obtain an image of the primary P-wave reflectivity, so the image could be called the "primary P-wave reflectivity image". All other arrivals/signals are treated as noise. As the name "primary P-wave reflectivity" suggests, multiples are treated as noise (as opposed to "primaries"); S-wave are treated as noise (as opposed to P-waves); refractions are treated as noise (as opposed to reflectivity). Therefore, we can define the signal-to-noise ratio as:

$$\frac{S}{N} = \frac{\text{Signal}}{\text{Noise}} = \frac{\text{Primary P-wave Reflection Energy}}{\text{All but Primary P-wave Reflection Energy}} \tag{5.1}$$

It can be seen now that processing of seismic data is to cancel out and/or remove all the energy which is not primary P-wave reflectivity energy, and "map" the reflectivity in depth from the time-recordings made at the surface. In terms of total impulse response of the earth $G(x, y, t)$, we want to obtain that part of the impulse response of the earth which is due to primary P-wave reflections:

$$G(x, y, t) \overset{\text{Processing}}{\rightarrow} G_{\text{primary,P-wave,reflectivity}}(x, y, z) \tag{5.2}$$

Making the seismic image: seismic velocity

The most important information that must be added to the data, is the *seismic velocity*. This is crucial for obtaining a proper image. In this chapter it is discussed how to obtain a first estimate of the seismic velocities of the subsurface, and how to use this information to make the final image. The problem can also be seen as being information we measure at the surface, which is a function of *time*, is mapped to the correct position in *depth*. In other words, we want to convert "time"-data to "depth"-data.

In this chapter, we will look at a basic processing sequence to obtain a seismic image from the raw seismic data, containing only reflections. The steps that will be considered here are common to seismic processing of data gathered on land (on-shore) as well as at sea (off-shore). They are: CMP sorting, velocity analysis and NMO correction (invoking velocities for imaging), stacking and migration (again using velocities for focussing the energy). Although this is a basic processing sequence, it does not mean that this will always give a good image: on land topography effects and the first layer can be the largest problem and have to be dealt with separately; at sea the source wavelet is not always a clean one and one has to compensate for this effect via so-called signature deconvolution.

5.2 Sorting of seismic data

Common-shot and common-receiver gathers

When data is shot in the field, we record the shots sequentially. So by a record we mean all the recordings from the sensors for a single shot experiment. Normally, the measurement for one source at one receiver location is called a trace, which is a time series of reflections. It is obvious that for each shot we will order these recordings (traces) by increasing (or decreasing) offset. The offset is defined as the distance from source to receiver. A simple simulated example of such a shot is given in figure 5.1. In this figure on the left hand side the ray paths from source to the receivers of the seismic waves are shown. Note that due to the different velocities in the different layers, the ray paths are bent according to Snell's law. For this record, one shot consists of the explosion from one charge of dynamite (supposed it is measured on land). The data is stored in the recording instrument and then put onto a magnetic tape, record by record.

When the next shot is fired, we do the same, record with the instrument and then write the data onto tape. We say that the data is shot ordered. A section as shown in

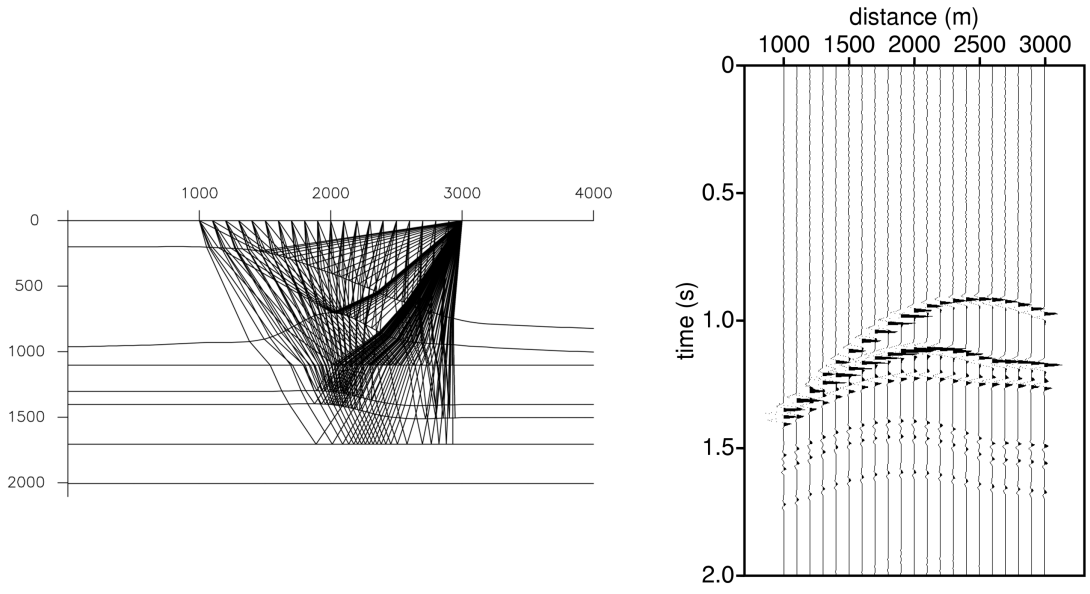

Figure 5.1: Shot gather measurement.

figure 5.1 is commonly called a *common-shot gather,* or common-shot panel: we show the recorded wave fields for one shot.

It can be guessed that if we talk about shot ordered data, we could also have receiver ordered data. This is indeed the case. One could get all the shots together, of course in an increasing shot position, belonging to one receiver position. Such a gather is called a *common-receiver gather (or panel).* However, this assumes that during acquisition the same receiver position is covered by different shots. In practice, we often make use of reciprocity: interchanging source and receiver will give exactly the same response (if the directional properties of the source and receiver can be considered identical). In fact figure 5.1 can also be considered as a common-receiver gather, where all ray paths from different shots come together at one receiver position.

Why should we need these distinctions? A nice feature about a common-shot gather is to see whether a receiver position has a higher elevation than its neighbors and thus gives an extra time shift in its record. This effect is called "statics". Therefore common-shot gathers are good for detecting geophone statics. In the same way, we can see on common-receiver gathers whether a shot was set deeper than the neighboring shot positions, and therefore common-receiver gathers are good for detecting shot statics.

Common-midpoint gathers

The way of organizing the data in common-shot gathers is just a consequence of the

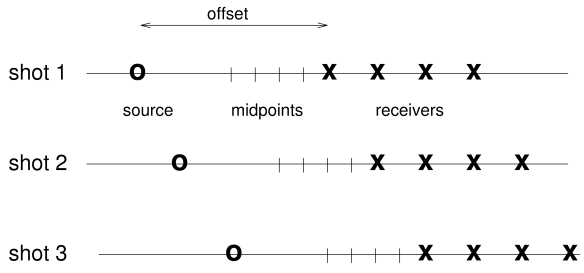

Figure 5.2: Midpoint definition in between sources and receivers.

logistics in the field, but for some processing steps it is not a convenient sorting the data. A commonly used way of sorting the data is in *common-midpoint gathers.* A mid-point is here defined as the mid-point between source and receiver position. An illustration of the mid-point is given in figure 5.2. We gather those traces that have a certain midpoint in common, like in figure 5.2, the record from receiver 3 due to shot 1, and the record from receiver 1 due to shot 2. Once we have gathered all the traces with a common-midpoint (CMP) position, we have to decide how to order these records for one CMP, and the logical choice is to order them by increasing (or decreasing) offset. A gather for one mid-point position with the traces for increasing (or decreasing) offsets is called a common-midpoint gather (or panel). Figure 5.3 shows a CMP gather for the same subsurface model as figure 5.1.

For what reason is the common-midpoint gather convenient? The most important one is for stacking which we shall discuss in one of the next sections. Suppose the earth would consist of horizontal layers as depicted in figure 5.4. Then the geometrical arrival from shot to receiver all reflect right below the midpoint between the source and receiver, and thus the reflection points in the subsurface then only differ in depths. With other words, all the reflections measured at the different offsets in a CMP gather carry information on the same subsurface points (below the midpoint position). If we would make a correction for the offset dependence of the traveltime for each trace, the reflections from the same place would arrive at the same time for all the traces, and thus we could add the traces together to increase the signal-to-noise ratio. This process is called NMO correction and stacking respectively, as will be discussed later. This argumentation is not valid for common-shot gathers since the reflection points in the subsurface do not coincide for each trace (for a horizontally layered earth). For a laterally varying medium also for a CMP the reflection points do not coincide, but they are coming still from a small region, as shown in figure 5.3, and the stacking procedure will often still give acceptable results.

Common-offset gathers

As can be expected, we can also form a *common-offset gather,* a gather in which we collect all those source-receiver pairs that have a certain offset in common. Usually, we shoot with fixed distances between source and receivers, and so we will have as many traces

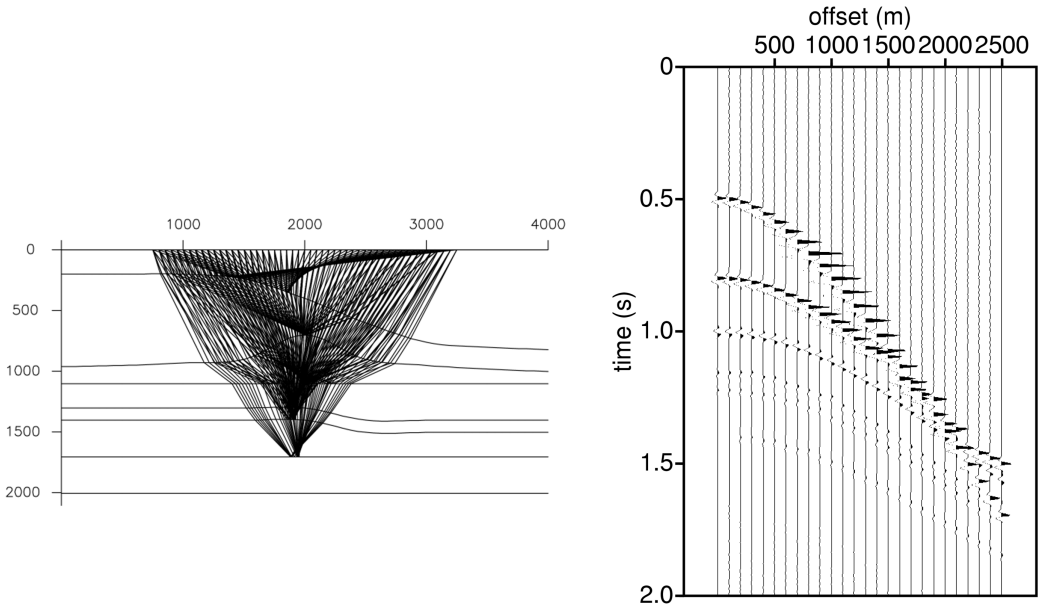

Figure 5.3: Common-midpoint gather.

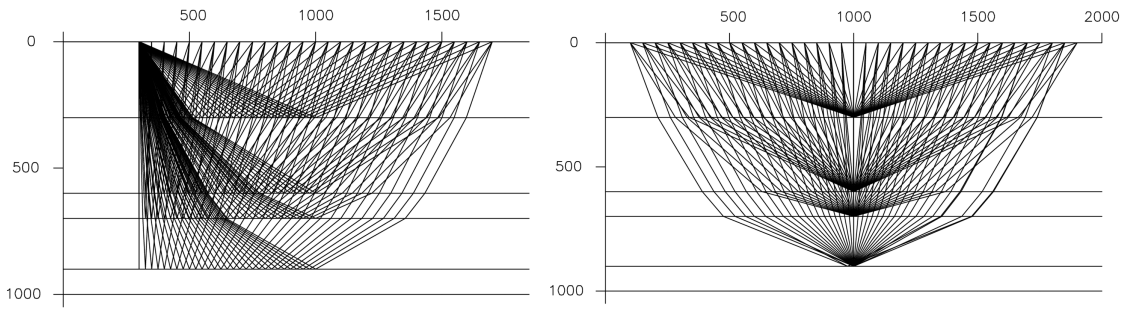

Figure 5.4: Common-shot and common-midpoint gather for horizontally layered earth.

in our common-offset gather as there are shots, thus often quite a large amount. For the model of figure 5.1 and figure 5.3 the zero-offset configuration (i.e. source and receivers at the same positions) is shown in figure 5.5. Note that in the zero-offset section the general structures can already be recognized. Common offset gathers are used in prestack

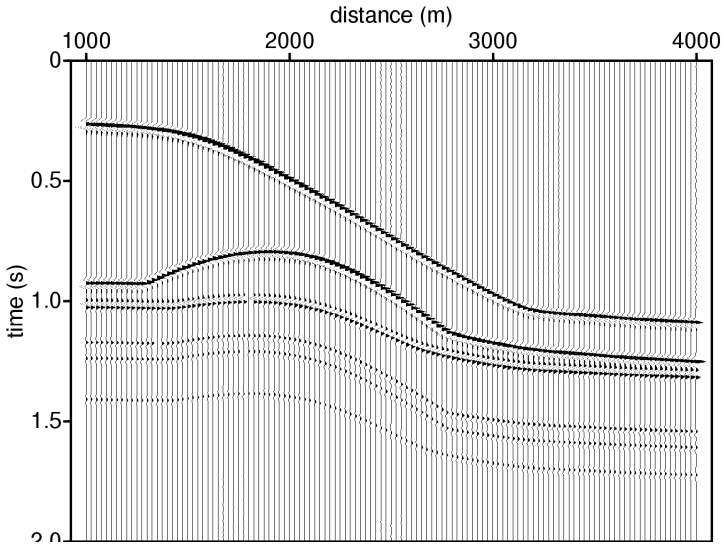

Figure 5.5: Zero-offset gather.

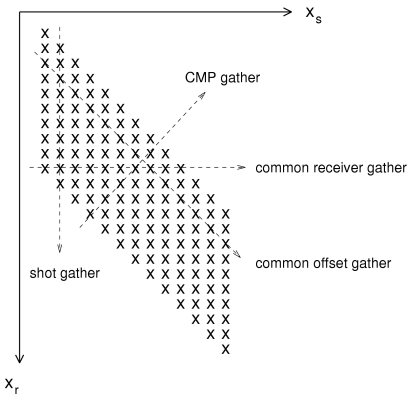

Figure 5.6: Relation between different sortings of seismic data.

migration algorithms since it can give a check on velocities. Migrating a common-offset gather for a small offset should give the same image as a migration of such a gather for a large offset, otherwise the velocity used in the migration is not the right one.

A graph combining all this information is given in figure 5.6. Here we assumed we have recorded along a line in the field, which we call the x-direction. Also, we have assumed

that we have 10 receiver positions with the first receiver at the source location (i.e. at zero offset). On the horizontal axis we have plotted the x–coordinate of the source (x_s), while on the vertical axis we have put the x–coordinate of the receiver (x_r). Then, each grid point determines where a recording has taken place. In this graph a column represents a common-shot gather, and a horizontal line a common-receiver gather. A common-midpoint gather is given by the line $x_s + x_r = constant$, which is a line at 45 degrees with a negative slope. A common-offset gather is given by the line $x_s - x_r = constant$, which is a line of 45 degrees but now with a positive slope.

What can be noticed in the graph, is that we started out with 10 receiver positions for each shot, while the CMP gather contains only 5 traces. Why that so? This can be seen in figure 5.2. When we shift one source position to the next, we actually shift *two* CMP's because the distance between each CMP is half the source spacing. So a factor two is involved. On the other hand there are twice as many CMP gathers, as the total of traces in the survey is of course constant.

In figure 5.6 we assumed the spacing between the shot positions and the receiver positions were the same but this does not need to be so. This also influences the number of traces in a CMP. The number of traces in a CMP is called the *multiplicity* or the *fold*. It can be shown easily that the multiplicity M is:

$$M = \frac{N_r}{2\Delta x_s/\Delta x_r} = \frac{L_r}{2\Delta x_s} \tag{5.3}$$

in which N_r is the number of receivers per shot, Δx_s is the spacing between the shot positions, Δx_r is the spacing between the receivers and L_r is the length of the receiver line ($=N_r\Delta x_r$).

In the above argumentation there is still one assumption made, and that is that the earth is horizontally layered. When the earth is not like that, the reflection points do not coincide any more, see figure 5.3. Still, the results obtained with this assumption are very good, it only gets worse results when the dips of the layers of the earth are becoming steep. We will come to that later on when discussing stacking.

5.3 Normal move-out and velocity analysis

NMO curve for single interface

The most important physical constant needed for obtaining an accurate image of the subsurface, is the velocity of the medium. We record our data at the surface *in time,* and what we wish to obtain is an image of the subsurface *in depth.* The link between time and depth is of course the wave velocity. Unfortunately, it is not so easy to obtain a good velocity model and this is often an iterative process. In this section we will discuss the effect of the velocity on the obtained data. We will first discuss some simple models in order to understand the features we can encounter in real data. As a consequence of this,

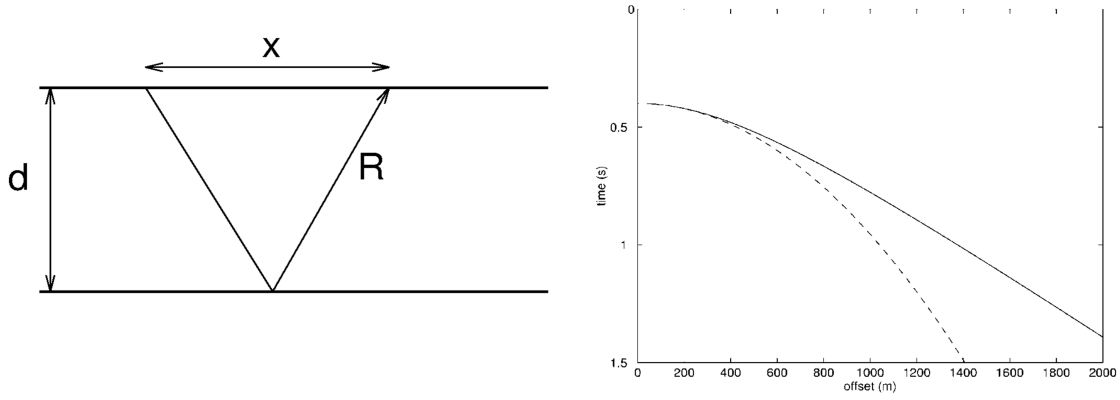

Figure 5.7: a) Distances in a subsurface model with one flat reflector. b) NMO curve for geometry of a) with depth 300 m and velocity of 1500 m/s. The dashed line is the parabolic approximation of the hyperbola.

we will discuss which operations have to be applied to the data in order to obtain the desired information. We assume here that we deal with a CMP gather.

Let us first consider the reflection from a single interface as depicted in figure 5.7. The time for the geometrical ray from source to receiver is given by:

$$T = \frac{R}{c} = \frac{(4d^2 + x^2)^{1/2}}{c} \tag{5.4}$$

in which x is the source-receiver distance, R is the total distance traveled by the ray, d is the thickness of the layer and c is the wave speed. When we write $2d/c$ as T_0, then we can write this as:

$$T = T_0 \left(1 + \frac{x^2}{c^2 T_0^2}\right)^{1/2} \tag{5.5}$$

note that this function describes a hyperbola. We can see that we have an extra time delay due to the factor $x^2/(c^2T_0^2)$. The extra time delay is called the Normal Move Out, abbreviated to NMO. This extra term is solely due to the extra offset of the receiver with respect to the source; at coincident source-receiver position this term is zero. Often, the square-root term in this equation is approximated by its one-term Taylor series expansion, i.e.:

$$T \simeq T_0 + \frac{x^2}{2c^2 T_0}. \tag{5.6}$$

Figure 5.7b shows the traveltime curve for a layer of 300 meter depth and a velocity of 1500 m/s. The dashed line in this figure shows the parabolic approximation according to equation (5.6).

In seismic processing we are not interested in the extra time delay due to the receiver position: the image of the subsurface should be independent of it. The removal of the extra time delay due to NMO is called the *NMO correction.*

NMO curve for more than one interface

Let us now move to a model with two interfaces, as depicted in figure 5.8. We call the source-receiver distance x, the horizontal distance the ray has traveled in the second layer x_2, the wave speed in the first layer c_1, and in the second c_2, the thickness of the first layer d_1, and of the second d_2. Then the traveltime from source to receiver is given by:

$$T = \frac{\left((x-x_2)^2+4d_1^2\right)^{1/2}}{c_1} + \frac{\left(x_2^2+4d_2^2\right)^{1/2}}{c_2} \tag{5.7}$$

$$= \frac{2d_1}{c_1}\left(1+\frac{(x-x_2)^2}{4d_1^2}\right)^{1/2} + \frac{2d_2}{c_2}\left(1+\frac{x_2^2}{4d_2^2}\right)^{1/2} \tag{5.8}$$

$$= T_1\left(1+\frac{x_1^2}{T_1^2c_1^2}\right)^{1/2} + T_2\left(1+\frac{x_2^2}{T_2^2c_2^2}\right)^{1/2}, \tag{5.9}$$

in which T_1 and T_2 are the zero-offset traveltimes through the first and second layer respectively, and $x_1 = x - x_2$. The problem with this formula is that, if we assume that c_1 and c_2, are known, we do not know x_2. Therefore we cannot directly use this expression to describe the move-out behaviour of this two-reflector model.

In order to tackle this, we first expand the square-root terms in equation (5.9) in a Taylor series expansion as we did for the one-interface case:

$$T \simeq T_1 + \frac{x_1^2}{2T_1c_1^2} + T_2 + \frac{x_2^2}{2T_2c_2^2}. \tag{5.10}$$

and we square this equation in order to obtain:

$$T^2 = (T_1+T_2)^2 + (T_1+T_2)\left(\frac{x_1^2}{T_1c_1^2}+\frac{x_2^2}{T_2c_2^2}\right) + O(x^4). \tag{5.11}$$

In this equation, we still have the distances x_1 and x_2 present. A relation between x_1 and x_2 can be found using Snell's law at the interface, being:

$$\frac{\sin\alpha}{c_1} = \frac{\sin\beta}{c_2}, \tag{5.12}$$

where α and β are the angles of the ray with the normal in layer 1 and 2 respectively, when crossing the first interface (see also figure 5.8). We make an approximation for small angles for which $\sin\alpha \approx \tan\alpha$ and $\sin\beta \approx \tan\beta$, such that equation (5.12) becomes:

$$\frac{x_1}{2d_1c_1} \approx \frac{x_2}{2d_2c_2}, \tag{5.13}$$

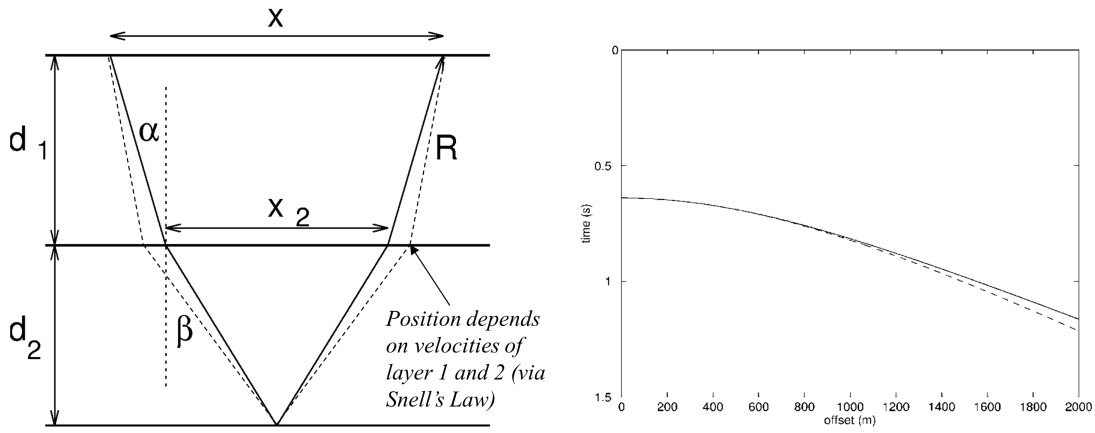

Figure 5.8: a) Distances in a subsurface model with two flat reflectors. b) NMO curve for second reflector with depth 300 m of each layer and velocities of 1500 m/s and 2500 m/s in the first and second layer respectively. The dashed line is the hyperbolic approximation of the traveltime curve.

or

$$\frac{x_1}{T_1 c_1^2} \approx \frac{x_2}{T_2 c_2^2}. \tag{5.14}$$

Writing this as $x_2 = (T_2 c_2^2)/(T_1 c_1^2) x_1$ and substituting this in $x_1 + x_2 = x$, we have:

$$x_1 = x \frac{T_1 c_1^2}{T_1 c_1^2 + T_2 c_2^2}, \tag{5.15}$$

Similarly for x_2, we obtain:

$$x_2 = x \frac{T_2 c_2^2}{T_1 c_1^2 + T_2 c_2^2}. \tag{5.16}$$

We can use equations (5.15) and (5.16) in the quadratic form of eq.(5.11) to obtain:

$$T^2 \approx (T_1 + T_2)^2 + (T_1 + T_2) x^2 \left(\frac{T_1 c_1^2 + T_2 c_2^2}{(T_1 c_1^2 + T_2 c_2^2)^2} \right) \tag{5.17}$$

$$\approx (T_1 + T_2)^2 + \frac{(T_1 + T_2)}{T_1 c_1^2 + T_2 c_2^2} x^2. \tag{5.18}$$

This equation is of the form:

$$T^2 = T_{\rm tot}(0)^2 + \frac{x^2}{c_{\rm RMS}^2}. \tag{5.19}$$

with $c_{\rm RMS}$ is what is called the root-mean-square velocity:

$$c_{\rm RMS}^2 = \frac{1}{T_{\rm tot}(0)} \sum_{i=1}^{N} c_i^2 T_i(0), \tag{5.20}$$

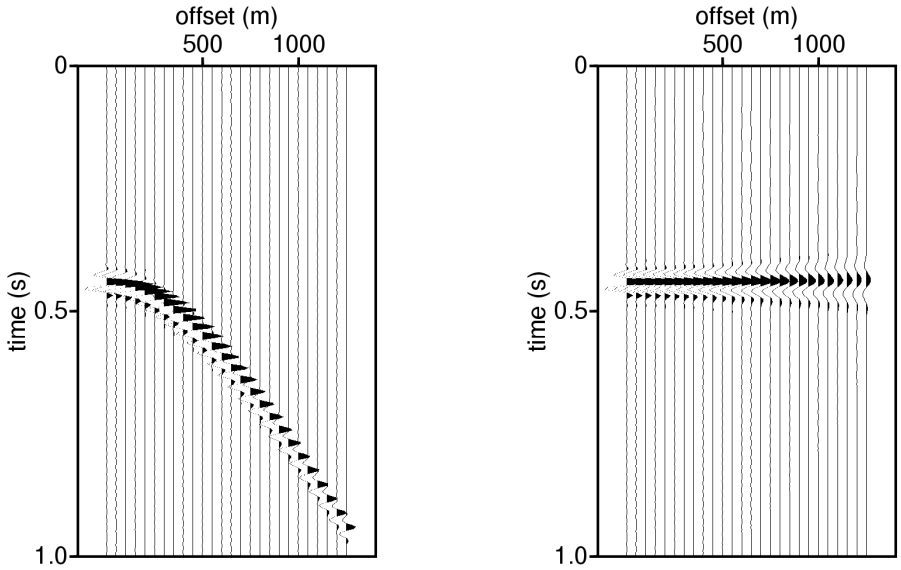

Figure 5.9: CMP gather with one reflection before and after NMO correction.

in which $T_i(0)$ denotes the zero-offset traveltime through the i–th layer; $T_{\rm tot}(0)$ denotes the total zero-offset time:

$$T_{\rm tot}(0) = \sum_{i=1}^{N} T_i(0). \tag{5.21}$$

We see here that with the assumptions made, a hyperbolic move-out for the interfaces below the first one is obtained. The approximation however is a very good one at small and intermediate offsets (for horizontal layers) but becomes worse when the offset becomes large. This effect can be observed in figure 5.8b, where the hyperbolic approximation of the second interface reflection is plotted with a dashed line.

Applying NMO correction

Then, how do we apply this NMO correction? First we have to determine the stacking (i.e. root-mean-square) velocities for each zero-offset time T_0 (see next section). Then, for each sample of the zero-offset trace will remain in its position. For a trace with offset x, we calculate the position of the reflection according to equation (5.19) and find the sample nearest to this time T. This sample is then time-shifted back with the time difference between T and T_0 (in fact it is mapped from time T to time T_0). In this simple scheme we have taken the sample nearest to the time T, but in general we can be much more accurate by using a better interpolation scheme. It is important to realize that with NMO we interpolate the data.

An artifact of the NMO correction is the NMO stretch. An example of this effect is shown in figure 5.9. How does this occur? We can see that the correction factor not only

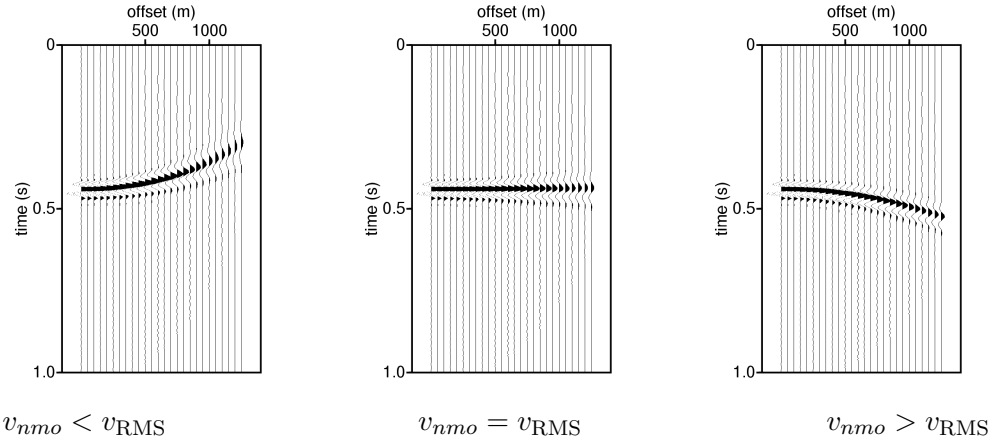

$v_{nmo} < v_{\mathrm{RMS}}$ $v_{nmo} = v_{\mathrm{RMS}}$ $v_{nmo} > v_{\mathrm{RMS}}$

Figure 5.10: CMP gather with one reflection after NMO correction with too low, correct and too high stacking velocities.

depends on the offset x and the velocity c_{RMS}, but also on the time T_0. So given a certain stacking velocity and offset, the correction $T - T_0$ becomes smaller when T_0 becomes larger. Thus, the correction is not constant along a trace, even if we have a constant offset and constant velocity. Also, we can see from this correction that the effect will become more prominent when the offset becomes larger as well. This effect is called NMO stretching.

Velocity estimation

In the application of the NMO correction, there is of course one big question: which velocity do we use? Indeed, we do not know the velocity on beforehand. Actually, we use the alignment of a reflection in a CMP gather as a measure for the velocity. Since, if the velocity is right, the reflection will align perfectly. However, when the velocity is taken too small, the correction is too large and the reflection will not align well; in the same way, when the velocity is chosen too big, the correction is too small, and again the reflection will not align. An example of these cases is given in figure 5.10.

As the earth is consisting of more than one interface, we need to determine the velocities, although they may just be root-mean square velocities for each layer. The goal is the same as in the case of just one interface: we would like all the reflections to be horizontally aligned. A systematic way of determining these velocities is to make common-midpoint panels which are each NMO corrected for a constant velocity. Then we can see for those velocities the reflector will align or not; usually the deeper the interface the higher the (root-mean-square) velocity. An example of such an analysis is given for a four reflector model (see figure 5.4) in figure 5.11.

Another way of determining velocities is via $t^2 - x^2$ analysis. For this analysis we have to pick the traveltimes for a certain reflector and plot them as a function of x^2. As we have seen with multiple interfaces, the slope of this curve should be $1/c_{\mathrm{RMS}}^2$, and thus we

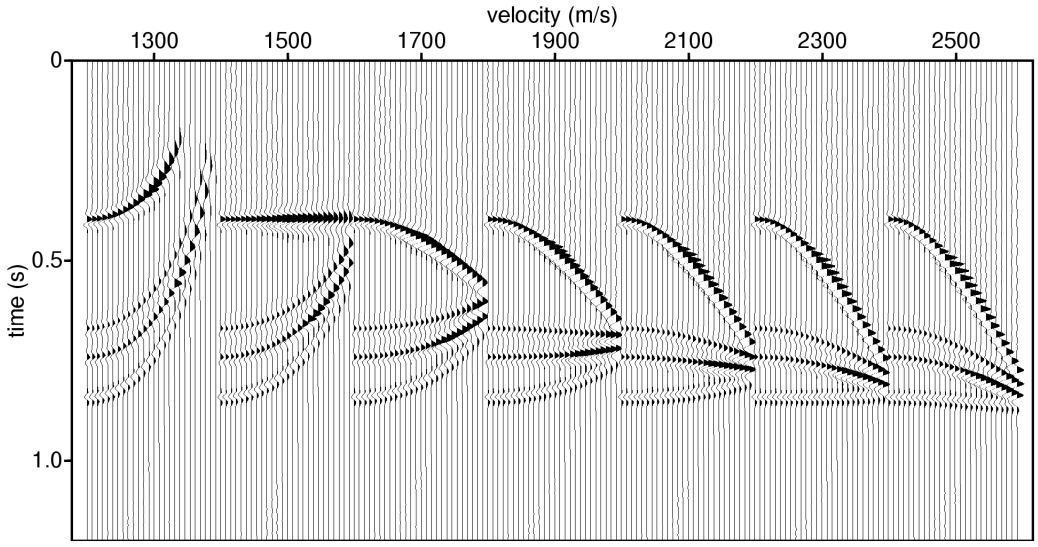

Figure 5.11: CMP gather NMO corrected with a range of constant NMO velocities from 1300 to 2700 m/s with steps of 200 m/s.

know the stacking velocity. This method can be quite accurate but depends on the quality of the data whether we are able to pick the reflection times from the data.

The most commonly used way of determining velocities is via the velocity spectrum, which has some relation to the aligning of reflectors. What we do with a velocity spectrum is that for a certain velocity, we correct the CMP gather and apply a coherency measure to the data. This gives us one output trace. Then, for a next velocity, we do the same. For a complete set of velocities, we plot these results next to each other, which is then called the velocity spectrum. On the vertical axis we then have the time, while on the horizontal axis we have the velocity. As an example we consider again the synthetic CMP gather in the model of figure 5.4, for which we calculate the semblance for velocities between 1000 m/s and 3000 m/s, see figure 5.12. The result we obtain is often displayed in contour mode or color mode.

As a coherency measure, the semblance is most often used. The semblance $S(t, c)$ at a time t for a velocity c is defined as:

$$S(t,c) = \frac{1}{M} \frac{\left(\sum_{m=1}^{M} A(x_m, t, c)\right)^2}{\sum_{m=1}^{M} A^2(x_m, t, c)}, \tag{5.22}$$

in which M is the number of traces in a CMP and A is the amplitude of the seismogram at offset x_m and time t after NMO correction with velocity c. For the definition of other coherency measures, the reader is referred to Yilmaz (1987, page 169, 173). Note that if an event is perfectly aligned with constant amplitude for all offsets, the semblance has value 1. Therefore, the semblance has always values between 0 and 1.

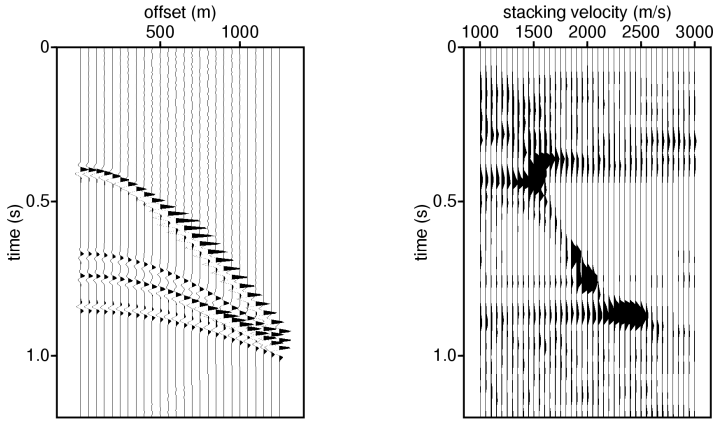

Figure 5.12: CMP gather with its velocity spectrum, using a semblance calculation with window length of 20 ms.

For a more extensive discussion on the velocity analysis we would like to refer to the book of Yilmaz (1987, pp.166—182).

5.4 Stacking

As stated before, an important goals in seismic processing is to increase the signal-to-noise ratio, and a very important, if not the most important, step towards this goal is stacking NMO-corrected CMP gathers. With stacking we add the NMO-corrected traces in a CMP gather to give one output trace; the word "stacking" comes from the old days when papers were stacked. A better nomenclature is perhaps horizontal stacking because we stack in the horizontal direction. This is in contrast to vertical stacking, which is recording the data at the same place from the same shot position several times and adding (i.e. averaging) these results. With (horizontal) stacking, we average over different angles of incidence of the waves, even in horizontally layered media. This means that we lose some information on the reflection coefficient since, as the reader may know, the reflection coefficient of an interface is angle-dependent. Therefore, the stacked section will contain *averaged* angle dependent reflection information.

In figure 5.13 a CMP gather with two -primaries and one multiple is shown before and after NMO correction in figures (a) and (b), respectively. What can be seen in the figure that after NMO, which is correct for the *primary* reflections, the multiple has not been corrected properly. For the multiple, the velocity that is chosen at that time, is too large compared to the velocity necessary for the multiple. Since the velocity is too large for the multiple, the correction is too small so the wrongly corrected multiple still shos some hyperbolic behaviour. The stacked result is obtained by adding all traces for a particular

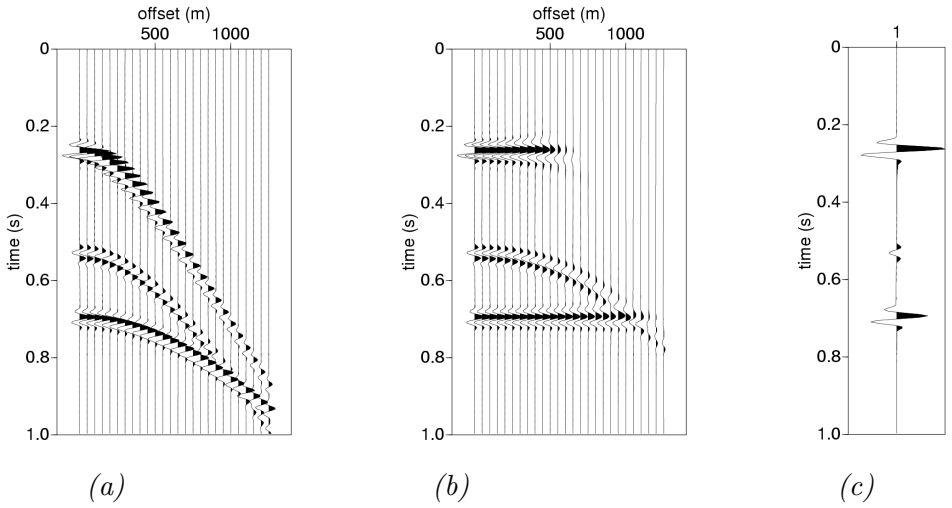

Figure 5.13: CMP gather with 2 primaries and 1 multiple before (a) and after (b) NMO correction and after stacking (c).

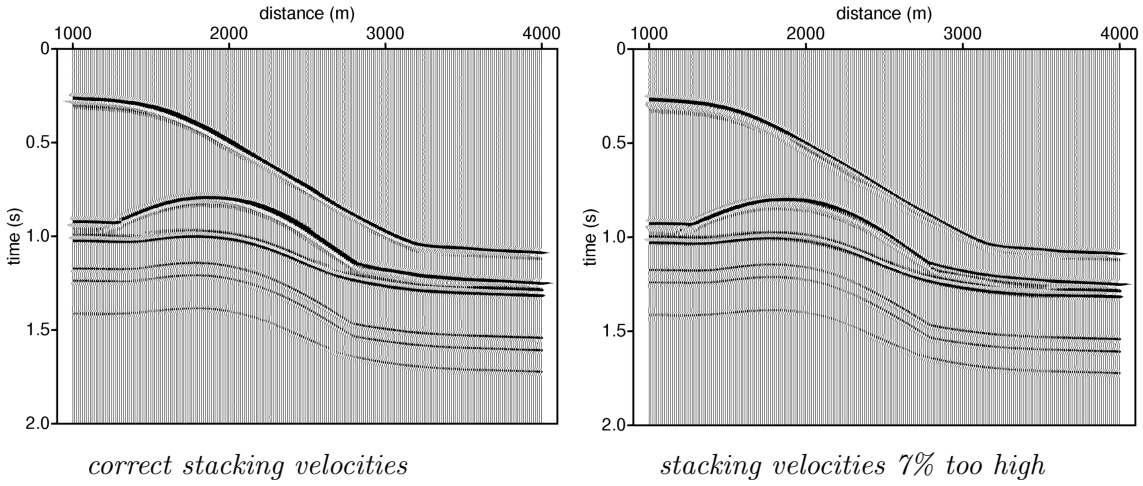

Figure 5.14: Stacked sections with correct and too high stacking velocities.

time, so we add along the horizontal direction. The result of this adding, or stacking, is given in figure (c). The resulting stacked trace shows a reduced multiple energy, which is a desired feature of the stack.

Although the signal-to-noise ratio is increased by stacking, we will also have introduced some distortions. We have already discussed the NMO stretch and the approximation with

the root-mean-square velocity. Therefore, when we add traces, we do not do a perfect job so we lose resolution. The effect of an erroneous velocity for the NMO is shown in figure 5.14, which shows a stacked section with the correct stacking velocities and with 7% too high stacking velocities for the data generated in the model of figure 5.1. One can see that the stacked trace is getting a lower frequency content and that the amplitudes are decreasing in some parts with the erroneous velocities. Note that a stacked section simulates a zero-offset section, but with much better signal to noise ratio. Compare therefore the stacked result to the zero-offset section of figure 5.5, which shows exactly the same region (1000 - 4000 m) in the model. Note the resemblance of the stack with the zero-offset section. Note also that the stack is twice as dense sampled in the trace direction, due to the fact that there are twice as many CMP positions as there are shot positions.

Finally, it should be emphasized that, with stacking, we reduce the data volume. The amount of data reduction is the number of added traces in a CMP gather. There are certain algorithms which are expensive to compute and are therefore applied to stacked data rather than on pre-stack data. An example of this is migration as shall be discussed in the next section.

5.5 Zero-offset migration

Introduction

Although we have removed some timing effects with the NMO correction, this does not mean that we have removed the wave effects: it is just one of many. We still need to "focus" the energy further. Migration deals with a further removal of wave phenomena via focussing in order to arrive at a section which is a true representation of the subsurface. After the NMO correction and stacking, we have only synthesized a zero-offset section, since we removed the offset dependence of the receiver position with respect to the source. That means, we have a section as if we did a seismic survey with source and receiver at the same place, thus zero-offset.

Let us now define migration, but will go into more detail in this subsection. Migration could be defined as :
Migration is the focussing process which results in a true image of the subsurface from primary-reflection data, assuming the velocity model is correct.
Equivalently, migration obtains the true image in (x, y, z) from data that are obtained in (x, y, t), where x, y and z stand for the two horizontal and vertical coordinate, respectively.

Some simple configurations, their zero-offset time sections and migration

Let us consider the simple example of a point diffractor in the subsurface. A point diffractor is like a "ball" in the subsurface: when a wave impinges on it, it scatters (reflects) energy back in all directions. When the source and receiver are at the same point at the surface, the receiver will only receive the ray that is scattered back as drawn in picture

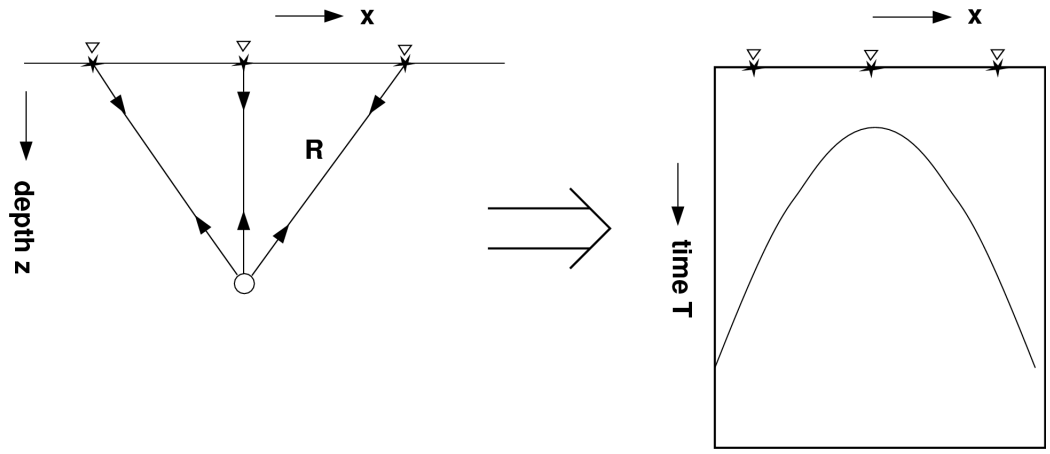

Figure 5.15: A diffractor (left) and its seismic response (right), a hyperbola in the zero-offset section.

5.15. So notice that even not right above the diffractor, we will receive energy. The (zero-offset) time section for a diffractor at position (x_d, z_d) is described by:

$$T^2 = \left[\frac{2R}{c}\right]^2 = T_d^2 + \frac{4(x - x_d)^2}{c^2}, \tag{5.23}$$

where R being the distance in a medium with a constant velocity c, T_d being the time $2z_d/c$ and x being the surface position of (zero-offset) source/receiver. This time section is a hyperbola (like for a *reflector* (!) in a CMP). As may be clear now, a zero-offset section is not a good representation of the subsurface, since that should be the left picture in figure 5.15. The process that converts the right picture (hyperbola) into the left picture (ball) is called *seismic migration*.

Let us consider a reflector. We can build up a reflector by putting point diffractors all along that reflector. When the spacing between the point diffractors becomes infinitely small, the responses become identical. This concept agrees with Huygens' principle. As example, consider four point diffractors, as depicted on the top left of figure (5.16). Each diffractor has the behaviour as discussed above, as can be seen on the right of figure (5.16), but the combination of the time responses shows an apparent dip. The actual dip goes, of course, through the apexes of the hyperbolae. In the bottom figures of (5.16), the number of point diffractors is increased to 8, 16 and 32. Note that for 32, the separate diffractors are hardly observable any more, and the response also looks more like a dipping reflector (with some end-point effects). Also here, the process that converts the right pictures into the left pictures is *seismic migration*.

Let us now look at a full dipping reflector, as shown in figure (5.17). Of course, it has some of the characteristics as we saw with the point diffractors, only with a full reflector we no longer see the separate hyperbolae. Actually, we will only see the apparent dip.

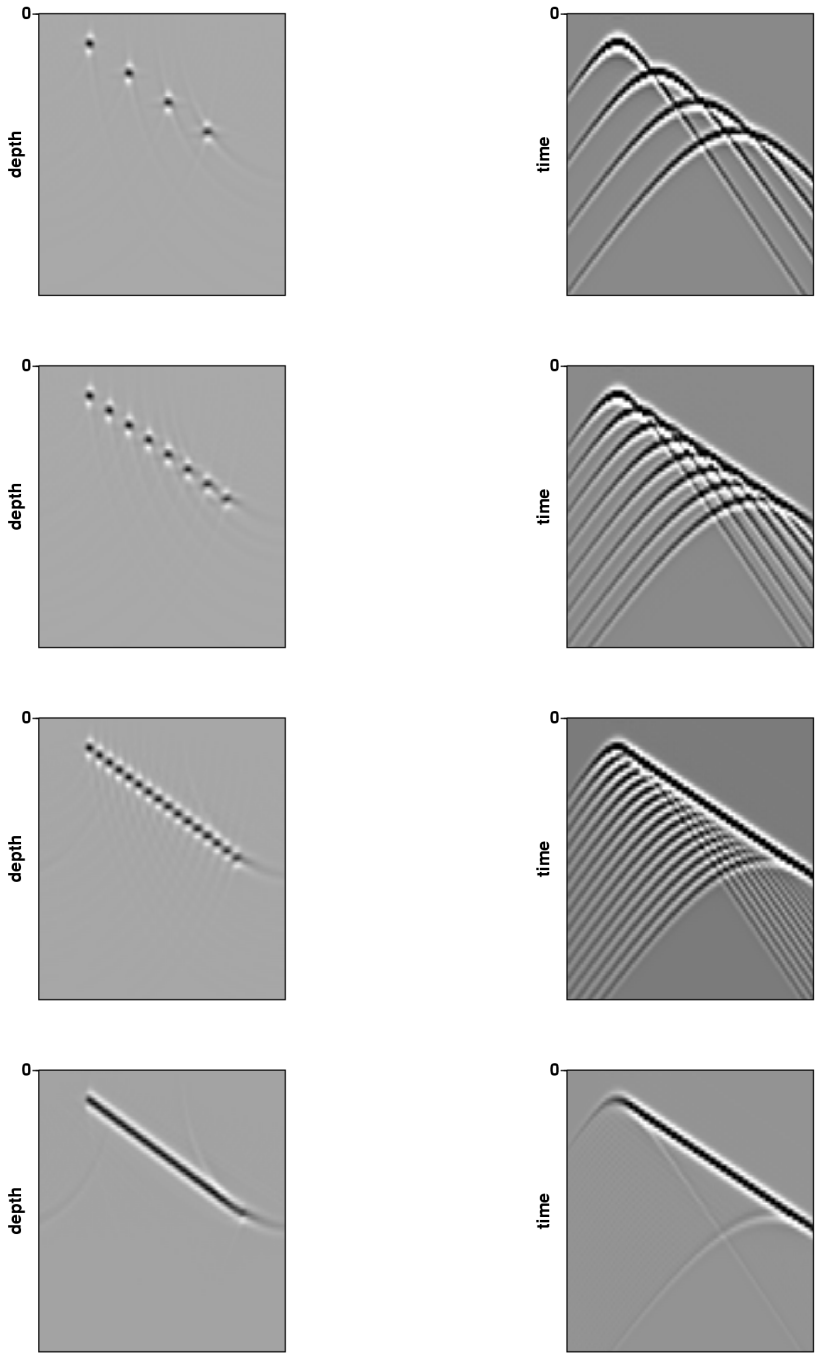

Figure 5.16: Point diffractors (left) and their seismic zero-offset responses (right). From top to bottom: 4, 8, 16 and 32 points.

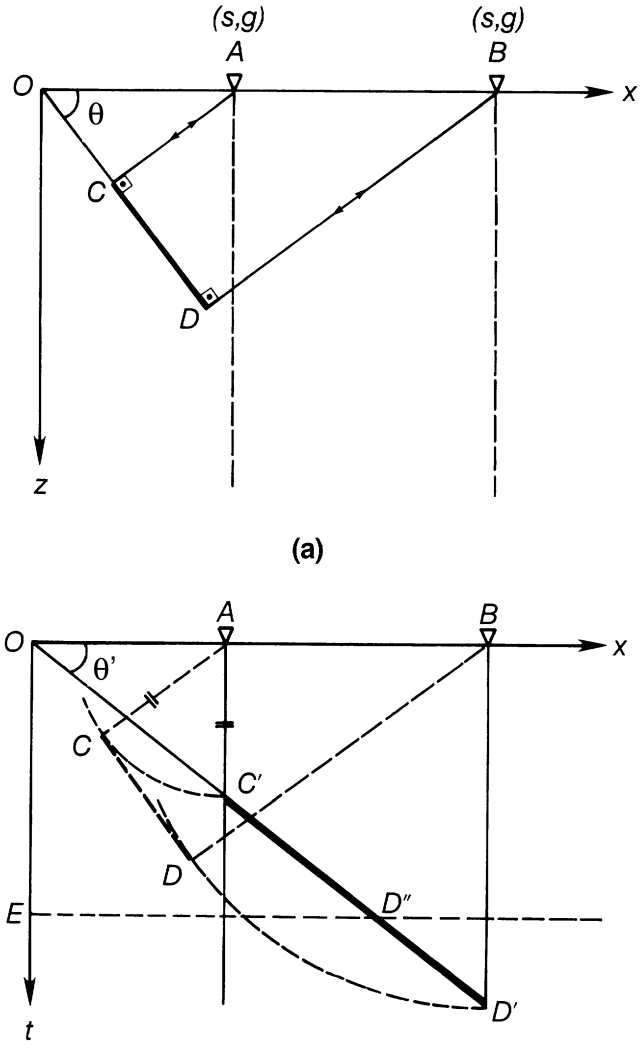

Figure 5.17: Relation between reflection points in depth (a) and traveltimes in zero-offset section (b) for dipping reflector (from Yilmaz, 1987, fig. 4-14).

For migration, as we saw with the point diffractors, we need to bring the reflection energy back to where they came from, namely the apex of each hyperbola. When connecting all the apexes of the hyperbolae, we get the real dip. This is also depicted in figure (5.17).

The next figure (5.18) quantifies the effect of migrating the energy to its actual location. In particular, compare the figures in the middle and and on the right: the difference is a factor $\cos\theta$, where θ is the dip of the reflector with the horizontal. The zero-offset traveltime at a certain x-value can be specified by $t_{ZO} = (2/c)x\sin\theta$, assuming that $x = 0$ corresponds to the point where the reflector hits the surface in figure 5.18a. The slope in

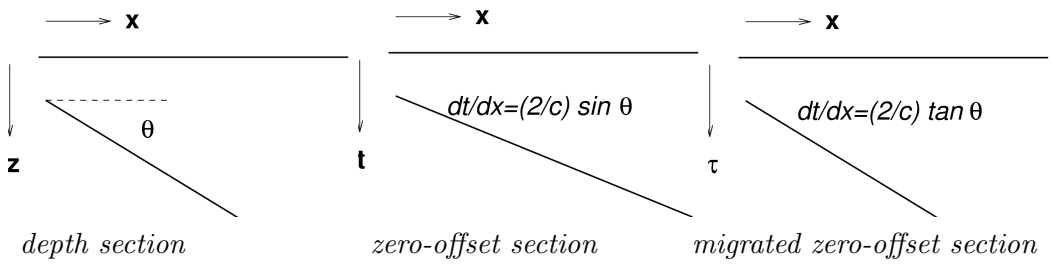

Figure 5.18: Migration increases dip in zero-offset section.

the zero-offset section is therefore $dt/dx = (2/c)\sin\theta$, see figure 5.18b. If this zero-offset section is migrated and the result is displayed in vertical time $\tau = z/c$, the resulting slope of the reflector is $d\tau/dx = (2/c)\tan\theta$ (figure 5.18c). Thus, migration increases the time dip in the section by $\cos\theta$ and thus reflectors in the unmigrated section are increased in their up-dip direction in the migrated section.

So far, we discussed some typical cases of point diffractors and a dipping reflector. From field data, the results are usually much more complicated. An example is given in figure 5.19. When we consider our typical configurations, we can (in a qualitative sense) understand the effect of migration of the real data set, as shown in figure 5.19. We can observe that all the diffractions in the stacked section are well focussed after the migration.

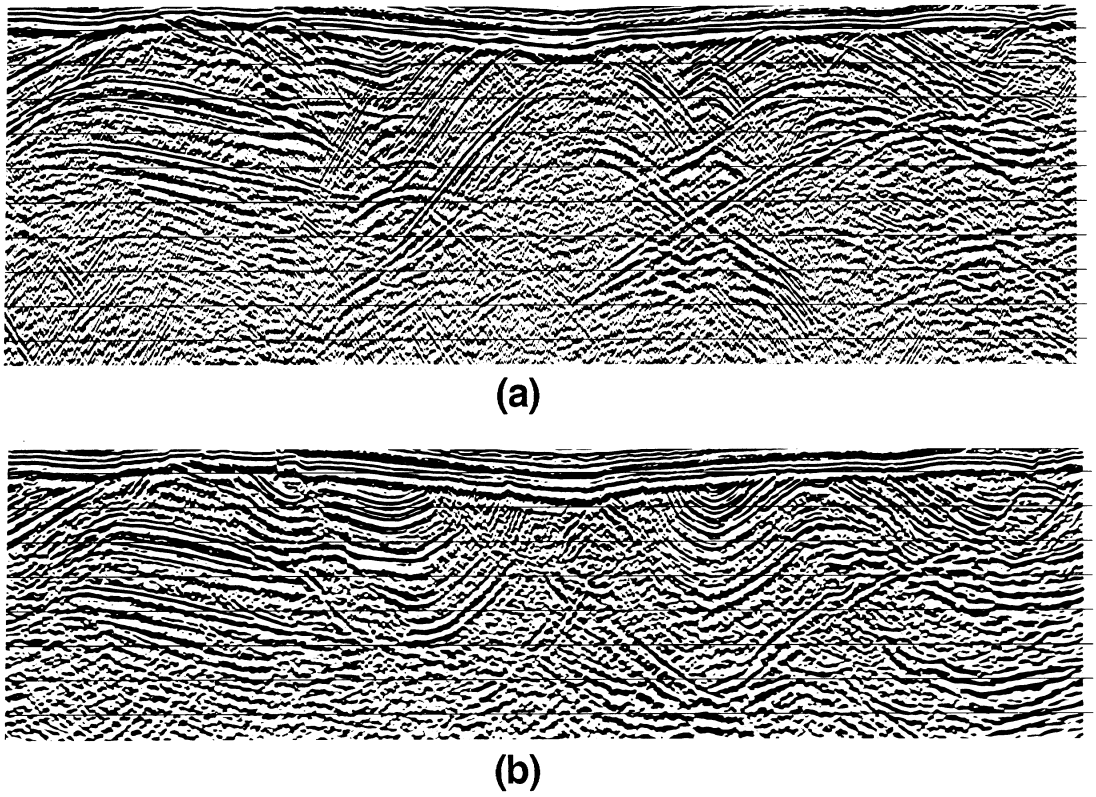

Figure 5.19: Stacked section (a) and its time migrated version (b) (from Yilmaz, 1987, fig. 4-20)

Creating zero-offset sections for reflectors with more complicated shape: Exploding-reflector model

In this subsection we are going to look at the so-called *exploding-reflector model*. It helps us understanding and how creating a zero-offset section. Consider a simple model with one reflector in the subsurface. When we have a source at the surface which emits a signal at $t = 0$, the signal will propagate through the medium to the reflector, will be reflected at a right angle to the reflector and will arrive back at the receiver (= shot position for a zero-offset experiment). This is shown in figure 5.20 at the left-hand side. Say the wave takes a time T to do this. Apart from some amplitude differences, the data recorded in such a way would be the same if we could fire off the sources on the reflector at time 0 but assume half the velocity of the medium in between; the path from source to reflector, and from reflector to receiver is the same for zero-offset data; the ray is perpendicular to

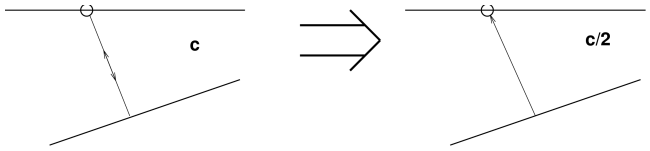

Figure 5.20: Exploding-reflector model for zero-offset data. A zero-offset measurement can be considered as an exploding-reflector response in a medium with half the velocity.

the reflector, entirely due to the zero-offset situation. Putting the imaginary sources this way on the reflector is called the exploding-reflector model. This is shown in figure 5.20 at the right-hand side. If we put the sources on the reflector and let them emit rays at a right angle to the reflector, we could synthesize the response at the surface.

This concept can be used for reflectors with a more complicated shape, like the syncline given on the left of figure 5.21. Taking the idea of the exploding-reflector model, we can follow the reflector from the left, emit a ray at a right angle to the reflector, track the ray to the surface, and determine the traveltime for that ray as needed for creating the zero-offset section. The resulting zero-offset section will be the shape as shown on the right of figure 5.21, often called a "bow-tie". Note that in figure 5.19 such structures are also visible.

The concept can also be used for cases when the seismic wave velocities are laterally varying. In those cases, the shapes in the zero-offset sections will not be perfectly hyperbolic any more. This is common for real data so for real data, the exploding-reflector model describes this too.

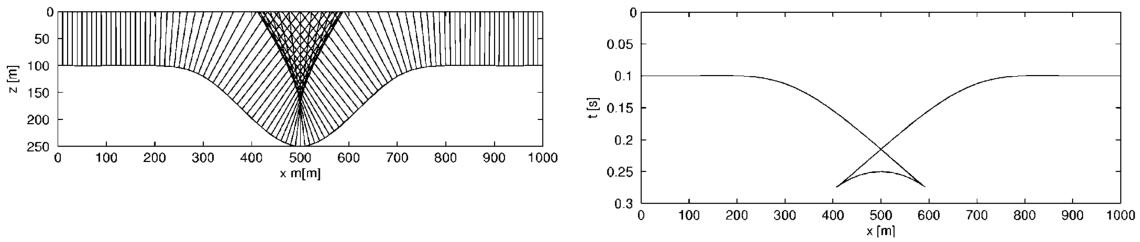

depth section with zero-offset ray paths *zero-offset section*

Figure 5.21: A syncline reflector (left) yields "bow-tie" shape in zero-offset section (right).

A simple migration algorithm: Diffraction stack

So far, we haven't described *how* to migrate a full dataset like the one shown in figure 5.19. The simplest case of a migration is adding (stacking) the data along hyperbolae. In that case, each point of the section (each time and space point!) is seen as a diffractor. As we saw in the 4-point-diffractor case compared with the dipping-reflector case, any reflector can be synthesized by point diffractors (although infinite). So if each point of the zero-offset time section is seen as a possible diffraction (and the velocity is known), we can add data along the particular diffraction hyperbola for that point. In case a real hyperbola is present in the observed time section, due to a real point diffractor in depth, energy will be added up constructively to give a relatively large output signal (=migrated) at that point. In case no diffractor is present at depth, the energy along the hyperbola at that point does not add up constructively and therefore the output signal (=migrated) will be small.

This method is called a diffraction stack. In the early days of computers the diffraction stack was the main migration algorithm. In formula form, the diffraction stack is given by (assumed to have a discrete number of x_{zo}'s, being the traces in a zero-offset section):

$$p_{zomig}(x,t) = \sum_{x_{zo}} p_{zo}\left(x_{zo}, T = \sqrt{t^2 + 4\frac{(x_{zo}-x)^2}{c^2}}\right), \tag{5.24}$$

where p_{zomig} stand for zero-offset migrated data, p_{zo} for zero-offset data, and c is the stacking velocity. From the formula it may be obvious that data are added along hyperbolae for each output point (x,t), being the apex of the hyperbola for point (x,t). What we do when stacking along hyperbolae, is actually removing a wave-propagation effect from a point diffractor to the zero-offset source/receiver positions. A nice feature about the diffraction stack is that it carries out our intuitive idea of migration, and is very useful in a conceptual sense. Of course, for this method to give proper results, we need to know the stacking velocity.

Zero-offset migration and wave theory

What is lacking in the approach of the diffraction stack is the basis on deeper physical principles than (kinematic) ray theory alone. The final migrated result may be correct in position (if the diffraction responses can be assumed to have a hyperbolic shape, i.e. if the subsurface exhibits moderate variations in velocity), but not in amplitude. The most well-known one is geometrical spreading, the effect that when observations are made at a larger distance, the amplitude is smaller due to wavefront spreading. In case of the exploding-reflector model, first each exploding source should have the strength of the reflection coefficient of the reflector, and second it should take into account the geometrical spreading. In this way, we will see that along a hyperbola (in case of constant velocity), the amplitude is changing.

An important item in migration has to do with the fact that we record in *time*, while we want to obtain properties in *depth*. In 3-D seismic, we record (x,y,t) and want to obtain

an image in (x, y, z). The link between these two is the so-called *imaging condition*. Say, we have recorded the data at time T, and would keep track of the time to get back from time T to the reflector. Then, we would obtain the image at time $t = 0$, again assuming we have taken the right (i.e. half the original) velocity. Because we take the time to be zero, the result does not depend on time any more, and we obtain an image in depth. The condition of $t = 0$ is called the imaging condition.

In the above, we have discussed aspects that can be derived from fundamental laws of physics but the derivation falls outside the scope of these lecture notes. When applying the fundamental laws to this migration problem, we get the formula known as Kirchhoff migration (Schneider, 1978). The data are recorded at the surface. Let us call our surface measurement p_{zo}, where the subscript zo stands for zero offset. Then we set $c \to c/2$ in order to correct for two-way traveltime. Then, we calculate the response for each point in the subsurface and put $t = 0$, the imaging condition, which images the exploding reflector which starts to act at $t = 0$. With other words, we start with our measurements at the surface and do a downward continuation (inverse wave field extrapolation) to all depth levels, and pick the $t = 0$ point at each subsurface point. If there was a reflector at a certain point, it will be imaged with this method. If there is no reflector at a certain depth point, no contribution at $t = 0$ is expected for that point. So we can obtain a depth section by integrating over the surface to obtain (Schneider, 1978):

$$p_{zomig}(\mathbf{x}) = p_{zomig}(\mathbf{x}, t = 0) = \frac{-1}{2\pi}\partial_z \int_{z_{zo}=0} \frac{p_{zo}(\mathbf{x}_{zo}, t = 2R/c)}{R}\, dA_{zo}. \tag{5.25}$$

Remember that R is the distance between the output point on the depth section and the particular trace location on the surface $z_{zo} = 0$. So as we integrate along the surface $z_{zo} = 0$ we are actually summing along diffraction hyperbolae (in the case of a constant velocity medium), defined by the time curve $t = 2R/c$, but then in a weighted fashion. Note the large resemblance with the diffraction-stack definition of equation (5.24). The extra $1/R$ factor takes the spherical divergence of the wave front into account and the factor ∂_z compensates for the frequency-dependent and wave-front angle-dependent effects of the lateral summation process. Note that the integral over surface A_{zo} will numerically be implemented as a summation over all (x_{zo}, y_{zo}) positions, i.e. a summation over all traces in the seismic zero-offset section. Although the diffraction stack of equation (5.24) has been written as a summation over x_{zo} only, the extension to 3D by adding a summation over the y_{zo} coordinate is straightforward; in that situation the hyperbola is replaced by a hyperboloid: $T_{zo}^2 = T^2 + 4[(x_{zo} - x)^2 + (y_{zo} - y)^2]/c^2$.

For inhomogeneous media where the velocities are not constant any more, the diffraction responses are no longer perfectly hyperbolic, and the diffraction stack is not right. With equation (5.25), we are doing the summation (migration) much better than the diffraction stack because we have included more wave effects.

Time migration using the stacking velocities

Our final result is a depth section, as we would obtain when we would make a geo-

logical cross-section through the subsurface (of course with a finite resolution). However, migration is not a simple process without any artifacts, and most importantly, we usually do not exactly know the velocity as a function of x, y and z. Therefore, we would like to be able to compare our original stacked section with the migrated section directly in order to see what the migration has done. Especially seismic interpreters need this type of comparison. To this aim, the depth coordinate z is mapped back onto time τ via:

$$\tau = \frac{z}{c} \tag{5.26}$$

for a constant-velocity medium. For an inhomogeneous subsurface, this mapping is more complicated. For this purpose often ray-trace techniques are used to locate the reflectors in time.

To overcome the problem of not knowing the interval velocities in your medium, we can use a work-around using the stacking velocities. As we have made a stack at this stage of the processing, the stacking velocities are already known. For a good migration we need to know the distance R from subsurface point to the surface (which depends on the velocities in the subsurface). It is often assumed that this path can be approximated by a straight line (as in a homogeneous medium) using the stacking velocity. Therefore, R is replaced by:

$$R/c \approx \tau' = (\tau^2 + \frac{4{x_{zo}}^2 + 4{y_{zo}}^2}{c^2_{\mathrm{RMS}}})^{1/2}. \tag{5.27}$$

Furthermore, the extrapolated data is considered in migrated time τ and not in depth. This describes a diffraction stack, but now in a weighted fashion, according to wave theory. In these type of migrations, it is assumed that the structures in the subsurface are simple enough to use the hyperbolic approximation of the response of an exploding-reflector source.

Effects of wrong migration velocities

The only important parameter we can actually set is the velocity distribution. It is therefore important to know how a wrong velocity distribution will manifest itself in the final result. This is shown in figure 5.22 where we see a correctly and incorrectly migrated a point diffraction. Note again the effect of migration: the focussing of the diffraction hyperbola into a point. When we put the velocity too low, the diffraction hyperbolae are not completely focussed yet and we keep a hyperbola in our result. Such a section is undermigrated. In the same way, when the velocity is too high, then the diffraction hyperbolae are corrected too much, and an over-migrated section will arise. As such, migration can also be used to determine velocities: it is thát velocity that images the diffractor(s) in its original point with no diffraction effects visible anymore. A well-known effect of over-migrated sections is the creation of so-called "migration smiles" and crossing events, as visible in figure 5.23.

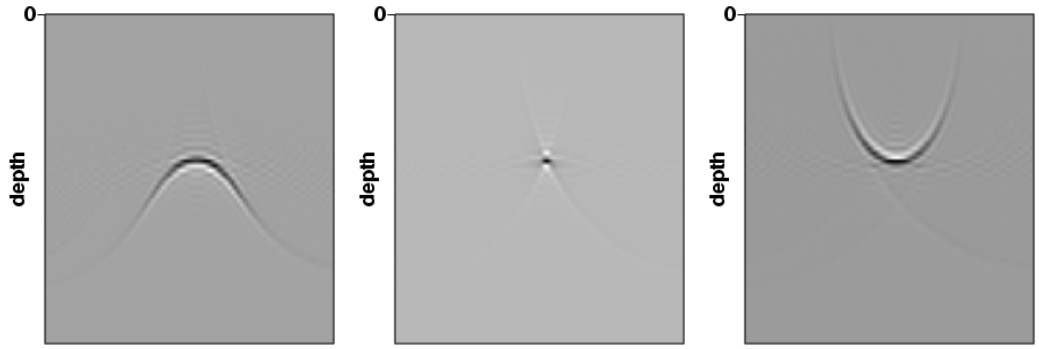

Figure 5.22: Point diffractor: migrated version with correct and wrong velocities.

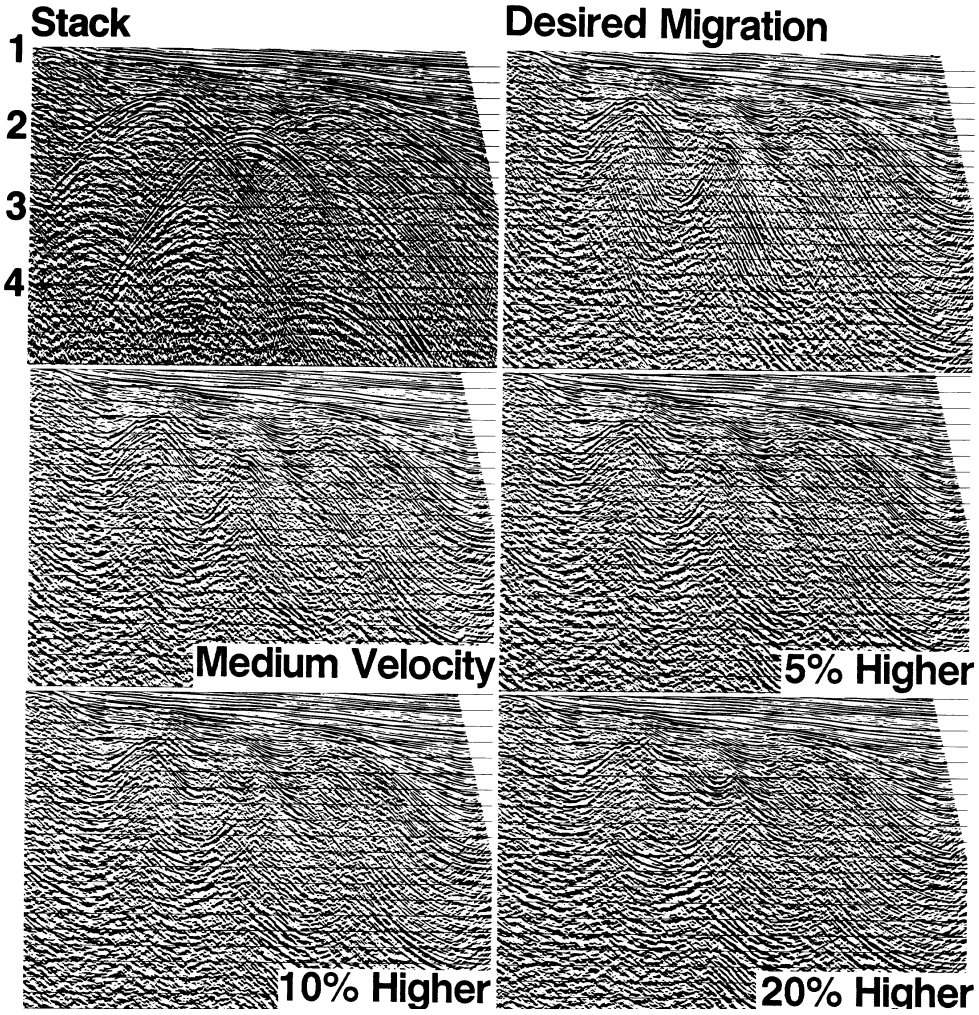

Figure 5.23: Stacked section and its time migrated version with the correct and wrong velocities (from Yilmaz, 1987, fig. 4-54).

5.6 Conversion from time to depth

In the previous section we have spoken of time and depth migration, referring to whether the output section is in time or depth, respectively. In time, we do not need to know the velocities that well, stacking velocities will often do. In depth migration we need to know the velocities very well, which is often a difficult task. Still, our goal is to obtain a section which is as close as possible to a geological cross-section; to that effect we want to have our section in depth. In this section we will briefly discuss the conversion from time to depth, via so-called Dix' formula, valid for media varying slowly in lateral direction.

Dix' formula: from RMS to interval velocities

Let us first consider a model with plane horizontal layers. We showed earlier in this Chapter that we could determine the root-mean-square velocities from the interval velocities via:

$$c^2_{\mathrm{RMS},N} = \frac{1}{T_{\mathrm{tot},N}(0)} \sum_{i=1}^{N} c_i^2 T_i(0), \tag{5.28}$$

where we have included an extra N in the notation of $c_{\mathrm{RMS},N}$ and $T_{\mathrm{tot},N}$. We can invert this formula, which means that we can determine the interval velocities from the root-mean-square velocities. When we consider the root-mean-square velocities for $N = 2$ and $N = 3$, we have:

$$c^2_{\mathrm{RMS},2} = \frac{c_1^2 T_1(0) + c_2^2 T_2(0)}{T_1(0) + T_2(0)} \tag{5.29}$$

$$c^2_{\mathrm{RMS},3} = \frac{c_1^2 T_1(0) + c_2^2 T_2(0) + c_3^2 T_3(0)}{T_1(0) + T_2(0) + T_3(0)} \tag{5.30}$$

We bring the denominator on the right-hand side to the left-hand side, subtract the first equation from the second, and obtain:

$$c^2_{\mathrm{RMS},3}(T_1(0) + T_2(0) + T_3(0)) - c^2_{\mathrm{RMS},2}(T_1(0) + T_2(0)) = c_3^2 T_3(0) \tag{5.31}$$

in which we recall that $T_3(0)$ is the zero-offset traveltime through layer 3, so in fact the difference between the total time up to the time at level 3 minus the time at level 2, so $T_3(0) = T_{\mathrm{tot},3}(0) - T_{\mathrm{tot},2}(0)$. So then the interval velocity c_3 becomes:

$$c_3 = \left(\frac{c^2_{\mathrm{RMS},3} T_{\mathrm{tot},3}(0) - c^2_{\mathrm{RMS},2} T_{\mathrm{tot},2}(0)}{T_{\mathrm{tot},3}(0) - T_{\mathrm{tot},2}(0)} \right)^{1/2} \tag{5.32}$$

The values for $c_{\mathrm{RMS},n}$ and $T_{\mathrm{tot},n}$ can directly be obtained from the velocity file as used for stacking the data. This is Dix' formula (Dix,1955). Dix' formula converts RMS-velocities to interval velocities.

Time-to-depth conversion using Dix' formula

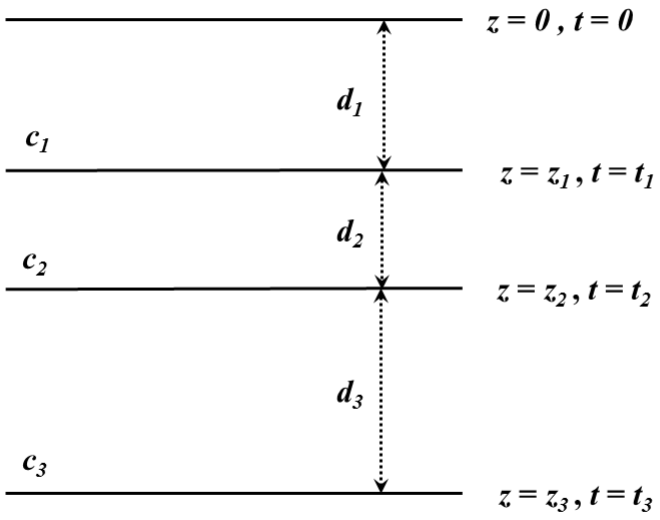

Figure 5.24: Definition of times, depths and velocities for time-to-depth conversion.

In our procedure to get a depth section for a model with horizontal plane layers, we convert the time axis on our (zero-offset) stacked section to a depth axis. This is done in the following way, using Figure 5.24: using this formula.

- We start at the top of the model, at depth $z = 0$ at time $t = 0$;
- The next reflection is at $t = t_1$. Since we know the velocity of the first layer, i.e., $c = c_1$, the depth z_1 can be determined from the time t_1 where that first reflection takes place: $z_1 = c_1\, t_1/2$. Please note the factor 2 because of two-way travel time;
- The next reflection is at $t = t_2$. The depth z_2 of that reflector can then be determined using the interval velocity $c = c_2$ of the second layer (which we know because of Dix' formula) and using the depth of the previous reflector: $z_2 = z_1 + c_2\,(t_2 - t_1)/2$;
- And the depth of the third reflector belonging to $t = t_3$ can then be found as: $z_3 = z_2 + c_3\,(t_3 - t_2)/2$;

  $\vdots$

- And the depth of the n^{th} reflector belonging to $t = t_n$ can be found as: $z_n = z_{n-1} + c_n\,(t_n - t_{n-1})/2$.

Although we derived the formulae for horizontal layers, the formulae will still be good when we have mild lateral velocity variations. It has been shown that even in the case of

dipping events, the formulae will still be good; however, in order to obtain a good depth section, we must first time-migrate the data before we can convert the time axis to a depth axis.

Check–shot survey or Vertical Seismic Profile (VSP)

In general, the velocities obtained from the velocity analysis is not very accurate for depth determination of reflectors. The RMS velocities are accurate in the sense that they align reflectors in a CMP gather. However, for a correct positioning in depth, the RMS velocities or updated velocities after migration must be converted to interval velocities. Still, the interval velocities determined this way are not good enough for accurate positioning.

Therefore, in practice, a so–called check-shot survey is done. A check–shot survey consists of a set–up where a geophone is put in a well while a source is put at the surface near the well. Another name often used, is a Vertical Seismic Profile, or VSP. In such a set–up we know the depth of the receiver as well as the time of the direct arrival. So from many recordings at many depths along the well, we can determine the velocities of the intervals between the subsequent recording depths and therefore the velocity model. This gives, at the scale of wavelengths of the surface seismics, a velocity model accurate enough to convert the seismic data from time to depth.

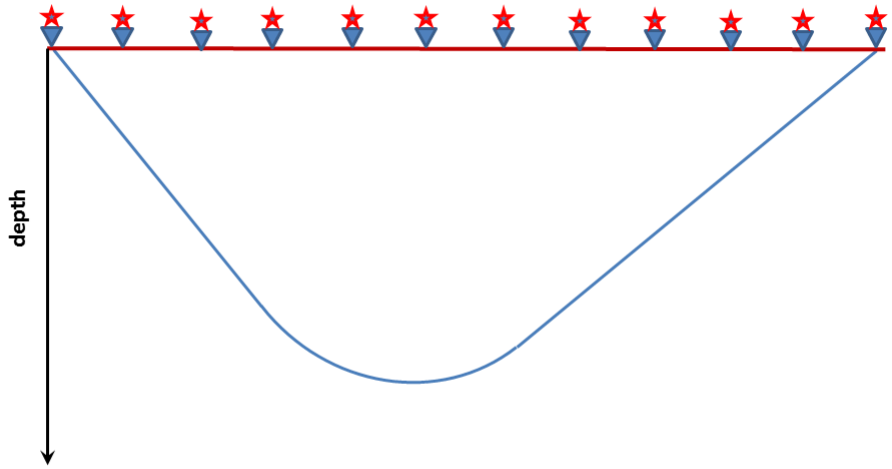

Figure 5.25: Subsurface with a valley, where the bend is part of a circle.

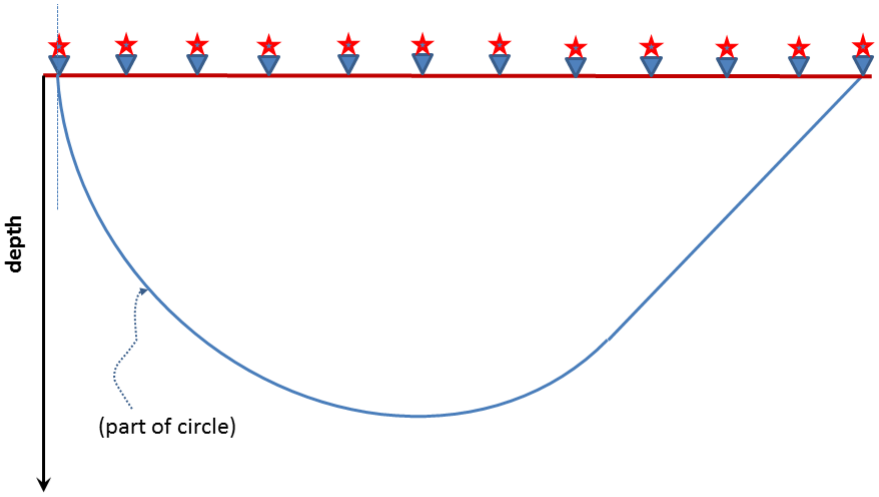

Figure 5.26: Subsurface with a circular reflector connected to a linearly dipping reflector.

5.7 *EXERCISES*

1. In figure (5.25), a valley is drawn. For this subsurface, construct the zero-offset section.

2. In figure (5.26), a circular reflector connected to a linearly dipping reflector is drawn. For this subsurface, construct the zero-offset section.

3. In figure (5.27), a dipping and horizontal reflector with a round boulder near their

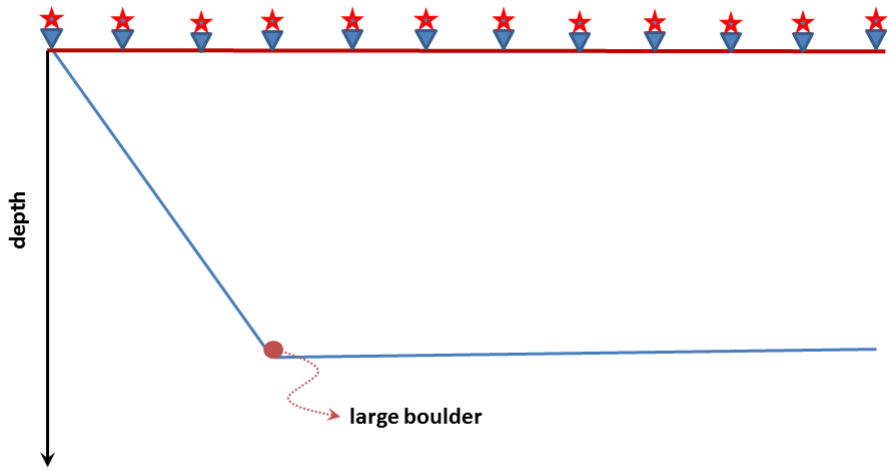

Figure 5.27: Subsurface with a dipping and horizontal reflector with a round boulder.

intersection are drawn. For this subsurface, construct the zero-offset section.

Appendix A

Discrete Fourier Transform and Sampling Theorem

In this appendix the discrete Fourier Transform is derived, starting from the Continuous Fourier Transform. As part of the derivation, the sampling theorem or Nyquist criterion is obtained.

Derivation

The continuous integrals are nearly always used in deriving any mathematical results, but, in performing transforms on data, the integrals are always replaced by summations. The continuous signal $a(t)$ becomes the discrete signal, or time series, a_k, in which k is an integer, and the sampling has taken place at regular intervals $k\Delta t$. Thus the discrete signal corresponds exactly to the continuous signal at times

$$t = k\Delta t. \tag{A.1}$$

Consider the inverse Fourier Transform (1.2) at the discrete times $k\Delta t$:

$$a_k = \int_{-\infty}^{\infty} A(f) \exp(2\pi i f k\Delta t) df \qquad k = ..., -2, -1, 0, 1, 2, ... \tag{A.2}$$

where a_k stands for the fact that time is now discrete so:

$$a_k = a(t), \text{when } t = k\Delta t \qquad k = ..., -2, -1, 0, 1, 2, ... \tag{A.3}$$

An important aspect of the integrand is that the exponential function $\exp(2\pi i f k\Delta t)$ is *periodic* with a period of $1/\Delta t$, i.e.,

$$\begin{aligned} f = F &: \exp(2\pi i F k\Delta t) \\ f = F + 1/\Delta t &: \exp(2\pi i (F + 1/\Delta t) k\Delta t) \\ &: = \exp(2\pi i F k\Delta t + 2\pi i k) \\ &: = \exp(2\pi i F k\Delta t) \end{aligned}$$

since $\exp(2\pi ik) = 1$, and therefore the exponential at $f = F$ is identical to the exponential at $f = F + 1/\Delta t$. Therefore, for all k, the integral above may be replaced by an infinite sum of pieces of the integral with period $1/\Delta t$:

$$\begin{aligned} a_k &= \left(\cdots + \int_{-\frac{5}{2\Delta t}}^{-\frac{3}{2\Delta t}} + \int_{-\frac{3}{2\Delta t}}^{-\frac{1}{2\Delta t}} + \int_{-\frac{1}{2\Delta t}}^{+\frac{1}{2\Delta t}} + \int_{+\frac{1}{2\Delta t}}^{+\frac{3}{2\Delta t}} + \cdots \right) A(f) \exp(2\pi i f k\Delta t) df \\ &= \sum_{m=-\infty}^{\infty} \int_{\frac{m}{\Delta t}-\frac{1}{2\Delta t}}^{\frac{m}{\Delta t}+\frac{1}{2\Delta t}} A(f) \exp(2\pi i f k\Delta t) df \end{aligned} \tag{A.4}$$

In order to get the bounds of the integral from $-1/(2\Delta t)$ to $+1/(2\Delta t)$, we change to the variable $f' = f - m/\Delta t$ to yield:

$$a_k = \sum_{m=-\infty}^{\infty} \int_{-\frac{1}{2\Delta t}}^{\frac{1}{2\Delta t}} A(f' + \frac{m}{\Delta t}) \exp(2\pi i \{f' + \frac{m}{\Delta t}\} k\Delta t) df' \tag{A.5}$$

Changing the order of the integration and summation, and noting that the exponential becomes periodic (so $\exp(2\pi imk) = 1$), this becomes

$$a_k = \int_{-\frac{1}{2\Delta t}}^{\frac{1}{2\Delta t}} \left[\sum_{m=-\infty}^{\infty} A(f' + \frac{m}{\Delta t}) \right] \exp(2\pi i f' k\Delta t) df' \tag{A.6}$$

The Fourier transform of the discrete time series is thus

$$a_k = \int_{-\frac{1}{2\Delta t}}^{\frac{1}{2\Delta t}} A_D(f') \exp(2\pi i f' k\Delta t) df' \qquad k = ..., -2, -1, 0, 1, 2, ... \tag{A.7}$$

provided

$$A_D(f') = \sum_{m=-\infty}^{\infty} A(f' + \frac{m}{\Delta t}) \tag{A.8}$$

So this is an infinite series of shifted spectra as shown in figure 1.3(b) in the main text. The discretisation of the time signal forces the Fourier transform to become periodic. In the discrete case we get the same spectrum as the continuous case if we only take the

period from $-1/(2\Delta t)$ to $+1/(2\Delta t)$, and else be zero; the signal must be *band-limited*. So this means means that the discrete signal must be zero for frequencies $|f| \geq f_N = 1/(2\Delta t)$. The frequency f_N is known as the Nyquist frequency.

Let us now look at the other integral of the continuous Fourier-transform pair, i.e. (1.1). We evaluate the integral by discretisation , so then we obtain for $A_D(f)$:

$$A_D(f) = \Delta t \sum_{k=-\infty}^{\infty} a_k \exp(-2\pi i f k \Delta t) \tag{A.9}$$

In practice the number of samples is always finite since we measure only for a certain time. Say we have N samples. Then we obtain the pair:

$$A_D(f) = \Delta t \sum_{k=0}^{N-1} a_k \exp(-2\pi i f k \Delta t) \tag{A.10}$$

$$a_k = \int_{-\frac{1}{2\Delta t}}^{\frac{1}{2\Delta t}} A_D(f) \exp(2\pi i f k \Delta t) df \qquad k = 0, 1, 2, ..., N-1 \tag{A.11}$$

This is the transform pair for continuous frequency and discrete time. Notice that the integral runs from $-1/2\Delta t$ to $+1/2\Delta t$, i.e. one period where one spectrum of $A_D(f)$ is present.

As said above, the values for frequencies above the Nyquist frequency must be set to zero. Equivalently, we can say that if there is no information in the continuous time signal $a(t)$ at frequencies above f_N, the maximum sampling interval Δt is

$$\Delta t_{\max} = \frac{1}{2 f_N} \tag{A.12}$$

This is the sampling theorem.

In practice the number samples in a time series is always finite. We wish to find the discrete Fourier transform of a finite length sequence. We approach the problem by dividing the definite integral (A.7) into the sum of N pieces of equal frequency interval Δf. Because $A_D(f)$ is periodic, with period $1/\Delta t$, we may first rewrite the integral with different limits, but with the same frequency interval:

$$a_k = \int_0^{\frac{1}{\Delta t}} A_D(f) \exp(2\pi i f k \Delta t) df \qquad k = 0, 1, 2, ..., N-1 \tag{A.13}$$

Writing the integral as a summation, we obtain

$$a_k = \Delta f \sum_{n=0}^{N-1} A_n \exp(2\pi i n \Delta f k \Delta t) \qquad k = 0, 1, 2, ..., N-1 \tag{A.14}$$

where

$$A_n = A_D(f), \qquad \text{when} \qquad f = n\Delta f. \tag{A.15}$$

We now notice that the series a_k is periodic with period N:

$$\begin{aligned} a_{k+N} &= \Delta f \sum_{n=0}^{N-1} A_n \exp(2\pi i n \Delta f \{k+N\} \Delta t) \\ &= \Delta f \sum_{n=0}^{N-1} A_n \exp(2\pi i n \Delta f k \Delta t + 2\pi i n \Delta f N \Delta t) \\ &= \Delta f \sum_{n=0}^{N-1} A_n \exp(2\pi i n \Delta f k \Delta t) \\ &= a_k \end{aligned} \tag{A.16}$$

since $N\Delta f = 1/\Delta t$ and so $\exp(2\pi i n) = 1$. Thus we arrive at the following discrete Fourier transform pair for a finite-length time series

$$A_n = \Delta t \sum_{k=0}^{N-1} a_k \exp(-2\pi i n k/N) \qquad n = 0, 1, 2, ..., N-1 \tag{A.17}$$

$$a_k = \Delta f \sum_{n=0}^{N-1} A_n \exp(2\pi i n k/N) \qquad k = 0, 1, 2, ..., N-1 \tag{A.18}$$

These two equations are the final discrete-time and discrete-frequency Fourier transform pair.

There needs to be some caution with applying these transforms. We have used both for the frequencies and the times N samples as if we had a choice. But in the frequency domain, we have negative and positive frequencies, while in the time domain we only have samples for positive times. Therefore, when transforming to the frequency domain, we must have enough space allocated for the negative frequencies. So we must always add zeroes to the time series, as many as there are (non-zero) samples.

Appendix B

Correlation

In this appendix the process of correlation is defined, and its Fourier counterpart is derived.

Definitions and derivations

Here we shall focus on correlation, specifically auto-correlation and cross-correlation, and relate it to the Fourier transformation. As we shall see, correlation can be written as a convolution, and in the frequency domain it is a simple operation.

Let us first define the time reversal of a signal $a(t)$:

$$a_{\text{rev}}(t) = a^*(-t) \tag{B.1}$$

where $b(t)$ is allowed to be complex and the asterisk * as superscript denotes complex conjugate. Normally of course we deal with real time signals. However, by allowing these signals to be complex it is easier to see their symmetry properties. When we apply a Fourier transformation to $a(t)$, and take the complex conjugate of each side, we obtain:

$$\begin{aligned} A^*(f) &= \left[\int_{-\infty}^{\infty} a(t)\exp(-2\pi i f t)dt\right]^* \\ &= \int_{-\infty}^{\infty} a^*(t)\exp(2\pi i f t)dt \\ &= \int_{-\infty}^{\infty} a^*(-t')\exp(-2\pi i f t')dt' \\ &= \mathcal{F}_t[a^*(-t')] \\ &= \mathcal{F}_t[a_{\text{rev}}(t')] \end{aligned} \tag{B.2}$$

which is the Fourier transform of $a_{\text{rev}}(t)$.

Now, the autocorrelation of $a(t)$ is defined as

$$\phi_{aa}(\tau) = \int_{-\infty}^{\infty} a(t)a^*(t-\tau)\,dt \tag{B.3}$$

Using the concept of the time reverse, equation (B.1), equation (B.3) can be written as

$$\phi_{aa}(\tau) = \int_{-\infty}^{\infty} a(t)a_{\text{rev}}(\tau-t)\,dt \tag{B.4}$$

That is, the autocorrelation of a signal is the convolution of the signal with its time reverse. Equation (B.4) may be transformed to the frequency domain. The convolution becomes a multiplication and the result is

$$\begin{aligned} \Phi_{aa}(f) &= A(f)A^*(f) \\ &= |A(f)|^2 \end{aligned} \tag{B.5}$$

The function $\Phi_{aa}(f)$ is the power spectrum of $a(t)$ and $|A(f)|$ is the amplitude spectrum of $a(t)$. Both the power spectrum and the amplitude spectrum are real. The power spectrum is the Fourier transform of the autocorrelation function.

The cross-correlation function $\phi_{ab}(t)$ is defined as

$$\phi_{ab}(t) = \int_{-\infty}^{\infty} a(\tau)b^*(\tau-t)\,d\tau \tag{B.6}$$

which can be recognized as the convolution of $a(t)$ with the time reverse of $b(t)$:

$$\phi_{ab}(t) = a(t) * b_{\text{rev}}(t) \tag{B.7}$$

In the frequency domain equation (B.7) becomes

$$\Phi_{ab}(f) = A(f)B^*(f) \tag{B.8}$$

The function $\Phi_{ab}(f)$ is known as the cross-spectrum. Note that the cross-correlation function and the cross-spectrum do not, in general, exhibit any symmetry. Also, it can be seen that the correlation of $a(t)$ with $b(t)$ is not necessarily the same as the correlation of $b(t)$ with $a(t)$, that is:

$$\phi_{ab}(t) \neq \phi_{ba}(t) \tag{B.9}$$

and

$$\Phi_{ab}(f) \neq \Phi_{ba}(f) \tag{B.10}$$

Appendix C

Advantages and disadvantages of Vibroseis and dynamite

This appendix gives a detailed discussion and list of advantages and disadvantages of dynamite and Vibroseis.

Nowadays, the Vibroseis is the most used seismic source on land. One may wonder why it is not normal practice in seismic exploration to use an impulsive source, since, after all, it is the earth's impulse response we are after. The most well-known impulsive seismic source, dynamite, is indeed used often in land seismic surveys. There are, however, some distinct disadvantages related to the use of an impulsive source like dynamite.

First of all, due to the high energy density of the dynamite explosion, severe harm can be done to the environment. In any case, the destructive nature of the dynamite source prohibits its use in densely populated areas. Second, a hole has to be drilled for every shotpoint in which the dynamite charge is placed. Third, the high energy-density of the explosion results in a non-linear zone surrounding the explosion. Although the ignition time of the dynamite itself is short compared with any time duration of interest in seismic exploration, this nonlinear zone results in a distorted wavelet. The high-frequency content of the signal decreases when the charge size is increased (the low frequency content increases). This yields a trade-off between penetration and resolution: a large charge size has better penetration, but lacks high frequencies. Another disadvantage of the creation of a nonlinear zone around the dynamite explosion is that effectively a wavelet is transmitted into the earth that is not an impulse, and has a shape which is not accurately known and cannot be measured easily.

The Vibroseis source has some distinct advantages over the dynamite source. First, the emitted signal contains an amount of energy that is (roughly) comparable to the energy contained in a dynamite signal. Because of the use of an expanded impulse, the energy density of the source wavelet in the Vibroseis technique is much less than the energy density of the dynamite wavelet. Therefore, destructive effects are much less severe. Secondly, Vibroseis provides us with a direct means to measure and control the outgoing wavelet.

	Advantages	Disadvantages
Vibroseis	1. Less destructive than dynamite : can operate in urban areas 2. Not labour-intensive : cheap in operation 3. Some control over outgoing signal	1. One truck does not deliver enough energy : arrays, so directivity 2. Surface source : many Rayleigh waves 3. Can only operate in areas which can support 20 tons 4. Correlation imperfect : correlation noise
Dynamite	1. Buried source : much less surface waves generated than Vibroseis 2. Signal close to δ-pulse	1. Destructive : cannot operate in urban areas 2. Labour intensive for making shotholes : expensive in operation

Table C.1: Advantages and disadvantages of Vibroseis and dynamite

Thirdly, there is no need to drill holes when using Vibroseis.

There are, however, also some disadvantages connected with the use of Vibroseis as a source. Firstly, a single vibrator in general does not deliver a sufficient amount of energy required for seismic exploration purposes, so that arrays of vibrators have to be used. Typically, 4 vibrators vibrate at each vibration location simultaneously. Second, as vibrators are surface sources, large amounts of Rayleigh waves are generated. The generation of Rayleigh waves can be suppressed in a dynamite survey by placing the charge at or below the bottom of the weathered layer. In Vibroseis surveys, the Rayleigh waves have a very high amplitude and are an undesired feature on the seismogram. Thirdly, the Vibroseis method can be employed only in areas which are accessible to the seismic vibrator trucks, whose weight may exceed 20 tons. Fourth, correlation noise (i.e. the noise generated by the correlation process that converts the Vibroseis signal into a pulse) limits the ratio between the largest and smallest detectable reflections.

In spite of many disadvantages, the Vibroseis method is now a standard method in the seismic exploration for hydrocarbons. Nowadays, Vibroseis is used more often in land seismics than dynamite The operational advantages of the Vibroseis method over the conventional dynamite survey result in an average cost per kilometre of Vibroseis which is less than the cost per kilometre for a dynamite survey. Also, the average number of kilometres that can be covered per crew month is higher for Vibroseis surveys than it is for dynamite surveys. This cost-effectiveness and efficiency, together with the increasing importance of signal control in the search for higher resolution of seismic data and the non-destructive character of the method explains the increasing popularity of Vibroseis. In table (C.1) the advantages and the disadvantages of the Vibroseis and dynamite are tabulated.

Appendix D

Network outline

This appendix gives, in tabular form, the impedances of a resistor, coil and capacitor. These results are being used in Chapter 3 (Seismic Instrumentation).

Table: Impedances for resistor, coil and capacitor

	Time	Frequency	Impedance
Resistor	$u = Ri$	$U = RI$	$Z_R = \frac{U}{I} = R$
Coil	$u = L\frac{di}{dt}$	$U = Lj\omega I$	$Z_L = \frac{U}{I} = j\omega L$
Capacitor	$i = C\frac{du}{dt}$	$I = Cj\omega U$	$Z_C = \frac{U}{I} = \frac{1}{j\omega C}$

Time-domain symbols: time t, voltage $u(t)$, current $i(t)$

Fourier-domain symbols: angular frequency $\omega(= 2\pi f)$, imaginary unit j, voltage $U(\omega)$, current $I(\omega)$

Impedances: resistance R, impedance Z, capacitance C, inductance L.

Table: Resistances and Impedances in series and parallel circuits

	Resistances	Impedances
In parallel	$\frac{1}{R_{\mathrm{TOT}}} = \frac{1}{R_1} + \frac{1}{R_2}$	$\frac{1}{Z_{\mathrm{TOT}}} = \frac{1}{Z_1} + \frac{1}{Z_2}$
In series	$R_{\mathrm{TOT}} = R_1 + R_2$	$Z_{\mathrm{TOT}} = Z_1 + Z_2$

Appendix E

Derivation of basic equations for 1-D acoustic wave motion

In this appendix the one-dimensional wave motion for an acoustic medium is derived, starting from the deformation law of Hooke and from conservation of momentum (Newton's Second Law). This results in the so–called deformation equation and equation of motion for acoustic waves.

Derivation

Here we will derive the basic equations for wave motion in homogeneous media, using the conservation of momentum (Newton's second law) and the deformation law, known as Hooke's Law of elasticity. In this derivation, we consider a single cube of mass when it is subdued to a seismic disturbance (see figure (E.1)). Such a cube has a volume ΔV with sides $\Delta X, \Delta Y$ and ΔZ.

We start with an elastic deformation of the cube, using Hooke's Law. This law states that the deformational force working on a piece of material is linearly related to the extension of that piece. Applying this to our cube of mass, the deformational force gives a relative change in volume:

$$p = -K\frac{dV}{\Delta V} \tag{E.1}$$

where the pressure p is introduced as being the force per unit area, K is called the bulk modulus and the minus sign expresses that the pressure is opposite to the deformation direction. Now we assume that the volume change is only in one direction (1-dimensional)

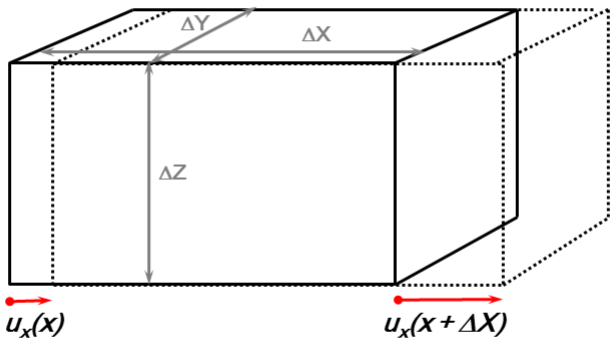

Figure E.1: A cube of mass, subjected to one-dimensional wave motion. Drawn line: original status. Dotted line: status after deformation.

as shown in Figure (E.1), so then we get:

$$\begin{aligned} \frac{dV}{\Delta V} &= \frac{u_x(x+\Delta X)\Delta Y\Delta Z - u_x(x)\Delta Y\Delta Z}{\Delta X\Delta Y\Delta Z} \\ &= \frac{u_x(x+\Delta X) - u_x(x)}{\Delta X} \end{aligned} \tag{E.2}$$

where u_x is the displacement in the x-direction. Using the situation that ΔX is rather small, we can approximate $u_x(x+\Delta X)$ by $u_x(x)+(\partial u_x/\partial x)\Delta X$; this then gives for Hooke's Law:

$$p = -K\frac{\partial u_x}{\partial x}. \tag{E.3}$$

Since we are finally interested in particle velocities rather than displacements (since geophones – seismic sensors on land – measure particle velocities), we differentiate both sides of Hooke's Law with respect to time t, and introduce $v_x = \partial u_x/\partial t$ to give:

$$\boxed{\frac{1}{K}\frac{\partial p}{\partial t} = -\frac{\partial v_x}{\partial x}} \tag{E.4}$$

This is the so-called deformation equation, in particular the equation of elastic deformation.. It is one basic relation needed for describing one-dimensional wave motion.

The other relation is obtained via Newton's Law, applied to the volume ΔV with mass M in the direction x, since we consider 1-dimensional motion:

$$\begin{aligned} F_x &= M\frac{\partial v_x}{\partial t} \\ &= \rho\Delta V\frac{\partial v_x}{\partial t} \end{aligned} \tag{E.5}$$

where F_x is the total force working on the element ΔV that is inducing motion. Consider the total force that is working on the cube in the x–direction, via the pressures working on the sides with area $\Delta Y \Delta Z$:

$$\begin{aligned} F_x &= -[p(x+\Delta X) - p(x)]\Delta S_x \\ &= -\frac{p(x+\Delta X) - p(x)}{\Delta X}\Delta V \end{aligned} \tag{E.6}$$

Using $p(x+\Delta X) \simeq p(x) + (\partial p/\partial x)\Delta X$ and combining it with Newton's Law as expressed in equation (E.5) gives:

$$\boxed{-\frac{\partial p}{\partial x} = \rho \frac{\partial v_x}{\partial t}} \tag{E.7}$$

since ΔV cancels. This equation is called the equation of motion. It is the other basic relation (next to the deformation equation) needed for describing one-dimensional wave motion.

Appendix F

Strain, P- and S-waves

In this appendix strain for an elastic solid is explained. Together with the stress (discussed in the main text), it is used to derive the basic equations for P- and S-waves: the deformation equations and the equations of motion.

Strain

Strain is a geometrical quantity. It is a *relative* displacement under applied forces, i.e., it is a measure of deformation, normalized by its original size. As for stress, strain may be divided into normal strain and shear strain, depending on the type of force that is applied. For a normal strain in the deformation of a volume, the strain is simply the change of volume divided by its original volume, i.e.,:

$$e_{\text{normal}} = \frac{\Delta V}{V} \tag{F.1}$$

where e is the strain, ΔV the change in volume and V the original volume itself. This volume change was also used to derive the acoustic wave equation (see appendix E).

Let us now look at figure (F.1), where the displacement $\underline{u}$ is given for at a point $\underline{x}$. Notice that the displacement is a function of $\underline{x}$, i.e., $\underline{u} = \underline{u}(\underline{x})$. When a force/stress is applied, we get a difference in displacement, described by:

$$\begin{aligned} \underline{u}(\underline{x} + d\underline{x}) &\simeq \underline{u}(\underline{x}) + \frac{\partial \underline{u}}{\partial \underline{x}} d\underline{x} \\ &= \underline{u}(\underline{x}) + d\underline{u} \end{aligned} \tag{F.2}$$

where the first term is a translation and the second term is the term associated with deformation, in accordance with the assumption of elasticity. Notice that the term $\partial \underline{u}/\partial \underline{x}$

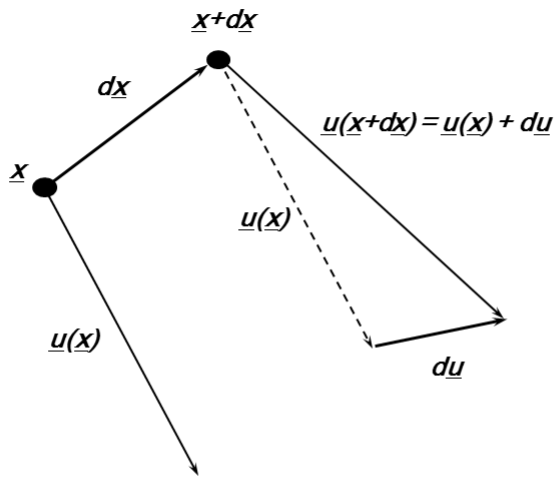

Figure F.1: Displacement field under presence of stress.

is a matrix since both $\underline{u}$ and $\underline{x}$ are vectors:

$$\frac{\partial \underline{u}}{\partial \underline{x}} = \begin{pmatrix} \frac{\partial u_x}{\partial x} & \frac{\partial u_x}{\partial y} & \frac{\partial u_x}{\partial z} \\ \frac{\partial u_y}{\partial x} & \frac{\partial u_y}{\partial y} & \frac{\partial u_y}{\partial z} \\ \frac{\partial u_z}{\partial x} & \frac{\partial u_z}{\partial y} & \frac{\partial u_z}{\partial z} \end{pmatrix} \tag{F.3}$$

The term $\partial \underline{u}/\partial \underline{x}$ can be written in a symmetric and anti-symmetric part:

$$\frac{\partial \underline{u}}{\partial \underline{x}} = \underline{\underline{e}} - \frac{1}{2}\underline{\underline{\xi}} \tag{F.4}$$

in which the elements of $\underline{\underline{e}}$ and $\underline{\underline{\xi}}$ are:

$$e_{ij} = \frac{1}{2}\left(\frac{\partial u_i}{\partial x_j} + \frac{\partial u_j}{\partial x_i}\right) \tag{F.5}$$

$$\xi_{ij} = \frac{\partial u_j}{\partial x_i} - \frac{\partial u_i}{\partial x_j} \tag{F.6}$$

where $\underline{\underline{e}}$ is the so-called strain tensor, and $\underline{\underline{\xi}}$ represents rigid rotation.

Tensile stress and strain, and P-waves in a solid

P-waves are associated with tensile stresses, so therefore we consider the tensile stress and strain for an infinitesimal rectangular parallelepiped as shown in Figure F.2. The sizes of

the parallelepiped are given by $\Delta X, \Delta Y$ and ΔZ, while the changes therein are given by $\delta U_x, \delta U_y$ and δU_z. We apply a tensile stress in the x-direction only. As was also given in the appendix on acoustic wave motion, Hooke's law states that a force needed to extend or compress a spring is linearly related to the length (u) of extension/compression of that spring, so $F = ku$. Stress is force per unit area, and strain is relative displacement, so Hooke's law applied to our parallelepedid gives:

$$e_{xx} = \frac{\partial u_x}{\partial x} = \frac{\delta U_x}{\Delta X} = \frac{1}{E}\tau_{xx} \tag{F.7}$$

where τ_{xx} is the tensile stress and e_{xx} the tensile strain in the x-direction, and E is called Young's modulus. When a tensile stress is applied, the size in the perpendicular directions y and z *decreases*, i.e., a lateral contraction occurs. This is quantified by the so-called Poisson's ratio, via:

$$e_{yy} = \frac{\partial u_y}{\partial y} = \frac{\delta U_y}{\Delta Y} = -\sigma e_{xx} \tag{F.8}$$

$$e_{zz} = \frac{\partial u_z}{\partial z} = \frac{\delta U_z}{\Delta Z} = -\sigma e_{xx} \tag{F.9}$$

We can follow the same procedure for a tensile stress in the y- and z-directions with tensile strains e_{yy} and e_{zz}, giving totally:

$$\begin{pmatrix} e_{xx} \\ e_{yy} \\ e_{zz} \end{pmatrix} = \frac{1}{E} \begin{pmatrix} 1 & -\sigma & -\sigma \\ -\sigma & 1 & -\sigma \\ -\sigma & -\sigma & 1 \end{pmatrix} \begin{pmatrix} \tau_{xx} \\ \tau_{yy} \\ \tau_{zz} \end{pmatrix} \tag{F.10}$$

So far, we have written down the basic expressions, but they are not in the desired form: we want to have a form in which the partial derivatives of the particle displacements are given (and not strains), and we want to have the stress on the left-hand side of the equation and the strains/particle-displacements on the right-hand side. To address the first issue, we have:

$$\begin{pmatrix} e_{xx} \\ e_{yy} \\ e_{zz} \end{pmatrix} = \begin{pmatrix} \frac{\partial u_x}{\partial x} \\ \frac{\partial u_y}{\partial y} \\ \frac{\partial u_z}{\partial z} \end{pmatrix} \tag{F.11}$$

To address the second issue, we have to invert the matrix in equation (F.10). Since the inverted matrix has terms that are not very simple, the so-called Lamé parameters are introduced:

$$\lambda = \frac{\sigma E}{(1-2\sigma)(1+\sigma)} \tag{F.12}$$

$$\mu = \frac{E}{2(1+\sigma)} \tag{F.13}$$

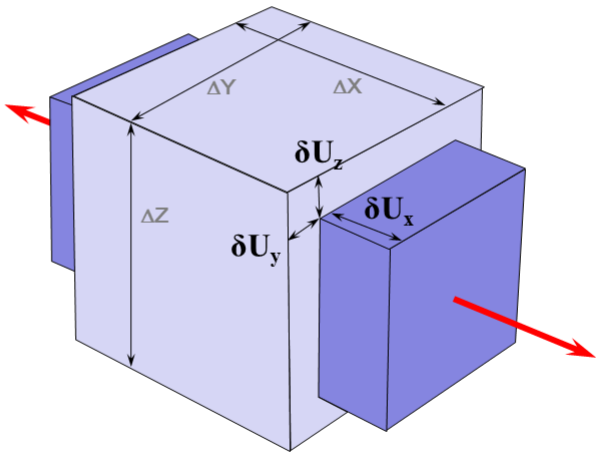

Figure F.2: Infinitesimal rectangular parallepiped deformed by tensile stress.

where μ is known as the shear modulus. Using these, we then get:

$$\begin{pmatrix} \tau_{xx} \\ \tau_{yy} \\ \tau_{zz} \end{pmatrix} = \begin{pmatrix} \lambda + 2\mu & \lambda & \lambda \\ \lambda & \lambda + 2\mu & \lambda \\ \lambda & \lambda & \lambda + 2\mu \end{pmatrix} \begin{pmatrix} \frac{\partial u_x}{\partial x} \\ \frac{\partial u_y}{\partial y} \\ \frac{\partial u_z}{\partial z} \end{pmatrix} \tag{F.14}$$

This the desired expression that we will use next.

Let us now derive the equations necessary to describe 1-D wave motion of a P-wave, travelling in the x-direction. To that end, consider figure F.3, in which again a infinitesimal block with size ΔX, ΔY and ΔZ is given. The mass ΔM of the little block is given by $\rho \Delta X \Delta Y \Delta Z$. We initiate a plane displacement field with displacements in the x-direction only (and therefore there is no contraction σ for this 1-D case):

$$\underline{u}(x, y, z, t) = \begin{pmatrix} u_x(x, t) \\ 0 \\ 0 \end{pmatrix} \tag{F.15}$$

In that case, Hooke's law gives $\tau_{xx} = (\lambda + 2\mu)\partial u_x / \partial x$. As for the acoustic case, we are finally interested in particle velocities rather than displacements (since geophones measure particle velocities), we differentiate both sides of Hooke's law with respect to time t, and introduce $v_x = \partial u_x / \partial t$ to give:

$$\boxed{\frac{\partial \tau_{xx}}{\partial t} = (\lambda + 2\mu) \frac{\partial v_x}{\partial x}} \tag{F.16}$$

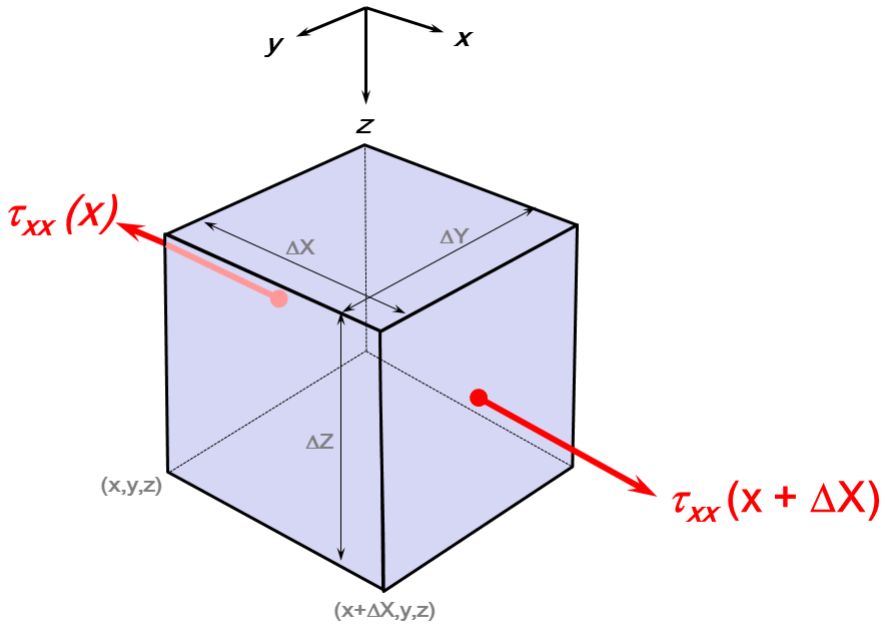

Figure F.3: Infinitesimal rectangular block under plane stress, used for deriving basic equations for P-wave motion.

Note that this equation has the same shape as the equation for acoustic waves, i.e.,

$$-\frac{\partial p}{\partial t} = K\frac{\partial v_x}{\partial x} \tag{F.17}$$

This equation alone does not describe wave motion; to that end we need to apply Newton's law as well. Referring to Figure F.3, the force is, in terms of stress:

$$F_x = \Delta Y \Delta Z[\tau_{xx}(x + \Delta X) - \tau_{xx}(x)] \tag{F.18}$$

and the force is given as mass times acceleration, i.e.:

$$F_x = \Delta M \frac{\partial^2 u_x}{\partial t^2}. \tag{F.19}$$

Equalizing these forces gives:

$$\frac{\tau_{xx}(x + \Delta X) - \tau_{xx}(x)}{\Delta X} = \frac{\Delta M}{\Delta X \Delta Y \Delta Z}\frac{\partial^2 u_x}{\partial t^2} \tag{F.20}$$

or, since $\tau_{xx}(x + \Delta X) \simeq \tau_{xx}(x) + (\partial \tau_{xx}/\partial x)\Delta X$:

$$\frac{\partial \tau_{xx}}{\partial x} = \rho\frac{\partial^2 u_x}{\partial t^2}. \tag{F.21}$$

Again, we need to introduce the particle velocity for the displacement, giving:

$$\boxed{\frac{\partial \tau_{xx}}{\partial x} = \rho \frac{\partial v_x}{\partial t}.} \tag{F.22}$$

This is the other desired equation, the equation of motion for P-waves. As expected, this equation has the same shape as the one for acoustic waves:

$$-\frac{\partial p}{\partial x} = \rho \frac{\partial v_x}{\partial t}. \tag{F.23}$$

Shear stress and strain, and S-waves in a solid

S-waves are associated with shear stresses. We will follow the same line of derivation as for the P-waves but then with shear stresses: consider the shear stress and strain for an infinitesimal rectangle, deformed into a parallelogram (2D) as shown in Figure F.4, with sizes ΔX and ΔZ. Let us first consider the left-hand figure (a), with τ_{xz}. The shear modulus μ is defined as the constant that relates the stress and displacement, in this case as:

$$\tau_{xz} = \mu \frac{\delta U_x}{\Delta Z} \tag{F.24}$$

which is the shear equivalent of Hooke's law for elastic deformation. Since the associated strain e_{xz} was defined as $(1/2)(\partial u_z/\partial x + \partial u_x/\partial z)$ (see equation (F.5)), which for the parallellogram becomes:

$$e_{xz} = \frac{1}{2} \frac{\delta U_x}{\Delta Z}, \tag{F.25}$$

the stress-strain relationship for shear deformation becomes:

$$\tau_{xz} = 2\mu e_{xz}. \tag{F.26}$$

This was the analyis for shear deformation in the horizontal direction, but deformation can also take place in the vertical direction, as shown in Figure F.4(b). In that case we have for the stress and strain:

$$\tau_{zx} = \mu \frac{\delta U_z}{\Delta X} \tag{F.27}$$

$$e_{zx} = \frac{1}{2} \frac{\delta U_z}{\Delta X} \tag{F.28}$$

$$\tau_{zx} = 2\mu e_{zx}. \tag{F.29}$$

The deformations as shown in Figures F.4(a) and (b) are actually deformations with a rigid-body rotation where $e_{xz} \neq e_{zx}$. We are interested in the deformation which show no rigid-body rotation, as shown in Figure F.4(c). For no rigid-body rotation $\xi_{xz} = 0$, so:

$$\frac{\partial u_x}{\partial z} = \frac{\partial u_z}{\partial x}, \quad \text{or} \quad \frac{\delta U_x}{\Delta Z} = \frac{\delta U_z}{\Delta X}, \tag{F.30}$$

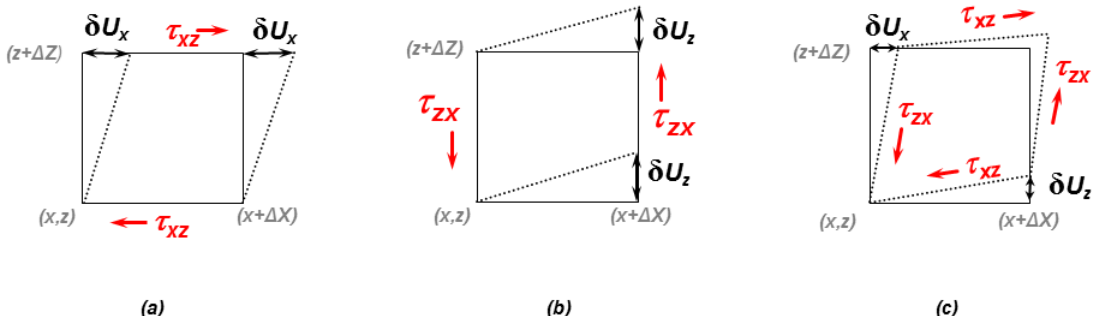

Figure F.4: Infinitesimal rectangle deformed to parallelogram by shear stress.

We then have:

$$e_{xz} = e_{zx}, \tag{F.31}$$

and therefore:

$$\tau_{xz} = \tau_{zx}. \tag{F.32}$$

Similarly, for no rigid-body rotation in 3-D:

$$e_{xy} = e_{yx} \tag{F.33}$$

$$e_{yz} = e_{zy} \tag{F.34}$$

$$\tau_{xy} = \tau_{yx} \tag{F.35}$$

$$\tau_{yz} = \tau_{zy} \tag{F.36}$$

Let us now derive the equations necessary to describe 1-D wave motion of an S-wave, travelling in the x-direction (as for the P-wave). To that end, consider the figure F.5 in which again a infinitesimal block with size ΔX, ΔY and ΔZ and mass $\Delta M = \rho \Delta X \Delta Y \Delta Z$ is given. We initiate a plane displacement field, giving displacements in the z-direction only (for P-waves they were in the x-direction only):

$$\underline{u}(x, y, z, t) = \begin{pmatrix} 0 \\ 0 \\ u_z(x, t) \end{pmatrix} \tag{F.37}$$

This means that there are no tensile stresses (since $u_z = u_z(x, t)$ only), and the other shear stresses τ_{xy} and τ_{yz} are zero. The shear equivalent of Hooke's law gives:

$$\tau_{zx} = 2\mu e_{zx} = 2\mu \cdot \frac{1}{2}\left(\frac{\partial u_z}{\partial x} + \frac{\partial u_x}{\partial z}\right) = \mu \frac{\partial u_z}{\partial x} \tag{F.38}$$

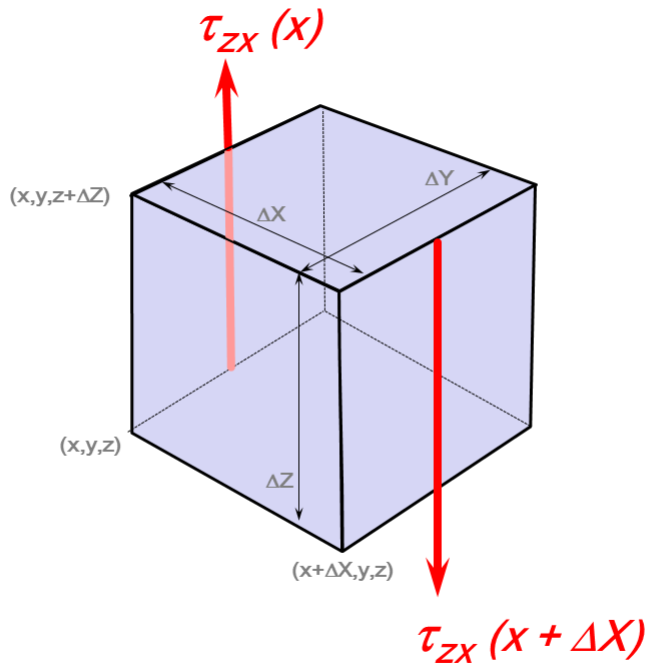

Figure F.5: Infinitesimal rectangular block under plane stress, used for deriving basic equations for S-wave motion.

As for P-waves, in order to introduce the particle velocity v_z, we differentiate both sides with respect to time t and take the particle velocity as $v_z = \partial u_z/\partial t$ to give:

$$\boxed{\frac{\partial \tau_{zx}}{\partial t} = \mu \frac{\partial v_z}{\partial x}.} \tag{F.39}$$

This is the desired expression for the deformation.

As before, this equation alone does not decribe wave motion since we need to apply Newton's law as well. Referring to Figure F.5, the force is, in terms of stress:

$$F_z = \Delta Y \Delta Z [\tau_{zx}(x + \Delta X) - \tau_{zx}(x)] \tag{F.40}$$

and the force is given as mass times acceleration, i.e.:

$$F_z = \Delta M \frac{\partial^2 u_z}{\partial t^2}. \tag{F.41}$$

Equalizing these forces gives:

$$\frac{\tau_{zx}(x + \Delta X) - \tau_{zx}(x)}{\Delta X} = \frac{\Delta M}{\Delta X \Delta Y \Delta Z} \frac{\partial^2 u_z}{\partial t^2} \tag{F.42}$$

or, since $\tau_{zx}(x + \Delta X) \simeq \tau_{zx}(x) + (\partial\tau_{zx}/\partial x)\Delta X$:

$$\frac{\partial \tau_{zx}}{\partial x} = \rho \frac{\partial^2 u_z}{\partial t^2}. \tag{F.43}$$

Again, we need to introduce the particle velocity via the displacement, giving:

$$\boxed{\frac{\partial \tau_{zx}}{\partial x} = \rho \frac{\partial v_z}{\partial t}.} \tag{F.44}$$

This is the other desired equation, the equation of motion for S-waves.